On Improving the Short-Wavelength Response and Efficiency of Photovoltaic Modules via Luminescent Down-Shifting of the Incident Light

Efthymios Klampaftis, BSc, MSc

Submitted for the degree of Doctor of Philosophy

On completion of research conducted at the

Department of Mechanical Engineering

School of Engineering and Physical Sciences

Heriot-Watt University

Edinburgh EH14 4AS

United Kingdom

March 2013

ABSTRACT

This thesis investigates the technology of luminescent down-shifting (LDS) of light for improving the short-wavelength response and efficiency of photovoltaic (PV) modules.

A critical literature review of previously published work is presented identifying the opportunity to include the luminescent species in the encapsulation layer of certain PV technologies.

A range of luminescent materials and mixtures thereof were tested in ethylene vinyl acetate (EVA) host. They all exhibited very high luminescent efficiencies and did not impair the transmittance of the encapsulant.

LDS EVA sheets were used to encapsulate multi-crystalline silicon (mc-Si) and chalcopyrite (CIGS) solar cells. An increase in short-λ external quantum efficiency of up to 25 % was achieved for mc-Si devices. For CIGS, the increase was up to 25 % and 40 % for 50-nm- and 100-nm-thick buffers respectively. The overall efficiency of mc-Si devices was improved by 0.2 % in the best case and gains of up to 0.2 mA / cm^2 and 0.6 mA / cm^2 were achieved for 50-nm- and 100-nm-thick buffer CIGS devices.

LDS offers the additional benefit of device colouration, which can encourage the further uptake of PV in applications where colour is a desirable property.

ACKNOWLEDGMENTS

I would like to first thank my parents and other members of my family, who have continuously encouraged and supported me during the years of this project. The successful completion of my PhD is the least I could bring home after their long-term sacrifices in order to provide me with the best possible education opportunities throughout my life.

I would like to express my sincere gratitude to my supervisor Professor Bryce S. Richards, whose influence in my academic life and not only has been decisive. After showing me what research about something novel is during our first collaboration, he offered me the opportunity to take on the challenge of a PhD. He did not stop believing in my potential even when my performance was not up to his high standards and this did not allow me to fail his trust. He continues to offer his advice and support like a true mentor and friend. I feel fortunate to have met him and proud to be a member of his research group.

Many thanks to all the members of our research group, who made my everyday life at uni more enjoyable. Brenda, Gavin, Dalila, Gudrun, Serena, Nabin, Sean, Giorgos, Jose, Aruna and Diego will always be a part of good memories from these years, together with other PhD peers who were not part of our group, like Daniel, Neruda and Mohammed. A special thanks to my good friend Dr. Nader Cooli, who showed me in practice how to not give up irrespectively of the difficulties one can find during a PhD and stimulated many thoughts in my mind with his life and the many interesting conversations we had.

I am grateful to the EPSRC and the JRI Energy for funding my PhD.

I am also grateful to the technical stuff of our department and in particular Richard who always tried to speed things up for me.

I would like to acknowledge the contribution of certain companies via supply of materials or access to equipment. These are: BASF that supplied Lumogen dyes, the first doped EVA sheets and EVA raw material (thank you Axel Grimm and Matthias Klueglein), NaREC for access to their solar simulator (thank you Alex Cole and Keith Heasman), E-Ton Solar for providing with solar cells (thank you Allen Guo), DuPont for supplying with Teflon FEP material (thank you Nicola Glassmaker) and finally ColorFlex for continuing to supply with Lumogen dyes till the end of the project (thank you Arno Böhm).

I am also grateful to certain people that kindly offered their help to me during this project having no vested interest in my work. These are: Professor Colin Hindle and Lynn Chalmers of Edinburgh Napier University, who helped me with the fabrication of EVA sheets, Bill MacPherson, who helped resolve the technical problem of our spectral response system and Jonathan Parry, who helped me with cutting solar cells.

I was fortunate during my project to have received the productive collaboration of Dr. Keith R. McIntosh of the Australian National University, Martina Congiu and Professor Neil Robertson of Edinburgh University and Sieghard Seyrling, Julian Perrenoud and Professor Ayodhya N. Tiwari of ETH Zürich University.

My sincere thanks to Professor John Wilson of Heriot-Watt University and Professor Zhiqun He of Beijing Jiaotong University for offering me the opportunity to experience the research and student life in China. Also, my thanks to my friend Zhao Zhi for making this experience much more interesting and enjoyable.

I cannot neglect to make a mention to a number of people that were not part of my university life, but who also helped me arrive to this moment with their friendship. Thank you Robin, Jon, Francois, Giannis, Calvin, Lee, Celin, Shane, Asazi, Jorge, Tasos, Dimitris, George, Marta, Molina, Juan, Alma, Pawel, Tomala, Dani, Christina and all my dear housemates and friends with who I shared parts of my life. I made so many friends during this PhD course that it makes it worth double to me.

Special thanks to the two fellow PhD students with whom I worked very closely and eventually became a good friend with. First thanks to Lindsay, the wonder boy with the so much potential in him. Our conversations over pretty much every aspect of life was a great parenthesis during the PhD hurdles, before going back to the practical problems in the lab, where he was always available to offer his help. Second but not least thanks to Dave, with who I shared the feeling of success by achieving together good results. However, it was his offering of friendship that I most appreciated and I feel fortunate to have had his support in the difficult moments of my PhD.

My final thanks to my dear Isidora who was my companion and everyday support during the most time-demanding years of this project. My feelings have grown stronger and I hope I will now be able to spend more time in your peaceful dream-world.

TABLE OF CONTENTS

GLOSSARY (ACRONYMS AND SYMBOLS)

AR	anti-reflective
AM0	air-mass zero
AM1.5d	air-mass 1.5 diffuse
AM1.5D	air-mass 1.5 direct
AM1.5G	air-mass 1.5 global
BIPV	building-integrated photovoltaics
BMA	butyl methacrylate
CIGS	copper indium gallium diselenide
DCM	dichloromethane
DSSCs	dye-sensitised solar cells
EMA	ethyl methacrylate
EQE	external quantum efficiency
EU	European Union
EVA	poly-(ethylene vinyl acetate)
FEP	fluorinated ethylene propylene
FF	fill-factor
LDS	luminescent down-shifting
LSC	luminescent solar concentrator
MMA	methyl methacrylate
NIR	near infra-red
OD	optical density
OPV	organic (polymer-based) photovoltaics
ORMOSIL	organic molecule silicates
PLE	photoluminescent excitation

PLQY	photo-luminescent quantum yield
PMMA	poly-(methyl methacrylate)
PV	photovoltaic(s)
PVA	poly-(vinyl acetate)
PVB	poly-(vinyl butyral)
QDs	quantum dots
RE	renewable energy
SR	spectral response
STC	standard test conditions
TCO	transparent conductive oxide
UV	ultra-violet

Al	aluminium
Ag	silver
AlGaAs	aluminium gallium arsenide
Alq_3	tris (8-hydroxyquinolinato) aluminium
Al_2O_3	aluminium oxide
a-Si	amorphous silicon
c	concentration
CaF_2	calcium fluoride
CdS	cadmium sulphide
CdTe	cadmium telluride
Cr^{3+}	chromium ion
c-Si	(mono)-crystalline silicon
Dy^{3+}	dysprosium ion

E_g	band gap
Eu^{3+}	europium ion
Gaq_2Cl	bis-(8-hydroxyquinoline)-chlorogallium
i	intrinsic
I_D	diode current
I_L	light generated current
I_{MPP}	maximum power point current
I_{SC}	short-circuit current
I_0	dark saturation current
InGaAs	indium gallium arsenide
In_2S_3	indium sulphide
I—*V*	current—voltage
J	current density
k	Boltzmann constant
$KMgF_3$	potassium magnesium fluoride
L	optical path
$LaVO_4$	lanthanum vanadate
mc-Si	multi-crystalline silicon
Mo	molybdenum
n	refractive index
$Nd:YVO_4$	neodymium-doped yttrium vanadate
Ni	nickel
P_d	power density
P_{in}	incident power flux
q	elementary charge

R_S	series resistance
R_{SH}	shunt resistance
Se	selenium
Si	silicon
SiO_2	silicon dioxide
Sm^{3+}	samarium ion
T	absolute temperature
T	transmittance
Tb^{3+}	terbium ion
TPD	N,N'-diphenyl-N,N'-(3-methylphenyl)-1,1'-biphenyl-4,4'-diamine
V_{MPP}	maximum power point voltage
V_{OC}	open-circuit voltage
W_p	watt-peak
Xe	xenon
ZnO	zinc oxide
$Zn(OH)_2$	zinc hydroxide
ZnSe	zinc selenide
ε	mass absorptivity
η	efficiency
λ	wavelength
ρ	density
σ	standard deviation
$\varphi(\lambda)$	photon flux

PUBLICATIONS RESULTING FROM WORK CONDUCTED FOR THIS THESIS

Journal articles

D. Ross, **E. Klampaftis**, B.S. Richards, J. Fritsche, M. Bauer, Increased J_{SC} of production line CdTe mini-module through luminescent down-shifting, *Solar Energy Materials & Solar Cells* 103 (2012) 11—16.

E. Klampaftis, D. Ross, S. Seyrling, A.N. Tiwari and B.S. Richards, Increase in short-wavelength response of encapsulated CIGS devices by doping the encapsulation layer with luminescent material, *Solar Energy Materials & Solar Cells* 101 (2012) 62—67.

E. Klampaftis, M. Congiu, N. Robertson and B.S. Richards, Luminescent Ethylene Vinyl Acetate Encapsulation Layers for Enhancing the Short Wavelength Spectral Response and Efficiency of Silicon Photovoltaic Modules, *IEEE Journal of Photovoltaics* 1(1) (2011) 29—36.

E. Klampaftis and B. S. Richards, Improvement in multi-crystalline silicon solar cell efficiency via addition of luminescent material to EVA encapsulation layer, *Progress in Photovoltaics: Research and Applications* 19 (3) (2011) 345—351.

E. Klampaftis, D. Ross, K. R. McIntosh and B. S. Richards, Enhancing the performance of solar cells via luminescent down-shifting of the incident spectrum: A review, *Solar Energy Materials & Solar Cells* 93 (2009) 1182—1194.

Conference papers

E. Klampaftis, D. Ross, S. Seyrling, A.N. Tiwari and B.S. Richards, Impact of luminescent down-shifting EVA layers onto CIGS solar cells, *Proceedings of PV SAT-8*, Newcastle, U.K., 2012, pp. 37—40 (Oral Presentation).

D. Ross, **E. Klampaftis**, J. Fritsche, M. Bauer and B. S. Richards, Measured increased J_{SC} in production quality CdTe cells and mini-modules through luminescent down-shifting, *Proceedings of 26th EU PVSEC*, Hamburg, Germany, 2011, pp. 2463—2466 (Oral Presentation).

Conference papers (continued)

E. Klampaftis and B. S. Richards. Optimisation of luminescent EVA encapsulation layers for silicon PV modules, *Proceedings of 26th EU PVSEC*, Hamburg, Germany, 2011, pp. 517—521.

E. Klampaftis, D. Ross, S. Seyrling, J. Perrenoud, A. N. Tiwari and B. S. Richards, Luminescent down-shifting for improving the efficiency of photovoltaic modules, *Proceedings of PV SAT-7*, Edinburgh, UK, 2011, pp. 5—8 (Oral Presentation).

E. Klampaftis and B.S. Richards. Improvement in multi-crystalline photovoltaic efficiency using luminescent encapsulation layers, *Proceedings of 25th EU PVSEC / 5th World Conference on Photovoltaic Energy Conversion*, Valencia, Spain, 2010, pp. 251—254 (Oral Presentation).

E. Klampaftis, B.S. Richards, L.R. Wilson, K .R. McIntosh, A. Cole and K. Heasman, Improving Spectral Response of mc-Si Cells via Luminescent Down-Shifting of the Incident Spectrum, *Proceedings of PV SAT-4*, Bath, UK, 2008, pp. 59—62 (Oral Presentation).

Other publications

B. S. Richards and **E. Klampaftis**, Luminescent encapsulation layers for multicrystalline silicon PV modules, *Photovoltaics International*, 11th Edition, February 2011, pp. 104–109 (Invited Paper).

CHAPTER 1 – INTRODUCTION

This chapter first introduces the reader to the general context in which this thesis was envisaged. It then introduces the technical challenge that it attempts to address and provides with a first description of the method that is used to do so. The structure of the thesis and the objectives of each chapter are finally described

1.1 The General Context

The global demand for energy has grown rapidly in the last decades and it is predicted to grow further in the foreseeable future [1]. The increasing population and the industrialisation of more societies on the planet are two forces that will continue to drive this trend. Mankind will need to address the major challenge of how to satisfy this growing energy demand in a sustainable way, if further progress in living standards for more people in the world is to be achieved.

The realisation that the growing energy demand cannot be satisfied with the use of fossil fuels has also grown in recent years. This is, firstly, because finite sources of energy cannot be considered as a sustainable solution in any medium- or long-term plan by definition. Secondly, because the burning of fossil fuels is associated with greenhouse gases emissions and the implication of disrupting the global climate with unpredictable and very likely disastrous consequences. Finally, fossil fuels, which are mined in certain regions of the planet only, are linked with supply uncertainty due to geopolitical reasons and this is an important security issue for our modern societies. Hence, there is a significant social and political shift towards greater utilisation of renewable energy (RE) sources, which are the only sustainable long-term solution to the energy challenge. RE technologies' contribution to the global energy production grows faster than any other energy sector in recent years and will most likely continue to do so in the foreseeable future [2].

In this context, the potential to harness the energy of our sun, which is the single biggest fountain of energy in the vicinity of our planet, seems to be a very attractive possibility. A typical argument that exhibits the potential of solar power is that the energy offered freely to us by the sun in one hour is in the order of the global consumption in one year [3]. At the same time, the sun is sending us in one year as much energy as this planet is ever going to produce by the use of all its non-renewable resources [4]. There is clearly an opportunity to pursue a long-term solution to our energy needs if we can exploit a fraction of this abundant energy resource that the sun is offering. This is already possible with the use of various existing technologies, before even considering what tools the applied science will be able to offer in the future.

1.2 Photovoltaics and the Pursuit for Higher Efficiency

Photovoltaics (PV) is one of the technologies that make use of the sun's great energy resource. They are devices based on semiconducting materials that directly convert the sun's irradiation to electricity. There has been a great progress in the field of PV devices' performance since the very first solar cells made in the late 19^{th} century based on bulk selenium (Se) specimens [5-7]. The first p-n junction silicon (Si)-based solar cell was developed in 1941 with the work of Ohl *et al.* [8, 9]. However, all these devices had less than 1% efficiency (η) and this had to be largely improved before any consideration on mass production of energy from PV could be made. This effort is on-going since the first major improvement in the 1950's with the work of Pearson, Chapin and Fuller [10, 11], who made the first silicon-based solar cells that reached an efficiency of 2.3 % and very soon arrived at 6 %. Within the next decade, the landmark of 10 % was exceeded, the first commercial products were on sale and the first solar powered telecommunications satellite Telstar-1 was launched.

The generic architecture of a typical p-n junction Si solar cell is shown in Figure 1. It is made from p-type Si wafer, which is subjected to high temperature diffusion of V group element (such as phosphorous) to form the n-type emitter homojunction. The top front contact is generally made from silver (Ag) in the form of fingers, so as to allow illumination, whilst the back contact is a continuous aluminium (Al) layer.

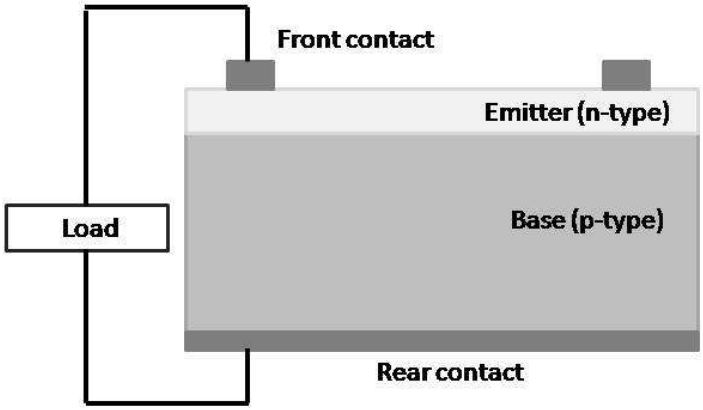

Figure 1: Schematic of the fundamental architecture of a p-n junction Si solar cell.

Today, the highest efficiencies for modern single p-n junction PV devices are 28.3 % for thin-film gallium arsenide (GaAs) and 25 % for crystalline silicon (c-Si) solar cells [12]. The efficiency of single p-n junction solar cells is restricted irrespectively of material quality and device structure to what is known as the Shockley–Queisser limit, which for a band gap (E_g) of 1.1 eV is just above 30 % [13]. To exceed this limit, sophisticated devices that make use of more than one solar cells stack on top of each other have been invented, so that each cell efficiently converts the more suited to its band gap fraction of the incident spectrum [14]. Other significant developments in the field of PV technologies are heterojunction amorphous silicon (a-Si) [15] and thin-film devices [16, 17] as well as dye-sensitised nanocrystalline solar cells (DSSCs) [18] and organic polymer-based PV (OPV) [19]. The performance of all these technologies is constantly improved, while more novel technologies are developed in the various PV laboratories of the world. The currently best research-cell efficiencies for all known technologies are shown in Figure 2.

The progress recorded in the area of PV devices' performance combined with the aforementioned motivation for greater utilisation of solar power have encouraged the development and rapid growth of a multi-billion industry in the recent decades. However, PV does not yet offer a major contribution towards satisfying our demand for energy. For example, PV satisfies just ~1.2 % of the European Union's (EU) total electricity demand, when the installed capacity in the EU represents ~75 % of the global total cumulative capacity [20]. There is clearly a long way to go before PV becomes a major player in the energy sector.

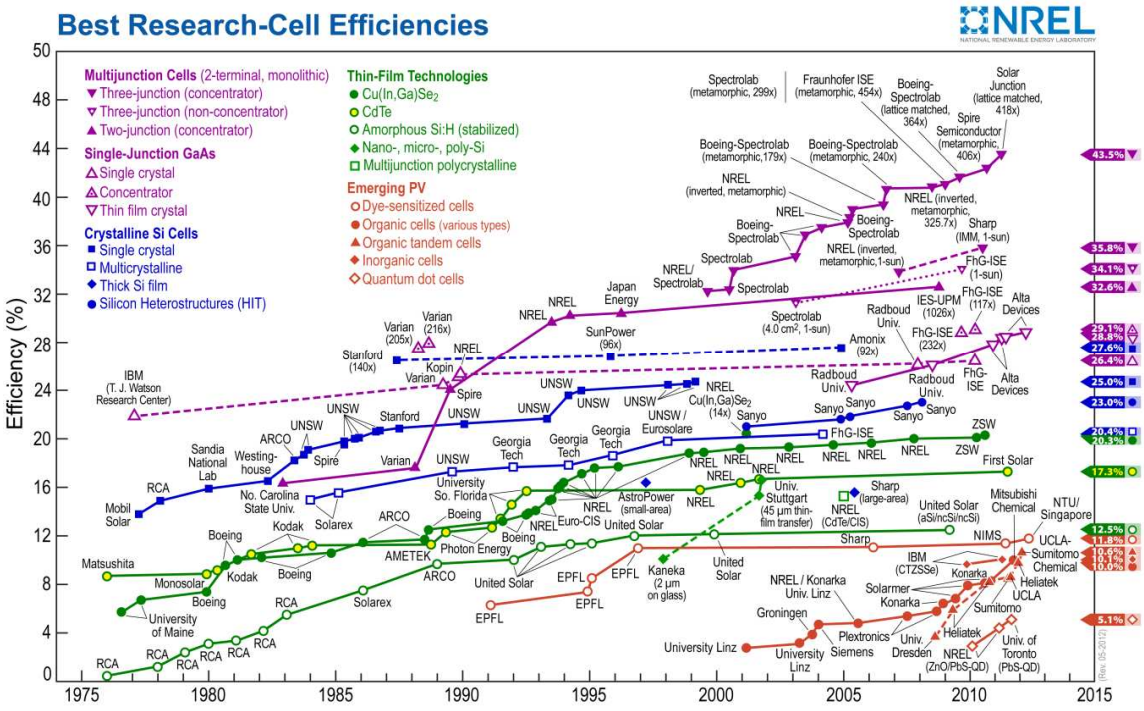

Figure 2: Best research-cell efficiencies [21].

Leaving aside for the political and financial actions that can increase the contribution of PV, scientists and engineers will also play a significant role. The primary aim is to further enhance the performance of existing PV devices with the use of more advanced methods. At the same time, novel technologies and applications of PV devices will come through. All these new ideas and practices that will be developed in laboratories must be successfully transferred to production if they are to make a practical contribution. This is not always a simple task either for technical or for financial reasons. The work presented in this thesis aims to make a contribution in the area of enhancing the performance of existing PV technologies, while considering the applicability of its suggestions to production.

1.3 Operating Principles and Characteristic Parameters of a Solar Cell

The solar cell action is generally described with the term "photovoltaic effect". In a classical p-n junction, such as that in the Si-based solar cell in Figure 1, photovoltaic effect describes the creation of voltage under illumination as follows:

i) Incident photons with sufficient energy ($hv > E_g$) get absorbed by the semiconducting material to create electron-hole pairs; and

ii) Free charge carriers are separated with the help of the built-in electrical field at the junction, resulting into electric potential.

The collection of light-generated minority charge carriers from the junction increases the number of electrons in the n-type region and that of holes in the p-type region. This charge separation creates an electric field which opposes the built-in field of the junction, thus reducing the barrier for the majority charge carrier diffusion current. If the light-generated charge carriers are prevented from exiting the device (open-circuit conditions), a new equilibrium is built where the light-generated and the diffusion currents balance each other out so that the net current is exactly zero. The voltage required to result to this new equilibrium is called the open-circuit voltage (V_{OC}). If the terminals of the device are connected with each other (short-circuit conditions), there is no charge build up due to illumination since the light-generated carriers exit the device and flow as current. This is called the short-circuit current (I_{SC}) of a solar cell.

Connected in an electrical circuit, the solar cell can be seen as a two-terminal device that conducts as a diode in the absence of light (dark), and generates a voltage if illuminated. Current can be driven by this voltage if a load is connected to the circuit. Figure 3 shows the equivalent circuit of a non-ideal solar cell and the currents that flow through the circuit's branches: the light generated current (I_L), the diode current (I_D) and the cell's output current (I). In the equivalent circuit are also included parasitic electrical losses arising from the fact that the solar cell is not a perfect conductor and due to current leakage between the two terminals if the insulation is not perfect. Parasitic losses are represented in the form of two resistances, one connected in series (R_S) and one in parallel (also called shunt resistance, R_{SH}) respectively. An ideal solar cell would exhibit $R_S = 0$ and $R_{SH} = \infty$.

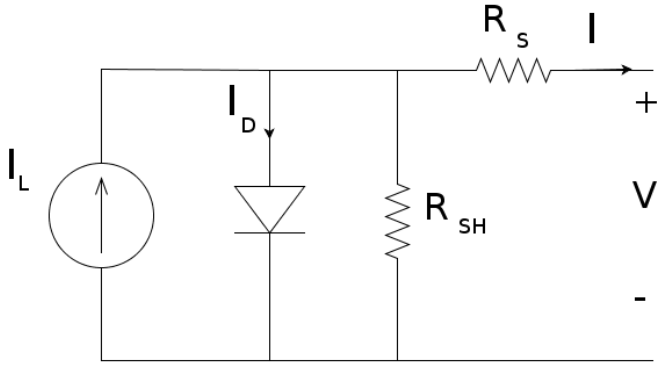

Figure 3: Equivalent circuit of a non-ideal solar cell.

The solar cell's output current can be expressed as the superposition of its J_L with its I_D and the losses due to the resistances:

$$I = I_L - I_0\left(e^{\frac{q(V+IR_S)}{kT}} - 1\right) - \frac{V+IR_S}{R_{SH}} \quad , \tag{1}$$

where q is the electronic charge, k is the Boltzmann constant, T the absolute temperature in K and I_0 the dark saturation current of the solar cell. Equation (1) is often written in the simplified explicit form of equation (2), which represents the case of an ideal solar cell with no resistive losses. This assumption is not very far from true for laboratory-quality high efficiency solar cells that will exhibit very low R_S (typically < 0.5 Ω cm^2 per unit of area) and very high R_{SH} (typically in the scale of MΩ cm^2 per unit of area).

$$I = I_L - I_0(e^{\frac{qV}{kT}} - 1) \tag{2}$$

Two important parameters that are used to characterise solar cells are the current that flows through the circuit when no load is applied (I_{SC}) and the voltage between the terminals when no current is drawn (V_{OC}). The equation that relates the V_{OC} and the I_{SC} of a solar cell can be derived from equation (2), given that at open circuit conditions no current is drawn from the solar cell (I=0), and that in the absence of resistive losses (or if they are not extremely high), the I_L and the I_{SC} are with very good approximation identical.

$$V_{OC} = \frac{kT}{q}\ln\left(\frac{I_{SC}}{I_0} + 1\right) \tag{3}$$

The maximum electrical power that can be generated from a solar cell occurs at a certain voltage between 0 (short circuit) and the V_{OC}. This voltage is called maximum power point voltage (V_{MPP}) and the corresponding current, maximum power point current (I_{MPP}). A third important parameter for solar cell characterisation is defined with the help of these quantities. This is the fill factor (FF), which is a measure of how much of the cell's I_{SC} and V_{OC} are utlised at the maximum power point of the device. The FF of a solar cell is given by equation (4):

$$FF = \frac{J_{MPP}V_{MPP}}{J_{SC}V_{OC}} \quad . \tag{4}$$

The final parameter that is used to characterise a solar cell is its overall η. This is a measure of how much power the device generates under certain conditions and is commonly given

as a fraction of the incident power flux (P_{in}). The efficiency is related to the three aforementioned solar cell parameters via the equation (5) and is usually determined for the standard test conditions (STC) of air-mass 1.5 global (AM1.5G) spectrum, P_{in} of 1000 W/m^2 and temperature of 25 °C.

$$\eta = \frac{I_{MPP}V_{MPP}}{P_{in}} = \frac{I_{SC}V_{OC}FF}{P_{in}} \quad (5)$$

These key solar cell parameters are shown in a characteristic *I–V* curve in Figure 4.

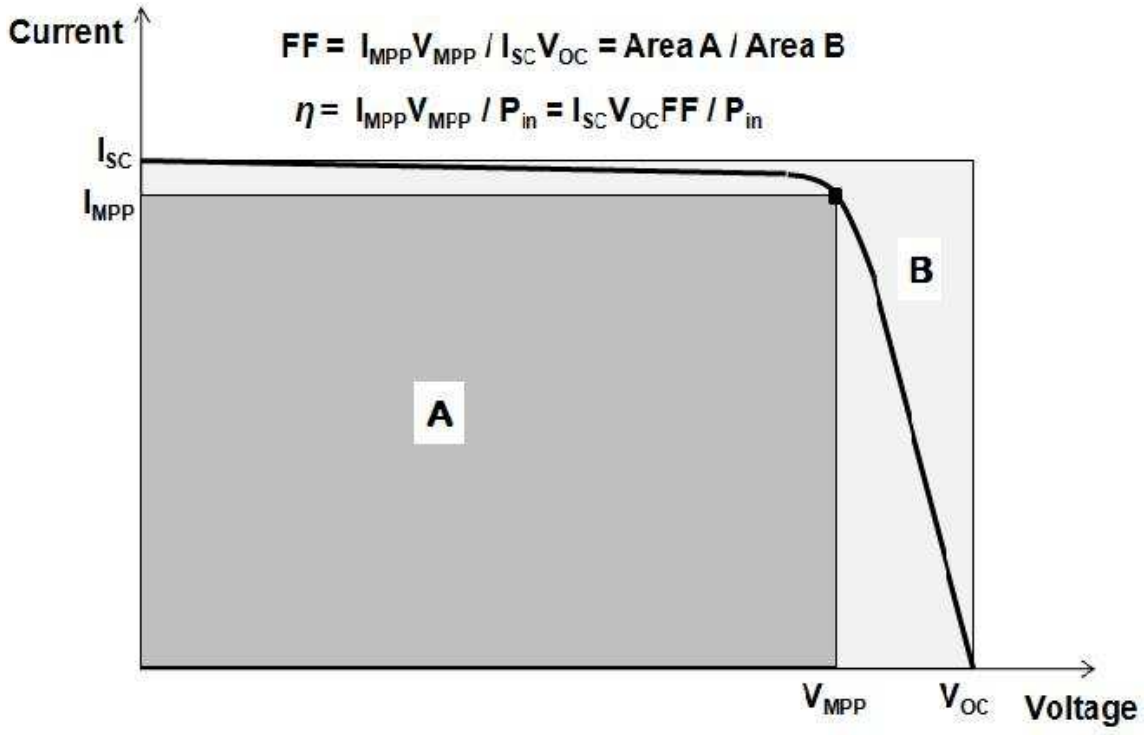

Figure 4: Characteristic *I–V* curve annotated with key PV parameters and equations.

1.4 Spectral Response of Solar Cells

Fundamental spectral losses, which arise from the limited spectral response (SR) of solar cells to the wideband solar spectrum, constitute the largest proportion of losses for every developed PV technology [13, 22]. Transparency losses arise from sub-band gap photons ($E < E_g$) that are not absorbed by the semiconducting material of the solar cell, while the excess energy of high-energy photons ($E > E_g$) is lost via non-radiative relaxation of

excitons to the conduction band in the form of heat. Figure 5 shows an energy band diagram of a p-n junction solar cell depicting fundamental processes within the device.

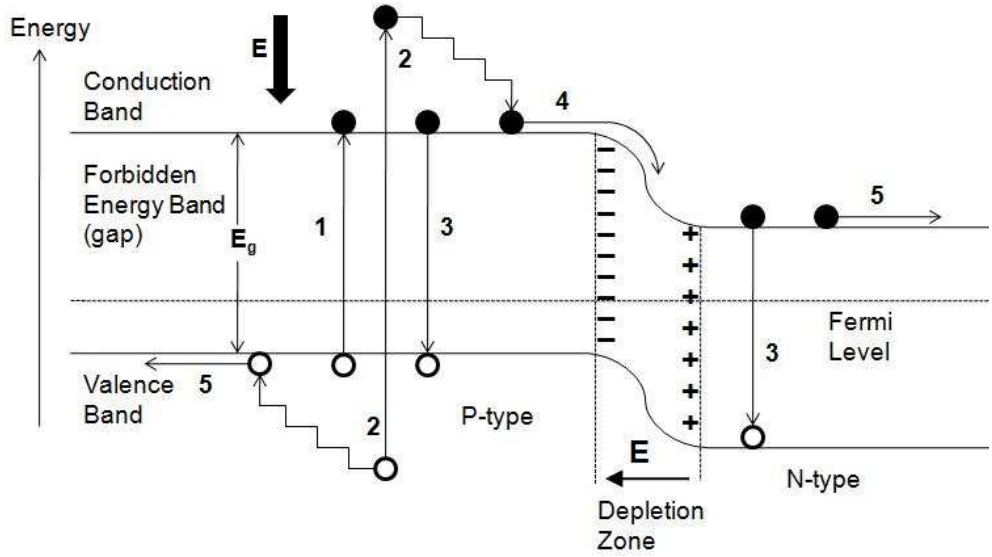

Figure 5: Energy band diagram depicting electron-hole pair excitation and separation in a p-n junction solar cell. Sub-band gap photons ($E < E_g$) will not be absorbed. Photons with $E = E_g$ will be absorbed and excite an electron-hole pair (1). Photons with $E > E_g$ will be absorbed and excite an electron-hole pair, however, the additional energy will be lost as heat (2). Some of the excited electron-hole pairs will recombine (3), whilst others will be separated by the electric field of the junction (4). Eventually some charge carriers will arrive to the terminals of the device (5).

In addition to the fundamental spectral losses, there are loss mechanisms that will further reduce the conversion efficiencies of PV devices. The response to short-wavelength (λ) photons, in particular, is inferior to the response to longer visible wavelengths, despite the higher energy content at short-λ. This is because the high-energy ultra-violet (UV) and blue λ photons will tend to interact fast with the front layers of a PV device, which do not contribute as effectively to photocurrent generation. Thus, the energy content of these photons is not harnessed efficiently. It is this weakness of PV devices that the work presented in this thesis aims to improve.

The λ-dependent performance of a PV device is best assessed by its external quantum efficiency (EQE) spectrum. The EQE is defined as the ratio of the number of charge carriers collected at the junction of the PV device to the number of the incident photons

(per units of time and area and for a certain bandwidth of the incident spectrum). Figures 6 (a) and (b) show the short-λ fraction of representative EQE spectra for various PV technologies, including c-Si, multi-crystalline silicon (mc-Si), GaAs, cadmium telluride (CdTe), copper indium gallium diselenide (CIGS), single and triple junction a-Si, a DSSC and the OPV poly(3-hexylthiophene)phenyl-C_{61}-butyric acid methylester (P3HT:PCBM), to exhibit the common trend of deteriorating performance with decreasing wavelength.

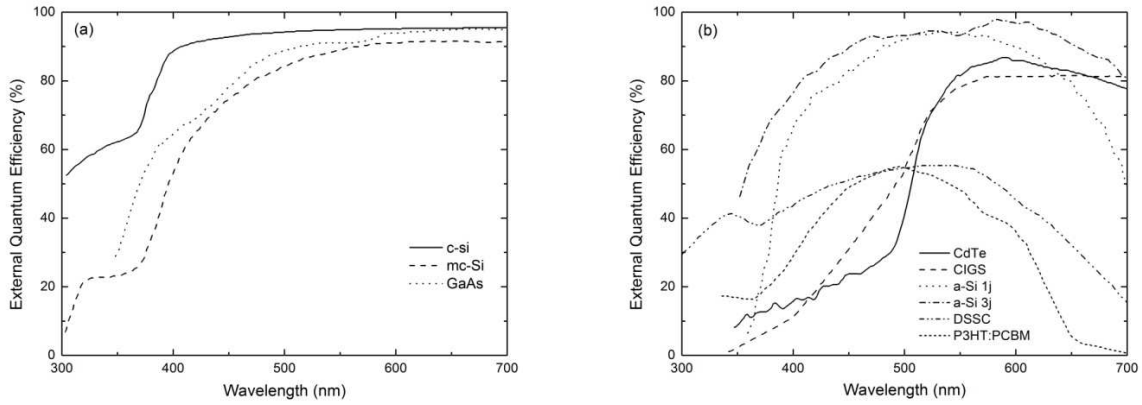

Figure 6: (a) Short-λ EQEs of wafer-based PV devices: c-Si [23], mc- Si [24] and single junction GaAs [25]. (b) Short-λ EQEs of thin-film PV devices: CdTe [26], CIGS [27], single junction a-Si [28], triple junction a-Si [29], DSSC [30] and P3HT:PCBM [31].

The high optical losses for short-λ photons arise from technical processing difficulties, necessary trade-offs in the design of a device and imperfect properties of the available materials to form the top layers of PV devices. The most dominant short-λ loss mechanisms for various in-production PV cell technologies are given in Table 1. At module level, there are further significant loss mechanism for short-λ photons: (i) absorption and reflection by the front cover (either glass or polymer); and (ii) absorption by the encapsulant where that exists.

There are three principal approaches to achieve a more efficient utilisation of the short-λ part of the solar spectrum. The first is to further improve the electronic properties of existing devices. This can be achieved by using advanced design concepts, such as very narrow junction(s), low doping levels or very thin window layers. These steps however, can prove difficult to implement and/or expensive in production, while they may also have detrimental effects in the overall performance of a device [32]. The second approach is the implementation of more sophisticated ‘‘third generation’’ cell structures, such as multi-

junction [14], hetero-junction [33] and intermediate band gap [34] cells, which can lead to better utilisation of the short-λ light. However, significant technical hurdles need to be overcome before these technologies will compete with first and second generation flat-plate PV technologies. The third approach is to modify the incident spectrum before it reaches the PV cell, so that it better matches the SR of the device. This is a passive approach that involves applying a luminescent species in a layer prior to the PV cell, thus, eliminating the need to interfere with the device's active material. This method is called luminescent down-shifting (LDS) of the incident light and it is the primary focus of this thesis.

Table 1: Major loss mechanisms for various in-production PV technologies.

Cell type	Major loss mechanism at short λ
c-Si	Emitter recombination, increased reflectance and absorption from the AR-coating
mc-Si	Recombination at the "dead" front surface layer due to heavily doped emitter, increased reflectance and absorption from the AR-coating
a-Si	Absorption in TCO window layer and recombination due to heavily doped semiconducting layers
GaAs	Absorption in AlGaAs or InGa**P** window layer
CdTe	Absorption in buffer (typically CdS) and TCO window layers
CIGS	Absorption in buffer (typically CdS) and TCO window layers
All	Absorption from glass & encapsulation material (except for superstrate grown thin-film technologies like a-Si and CdTe).

Acronyms: anti-reflective (AR), transparent conductive oxide (TCO), aluminium gallium arsenide (AlGaAs), indium gallium arsenide (InGaAs) and cadmium sulphide (CdS).

1.5 Introduction to LDS

The enhancement of the short-λ response of PV devices via LDS of the incident spectrum first appears in the literature in the late 1970s. It was observed and reported during research conducted for the luminescent solar concentrator (LSC) technology as a beneficial consequence of the concentration process [35, 36]. Hovel *et al.* [32] were the first to apply the concept of LDS in a planar luminescent sheet positioned on top of PV cells. They identified and exhibited the potential of this method, experimenting with a range of PV technologies. While these first results were encouraging for the LDS concept, it is

important to note that the efficiencies of the solar cells used were considerably lower than the ones of today, thus, allowing a larger margin for improvement. At the same time, their final results were severely limited by the inadequacy of the luminescent materials available at that time. The performance of both the solar cells as well as the luminescent materials that are available today is substantially better than what used to be in the late '70s. This means that the overall improvement that LDS can potentially offer to PV devices is of smaller magnitude, but we have better tools to realise it in practice.

The principle of LDS is to absorb the fraction of incident sunlight where a solar cell performs suboptimally with the use of a luminescent species and before the photons reach the semiconducting material of the cell. Consequently, longer-λ photons will be emitted by the luminescent species, in a spectral region where the solar cell exhibits higher SR. As a result, more electron-hole pairs can be potentially created per incident photon and a higher photocurrent will be generated. Thus, the short-λ EQE of the cell will increase. The V_{OC} and FF of the PV device will not change significantly, since there is no change in the electronic properties of its semiconducting material and/or its resistances. Hence, an increase in overall conversion efficiency can be achieved.

It is worth noting that LDS is an one-to-one photon process as opposed to two other spectral conversion techniques that are also used for improving the SR of solar cells. Down-conversion can also be used to improve their short-wavelength response. However, this is an one-to-two photons process, where one UV or blue photon can excite an electron to a higher electronic state, which will then relax via a two step radiative sequence and will emit two visible wavelength photons. This process is also often described with the term quantum splitting. Up-conversion is the third spectral technique that can be used to improve the long-wavelength response of solar cells. This is a two-to-one process, where two infra-red photons can be sequentially absorbed by the same electron, which will then relax by emitting one visible wavelength photon. A simplified energy diagram that describes this fundamental difference between these three spectral conversion techniques is shown in Figure 7.

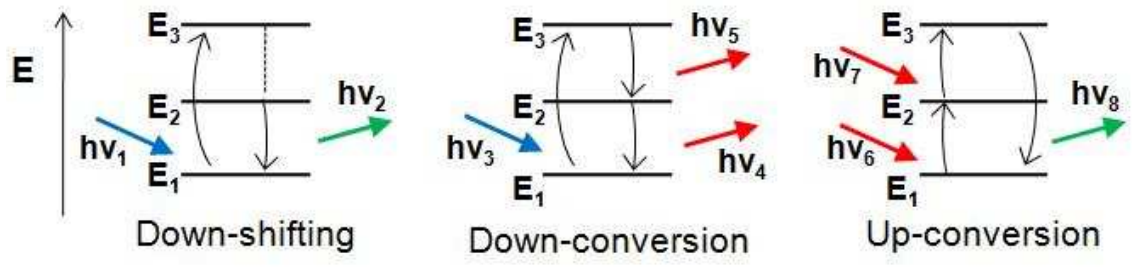

Figure 7: Simplified energy diagram depicting the fundamental difference between three spectral conversion techniques used to improve solar cell response. Down-shifting is an one-to-one photon process and can be used to improve the UV and blue response of solar cells. Down-conversion can also be used for the same reason, but it is an one-to-two photon process. Up-conversion can be used to improve the infra-red response of solar cells and it is a two-to-one photon process.

A visual description of how the LDS process is shifting parts of the spectrum to a region of higher cell EQE is given in Figure 8. The CdTe cell exhibits a sharp decrease in EQE for $\lambda < 550$ nm, primarily due to parasitic absorption by the CdS buffer layer [26]. A fluorescent organic dye that absorbs in the region $\lambda < 500$ nm and emits at $\lambda > 500$ nm is shifting parts of the incident irradiation from wavelengths where the cell is performing poorly (EQE of 0 – 25 %) to longer ones where the cell is performing better (EQE of 30 – 80 %). The spectral distribution of the photon flux for the standard AM1.5G solar spectrum is also plotted in order to consider the process in terms of available photons for LDS.

The introduction of a luminescent material in the design of a PV device will, however, result in additional interactions with the incident photons and new optical loss mechanisms will be created. Therefore, the potential gains from the better response of the PV device to the modified spectrum must exceed these losses for LDS to afford an overall efficiency improvement.

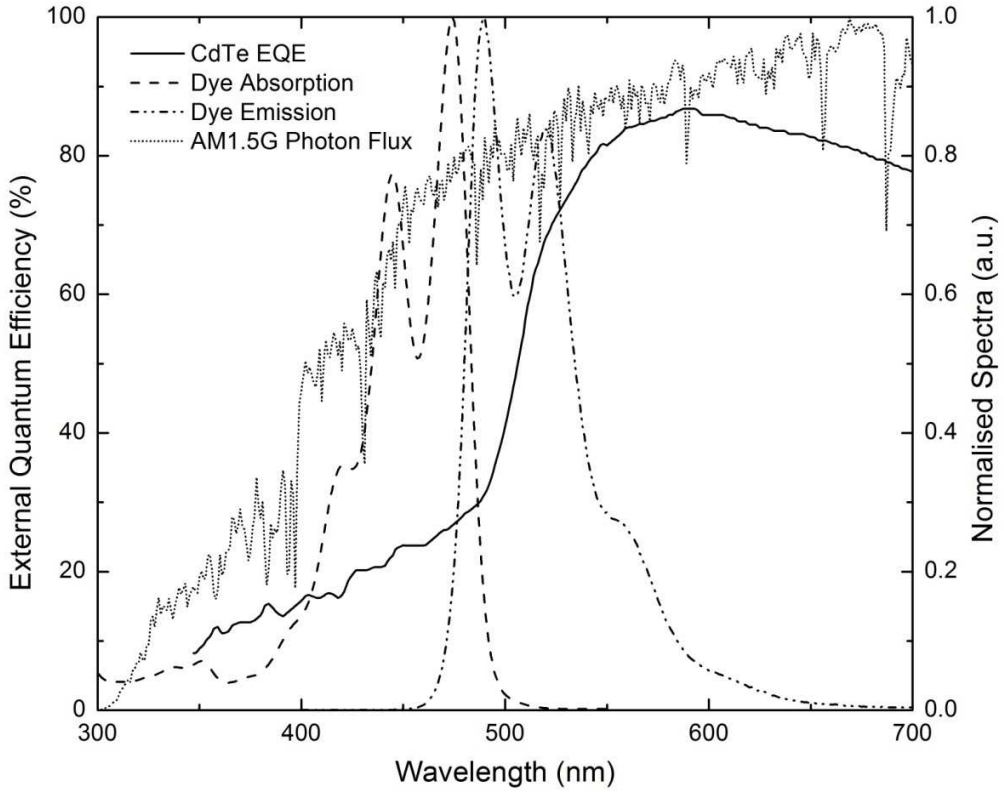

Figure 8: Visual representation of the LDS method. Normalised absorption and emission bands of a fluorescent organic dye (BASF Lumogen F Yellow 083) [37], along with the AM1.5G solar spectrum [38] and the EQE of a production line CdTe PV module [26].

The added optical losses originate from two sources: the luminescent species used to perform LDS and the host material. Figure 9 shows a simplified diagram of a planar LDS layer on top of a PV module, highlighting the new optical processes that will be created by the introduction of the LDS layer. These include:

(i) parasitic absorption from the host material;

(ii) emission from the luminescent species at less than unity photo-luminescent quantum yield (PLQY);

(iii) losses through top and side planes of the layer because luminescent light is not emitted towards the underlying solar cell only;

(iv) re-absorption from the luminescent species due to partial overlapping of the absorption and emission bands, where that is the case, which will increase the losses from the top and side planes of the LDS layer; and

(v) higher reflection losses due to the introduction of an additional interface between the LDS layer and the PV device.

A quantitative description of these processes can be found in 2.4.

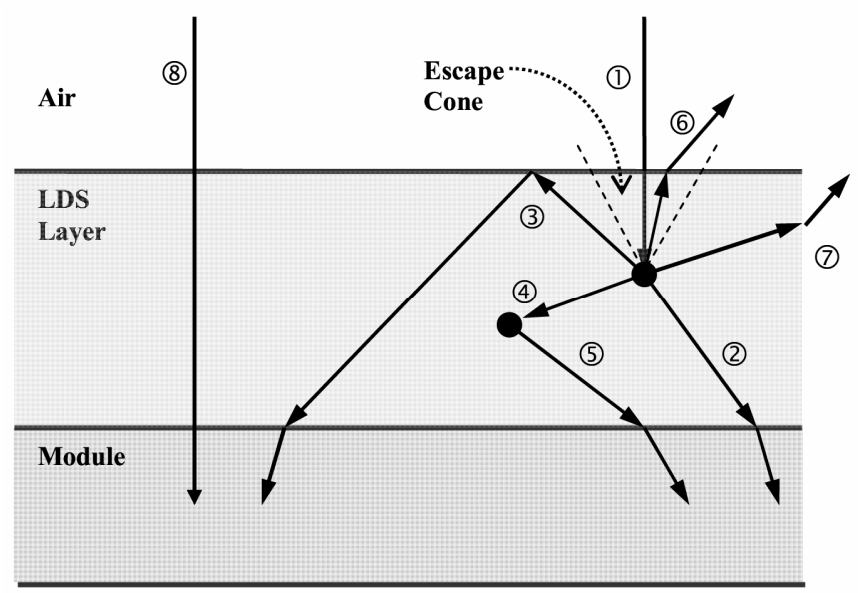

Figure 9: A diagram of a PV module with an LDS layer on top. Light having λ within the absorption band of the luminescent species ① will be absorbed and re-emitted at longer λ. Assuming that the emission is isotropic, the majority of the light will be emitted to the cell, either directly ② , or following internal reflection at air : LDS interface ③, or via re absorption ④ and re-emission ⑤ by another luminescent species. A fraction of the luminescence will be emitted out of the module through the top escape cone ⑥ or through the side of the LDS layer ⑦. Light that is not absorbed by the luminescent species will be transmitted to the cell ⑧. Reflection at the LDS : module interface has been neglected since the refractive indices of these layers are likely to be very similar.

1.6 Ideal Luminescent and Host Materials

Certain highly desirable properties can be identified for the luminescent and host materials to be used for successful LDS, if the list of additional optical loss mechanisms is considered together with the general processing requirements for all materials to be used in PV manufacturing.

An ideal for LDS luminescent species would exhibit unity PLQY, which means that for each photon that is absorbed there is one emitted. It should absorb as much light as possible in the spectral region where the PV device exhibits low SR. This implies the need for a wide absorption band as well as a high absorption coefficient. In addition, an ideal for

LDS luminescent material would emit light with a large Stokes shift and near the peak of the underlying solar cell's EQE. Thus, the absorption and emission bands of the luminescent species would ideally not overlap to avoid re-absorption events that will increase losses due to luminescence outwards the module (top and side plane losses).

The ideal host material must exhibit excellent broadband transmittance and low scattering of light, which are general requirements for any materials to be used in PV devices. It must also provide a suitable environment for the hosting of the luminescent species. In addition, its refractive index (n) must be suitable for minimal reflection losses at the interfaces between the LDS layer and the other layers (above or beneath) of the PV device.

All materials — both luminescent and host — must also be able to endure the treatment that will be subjected during the PV module manufacturing. In addition, they must exhibit prolonged photostability over the extended periods of 20–25 years that the PV manufacturers guarantee a minimum performance for their modules. Finally, the cost should be as low as possible as for all components of a commercial product. The weaknesses of existing materials versus the ideal properties described in this section will be exhibited in more detail in the following chapters, where the experimental application of LDS layers is presented and discussed.

1.7 Outline of This Work

Following this introduction to the concept of LDS and the general context in which this project refers to, the main body of this thesis is separated in six chapters. The overall objective of this work is to investigate how to incorporate the LDS technology into the architecture of a commercial PV module in order to increase its conversion efficiency, using a methodology that is feasible to be applied in practice and in the near future.

A thorough critical literature review is presented in the second chapter of the thesis, which includes all previous experiments on the LDS technology for all known PV technologies to-date. The results of the various works are comparatively evaluated on a PV technology-specific basis. In this way, the absence of a uniform protocol for reporting results in this area, and the consequent difficulties that this creates, are highlighted. Suggestions to the direction of establishing such a uniform protocol are made. In addition, certain experimental conditions, including the importance of the illuminating spectrum and the size

of the under investigation PV devices, are considered. A quantitative analysis on the impact of these conditions to the results of experiments on the LDS technology is presented and discussed. Finally, through this process, strengths and weaknesses of the previous works are identified and the specific methodology that comprises the experimental focus of this work is introduced to the reader.

The materials and methods used in this work are then presented in the third chapter of this thesis. The fourth chapter first reports characterisation results for the poly-(ethylene vinyl acetate) (EVA) encapsulation sheets manufactured for this work and the performance of the chosen luminescent materials in this matrix. Then, the impact of doped EVA sheets onto mc-Si single-cell mini-modules is determined. Suggestions on how to further increase the reported benefit via LDS are made during the discussion of these results. Finally, additional considerations relating to the cost, the photostability and the colouration due to LDS of mc-Si devices are discussed.

The fifth chapter investigates certain suggestions made in the literature and in the fourth chapter about how to further increase the benefit of LDS for mc-Si devices. The concept of mixing multiple luminescent materials in the same layer is focused on. Also, an optimisation study for the concentration of the most promising luminescent candidate materials is presented. Finally, the suitability of a novel organolanthanide complex to perform LDS is investigated, resulting in observations that are interesting to chemists working in this area for future research.

The sixth chapter first reports additional characterisation results on EVA sheets doped with one more luminescent material. The impact of these LDS EVA layers onto thin-film CIGS devices is then investigated. Two different CIGS solar cell configurations are studied in order to exhibit that the EQE profile of the devices is detrimental for the correct choice of the optimal luminescent species. Finally, it is suggested that the successful narrowing of the incident spectrum can afford the reconsideration of certain configurations of CIGS devices, such as the choice of the buffer material and the optimal AR scheme. The seventh and final chapter of this thesis highlights the most important findings and conclusions of the previous chapters. It finally makes specific suggestions for future research on the LDS technology.

CHAPTER 2 – REVIEW OF MATERIALS AND EXPERIMENTS, ANALYSIS AND RECOMMENDATIONS

This chapter reports the outcome of a critical literature review of all previous applications of the LDS technology to PV devices. These are grouped in Tables on a PV-technology specific basis. The impact of certain experimental conditions on the obtained results is highlighted and quantification is carried out for the impact of the size of PV devices and LDS layers as well as for the use of different illuminating spectra. At the end of this chapter, the experimental focus of this thesis is introduced based on the evaluation of the strengths and weaknesses of the previous applications.

This chapter expands on material from the following publication:

E. Klampaftis, D. Ross, K. R. McIntosh and B. S. Richards, Enhancing the performance of solar cells via luminescent down-shifting of the incident spectrum: A review, Solar Energy Materials & Solar Cells 93 (2009) 1182—1194.

2.1 Introduction

Since the first mention of LDS in the literature more than 30 years ago [32], a large number of experiments have been reported for nearly all existing PV technologies. Researchers have used a wide range of luminescent and host materials. They investigated different designs and methodologies to introduce the LDS technology to PV modules. However, certain experimental conditions were not the same between different experiments, thus complicating the comparison of results in different works.

The previous experiments in the literature on the LDS technology are presented and critically discussed in this chapter. A review on the host and luminescent materials that researchers used is first given, highlighting certain aspects of the chosen materials and discussing their suitability for LDS. Certain experimental parameters are focused on to

exhibit the need for a more uniform methodology of presenting results on the LDS technology. The complete list of reported experiments in the literature is then presented. The works are grouped based on the PV technology that was investigated, since the potential for improvement via LDS is dependent on the technology under consideration and its spectral response at short-λ. Concentrator systems are not considered here, as these usually utilise highly sophisticated and efficient cells that allow less space for improvement via LDS. The experimental focus of this thesis is introduced at the end of this chapter by identifying the best opportunity to introduce the concept of LDS to certain in-production PV technologies.

2.2 Host Materials Review

Researchers used a large variety of materials to host the luminescent species. The most frequent types of material were polymers, such as poly-(methyl methacrylate) (PMMA) [30, 39, 40] or poly-(vinyl acetate) (PVA) [41, 42], and inorganic crystalline materials such as aluminium oxide (Al_2O_3) [32] or calcium fluoride (CaF_2) [43]. Other choices in the literature were various types of glass [44-46], organic molecule silicates (ORMOSIL) [47-49] and organic paint thinners [50-52].

Polymeric materials can exhibit high transparency in the visible region of the spectrum, adequate resistance to heat and humidity variations and high mechanical strength [53]. They also provide very good host environment for organic dye molecules [32]. Additionally, the PV industry has a long experience in using polymeric materials, especially in the case of the EVA copolymer, which is the standard encapsulant used for wafer-based Si solar cells [54]. On the other hand, photodegradation under extended UV exposure is a major issue for polymeric materials. Manufacturers are addressing this by utilizing UV stabilisers and absorbers, such as Tinuvin 770 and/or Cyasorb UV 531 [53, 54]. These are molecules that strongly absorb UV photons that would otherwise interact with the polymer, turning their energy into heat. This means that the energy of these photons is wasted from the point of view of electrical power generation. Finally, the cost of polymers is relatively low compared with other available options for the host material.

Inorganic crystalline materials exhibit high transparency for the whole spectrum and long-term photostability [32]. They are, however, expensive and difficult to process, hence, unlikely to be considered as a feasible option on a commercial basis. Glass is already used

as a front cover for most of the commercial PV modules and it fulfills all relevant criteria. It is, however, more expensive and difficult to mix with luminescent materials compared with polymers. ORMOSIL and paint thinners are easier to process with luminescent materials, but they are not readily implantable in an existing production line and are not currently used in any commercial PV product.

2.3 Luminescent Materials Review

The luminescent materials that were investigated for LDS can be separated into three main categories: semiconducting quantum dots (QDs) [45, 55-58], fluorescent organic dyes [24, 30, 39, 40, 50-52, 59-65] and rare-earth-based compounds [41-44, 46-49, 66-68].

QDs are nanosize semiconducting crystals with tunable absorption and emission bands, according to their size. They exhibit a wide absorption band (typically several hundreds of nanometers), high emission intensity and relatively good photostability [58]. On the other hand, they result in high re-absorption losses due to their large overlap of absorption and emission bands [69], exhibit relatively poor PLQY and they remain generally expensive [69].

Organic dyes exhibit relatively high absorption coefficients [64], close to unity PLQY values [70] and are easy to process in polymeric matrices [64, 70]. Their drawbacks are their narrow absorption bands (typically ~100 nm), their relatively small Stokes shift and the partial overlap of their absorption and emission bands, which result in re-absorption events that increase optical losses due to multidirectional emission of luminescence [71]. It has been suggested in the literature [24, 40] and exhibited experimentally in PMMA host [27] that several dyes can be mixed within a single layer in order to broaden their absorption bandwidth and to pursue a greater wavelength shift. Their photostability over prolonged periods of UV exposure remains questionable in most cases, although significant improvements have been reported in recent years and there are already commercially available organic dyes that are photostable for many years [70].

Rare-earth ions exhibit high PLQY values [69, 72], but have extremely low absorption coefficients [72]. The latter can be improved by increasing the doping concentration and/or sample thickness. Also, via the more promising approach of using an organic antenna structure (ligand) with much higher absorption coefficient, which will absorb light and then

transfer the energy to the rare-earth ion for emission [41, 42, 69, 72]. However, this approach usually comes at a cost in terms of overall PLQY, due to losses during the transfer of energy from the ligand to the rare-earth ion [73]. Such compounds are generally referred to as organolanthanide complexes. A qualitative comparative evaluation of the aforementioned types of materials in terms of suitability for LDS is given in Table 2.

Table 2: Comparison of different material options for performing LDS in terms of desirable properties.

Property	Organic dyes	QDs	Organolanthanide complexes
High PLQY	Yes	No*	No*
Broadband absorption	No	Yes	No
Large Stokes shift	No	No	Yes
Long-term photostability	Yes†	No	Unknown‡
Cost	Moderate	High	Unknown‡

* For commercially available materials. †Not all. ‡ For compounds synthesised for LDS applications.

2.4 Additional Optical Losses due to LDS

Parasitic absorption by the host material is one of the additional optical loss mechanisms that the introduction of an LDS layer to a PV module's design will introduce (as described in section 1.4). The magnitude of the absorption losses associated with the host material depends on the material's inherent properties and the thickness of the LDS layer. Given that highly transparent materials are naturally desirable for PV applications, the thickness of the luminescent layer is critical. Thin polymeric films seem to be a good candidate to fulfill all the requirements for successful LDS. For the case of a 1 mm thick sheet of commercially available PMMA, the absorption losses are in the order ≈1 % of the total incident energy, as found in the ray-tracing simulation presented in Tables 3 and 4 (host absorption is not reported in the Tables).

The luminescent species introduces the most significant additional optical losses resulting from the addition of an LDS layer to a PV module. If a non-radiative pathway (either

molecular or ionic) is available for the relaxation of the excited luminescent species, it can result in energy losses expressed in the form of non-unity PLQY value. As discussed in section 1.5, an as high as possible (ideally unity) PLQY value is a necessary requirement for successful LDS.

Mechanisms ⑥ and ⑦ as shown in Figure 9 are additional losses due to isotropic profile of luminescence (although this is not necessarily always the case). However, not all photons emitted towards the top or the sides of the LDS sheet will escape, but only those with an angle of incidence smaller than the critical angle for transmission. The remainder of the photons will be internally reflected with a high probability of eventually reaching the solar cell. The fraction of emitted photons that escape from the top plane for a single absorption-emission event has been predicted from theory to the range of ≈12.5 % for the case of air and a host material with $n = 1.5$ [32, 64]. This figure will be higher for multiple re-absorption events, which can happen when the absorption and emission bands of the luminescent species overlap. This is the case for QDs and organic dyes [69], particularly when high concentrations are used [30]. It has been shown that in practice more that 25 % of the emitted photons will in fact escape from the top surface of a doped polymeric ($n \approx 1.5$) sheet [74].

The losses from the side planes of the LDS layer are commonly not included in calculations and estimations for the overall losses in the literature. This is despite having been identified at least once as the main loss mechanism when small area devices are tested [27], although again, without quantification. Simulations for these losses were performed using the in-house ray-tracer *RAYLENE* (see 3.7 for details). The LDS layer input parameters for these simulations were those of a PMMA sheet doped with a three-dye mixture (BASF Lumogen violet 570, yellow 083 and orange 240) of combined PLQY = 93 % and at concentrations equivalent to an optical density (OD) of 2 for more than half of its absorption band. OD = 2 means that 1 % of the incident light is transmitted through the sheet or otherwise, that 99 % of the light is absorbed (see 3.1.1 for the definition of OD). The results of these simulations are shown in Tables 3 and 4.

Table 3: Side losses dependence on module area for luminescent and non-luminescent sheets. The optical losses are given as percentage of the incident power (0.1 W / cm^2, AM1.5G).

Module area (cm^2)	Side losses	
	OD = 0	OD = 2
1	1.3 %	4.3 %
4	0.7 %	2.6 %
9	0.5 %	1.8 %
16	0.4 %	1.5 %
25	0.3 %	1.2 %
56	0.2 %	0.8 %
100	0.1 %	0.6 %
225	0.1 %	0.5 %

Table 4: Side losses dependence on dimensions of the luminescent layer for constant dye concentration of OD = 2. The optical losses are given as percentage of the incident power (0.1 W / cm^2, AM1.5G).

Thickness	Side losses by module area			
(mm)	1 cm^2	9 cm^2	225 cm^2	7200 cm^2
0.25	0.4 %	0.1 %	0.1 %	0.0 %
0.5	2.6 %	1.0 %	0.3 %	0.1 %
1	4.3 %	1.8 %	0.5 %	0.1 %
2	6.7 %	3.2 %	0.8 %	0.2 %
4	8.9 %	5.1 %	1.5 %	0.3 %

The results of Table 3 show that there are losses from the side planes of the added layer even when that is undoped (OD = 0). The origin of these losses is reflection from the textured surface of the underlying solar cell, since scattering of light in these layers is not simulated in the ray-tracer. The losses from the sides are significantly increased when the luminescent species is added in the layers. The magnitude of the increase is strongly dependent on the dimensions of the LDS layer, as can be seen in Tables 3 and 4. Thin

large-area sheets will lose smaller fraction of photons through the sides comparing with thicker, smaller area ones. This is because, under these circumstances, the emitted photons are more likely to be transmitted towards either the solar cell or out of the sheet through the top plane, than to be incident on the sides at suitable angles for transmission out of the sheet. These losses are a much more important issue when smaller area cells and sheets are used, which however, are the norm in laboratory-scale experiments.

The multi-directional emission profile of luminescence will also result in an altered distribution of the photons' angles of incidence to the interface between LDS layer and module as well as to the already-existing interfaces within the module itself. PV devices are usually characterised using small angles of incidence only [75]. However, larger angles are also present in real applications; especially where tracking of the sun is not applied or under diffuse solar conditions. Multi-directional luminescence will result in a much wider distribution of incident angles. Since reflection is dependent on the angle of incidence and is higher with increasing angle [75], LDS may result in slightly increased reflection losses as well.

If we consider altogether the losses due to the introduction of an LDS layer to a PV module, then the estimates in the literature for the total sum of losses vary from 15–50 % [30, 32, 56]. As previously discussed, the gains from the better response of the PV devices to the modified spectrum must exceed these additional losses in order to justify the introduction of the LDS technology to PV modules.

2.5 The Impact of the Illuminating Spectrum

The spectral energy distribution of the incident light is of paramount importance for the magnitude of gains that are possible to be achieved via LDS. This is simply because higher gains can be made when more photons are available to be down-shifted in the first place. LDS will therefore result in higher performance improvement under blue-weighted spectra. This was first observed in one of the early works on the LDS technology [62], where researchers reported 25 % and 35 % relative efficiency increases using the same solar cells and luminescent sheets, but under different incident spectra. Simulation results indicated that, keeping all other parameters the same, the standard air-mass 1.5 diffuse (AM1.5d) spectrum will result in three times higher relative improvement in comparison to the AM1.5G and four times in comparison to the air-mass 1.5 direct (AM1.5D) [57]. A more

recent experimental study reported results that were 50 % relatively higher when using the extra-terrestrial air-mass zero (AM0) standard spectrum compared to when using the AM1.5G [65]. It must be noted at this point that when speaking about higher relative improvement due to LDS, this refers to the overall conversion efficiency enhancement of PV devices and not their absolute output power. The latter primarily depends on the power density of the incident spectrum.

For laboratory experiments, the relevance of this issue lies in the choice of the spectrum under which measurements are taken. Although the PV community established standard test conditions to report results (see 1.3), this is not always the case with reported experiments on the LDS technology. This is particularly true when referring to early experiments during the 80's and the 90's, but not only. There has been a great disparity in the literature regarding the spectra that various researchers used in their experiments, which complicates the direct comparison of their results.

Simulations were performed using the in-house ray-tracer *RAYLENE* (see 3.7 for details) to demonstrate the effect of different spectra upon two in-production PV technologies: mc-Si and CdTe. CdTe is the PV technology that exhibits the greatest potential for efficiency enhancement via LDS. Hence, the impact of different spectra is more pronounced. The LDS layers were made by PMMA doped with the dye mixtures previously identified via simulations as optimal for mc-Si [24] and CdTe [40] solar cells. The spectra that were studied were those of an unfiltered 1000 W xenon (Xe) arc [76] and a halogen [77] lamps, the extra-terrestrial standard AM0 [78] and the terrestrial AM1.5G and AM1.5d. The AM1.5d spectrum is a component of AM1.5G and is defined via two other standard spectra as: AM1.5d (λ) =AM1.5G (λ) – AM1.5D (λ). It has a higher relative UV and blue content than all the other spectra, which explains the higher experimental results when it is used. The AM0 is second in relative power density in the short-λ region of the spectrum. On the contrary, the spectrum of a Xe arc exhibits a much higher near infra-red (NIR) and lower visible relative content than the rest, due to the NIR spikes of the Xe arc. The AM1.5G and AM0 also exhibit a relatively high NIR content. The halogen lamp has a blue-poor spectrum and emits most of its light in the visible and NIR. The EQE curves of the two solar cells and the spectral irradiance of the various spectra used in these simulations are shown in Figure 10. The relative power contents of the five different spectra for the

regions of 280–300 nm and 280–400 nm are given in Table 5. The results of the simulations are presented in Table 6.

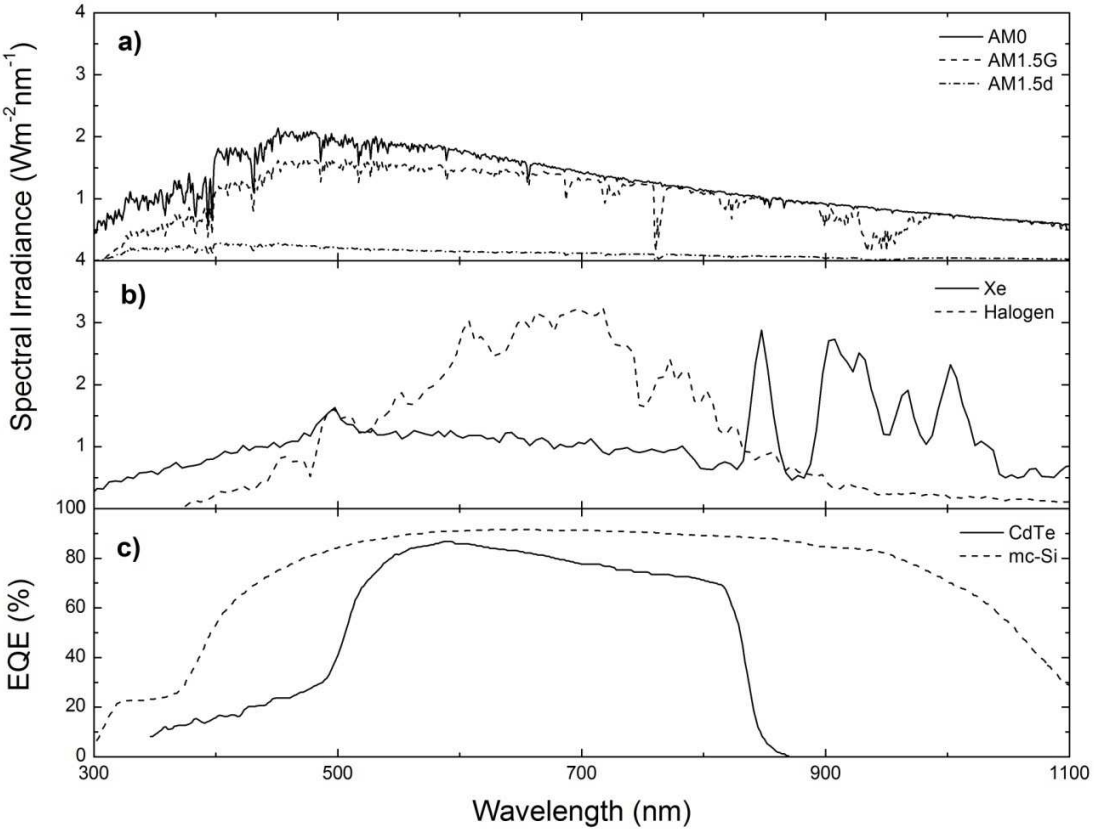

Figure 10: a) The standard spectra under investigation, b) the spectra of the two light sources used in the simulations and c) the EQE curves of the mc-Si and CdTe cells used for the simulations. Data: Xe lamp spectrum [76], Halogen lamp [77], AM1.5G [38], AM0 [78], mc-Si EQE [24] and CdTe EQE [26].

Table 5: The relative power content of five spectra for two spectral regions.

Spectra	Relative power content for 280–400 nm (%)	Relative power content for 280–500 nm (%)
AM0	15.2	29.0
AM1.5G	9.2	23.2
AM1.5d	27.1	48.3
Xe arc	6.7	18.1
Halogen arc	0.5	8.1

Table 6: Simulated efficiencies for the mc-Si and CdTe cells under different incident spectra.

Incident spectrum	mc-Si				CdTe			
	Bare cell η (%)	η: Clear PMMA (%)	η: LDS PMMA (%)	LDS impact (% rel.)	Bare cell η (%)	η: Clear PMMA (%)	η: LDS PMMA (%)	LDS impact (% rel.)
Xe	19.4	20.0	20.2	+ 1.0	8.3	8.2	9.6	+ 17.1
AM0	14.5	15.0	15.2	+ 1.3	8.7	8.7	10.3	+ 18.4
AM1.5G	16.4	16.9	17.0	+ 0.6	10.0	10.0	11.5	+ 15.0
AM1.5d	14.8	15.2	15.9	+ 4.6	10.7	10.3	14.3	+ 39.0
Halogen	20.8	21.0	21.0	0	16.9	16.9	17.5	+ 3.6

The differences in these results highlight the significance of the choice of the illuminating spectra for experiments on the LDS technology. The use of a halogen lamp results in the best absolute efficiencies for both devices, since most of its photon flux is in the visible and NIR regions of the spectrum, where the devices exhibit their peak performance. This is particularly relevant to CdTe devices that operate in the narrow region of 500–850nm.The Xe lamp with the intense spikes in the NIR region of the spectrum results in a very good absolute efficiency for the case of mc-Si, due to the high EQE of this PV technology in this region of the spectrum. On the other hand, the AM0 and AM1.5dif give the lowest efficiency results for the mc-Si device. This is due to the relatively higher UV and blue content of these spectra in combination with the relatively poor EQE of mc-Si cells in this region. The CdTe cell exhibits its lowest absolute efficiency result under the Xe spectrum, due to its poor SR in both the UV and NIR regions, where the Xe spectrum is rich. The impact of LDS in terms of relative efficiency increase is significantly more pronounced for both cells under the blue-weighted spectra AM1.5d. This is in agreement with the theoretical expectation, since there are proportionally more photons to be down-shifted when using this spectrum, as well as with the experimental results obtained with it [57, 62]. The AM0 results in the second best relative cell efficiency improvements via LDS, since it is the second richest spectrum in short-λ photons. Note, that this comparison is based on normalised to one- sun intensity spectra and the results presented refer to relative rather than absolute improvements. Naturally, the AM1.5d spectrum will result in lower absolute

photocurrent, since it has the lowest overall power flux, but it is the spectrum that results in the greatest efficiency improvement due to LDS in relative terms.

The impact that the different spectra have upon the efficiency results of PV devices is not new knowledge for the PV community. However, the results of Table 6 highlight that this impact is far more significant for a technology that concentrates on a narrow region of the illuminating spectrum only. This should always be taken into consideration for the analysis of results on the LDS technology and reports should always refer clearly to the illuminating spectrum. When no particular reason exists for a different choice of the illuminating spectrum, it is desirable to use the standard method of reporting results, as established by the PV community, to afford uniform experimental conditions. Direct comparison of results obtained from different research groups should be made with caution when they have used different spectra.

2.6 Silicon Wafer-Based Devices

The impact of any new concept upon Si wafer-based devices is particularly important for the PV world, since they comprise the vast majority of the global PV cell production since the dawn of the industry with a share of about 87.9 % in 2011 [79]. The term silicon wafer-based devices used here includes the mono- and multi-crystalline as well as the ribbon crystalline silicon technologies, which comprised ~ 30.9 %, 57 % and < 0.1 % of the global PV cell production in 2011 respectively [79]. Representative EQE curves for production-line high efficiency c- Si and screen-printed mc-Si solar cells are shown in Figure 6 (a). These cells exhibit very high EQEs for the most part of the solar spectrum. The mc-Si technology exhibits EQEs higher than 80 % for most of the visible part of the spectrum, whereas the c-Si reaches at 90 % in the same region. The poorer EQEs exhibited by the mc-Si cell at $\lambda < 500$ nm are due to higher reflection and absorption by the AR-coating, which is optimised to perform optimally for longer wavelengths, and high emitter recombination due to its heavy doping. The EQE of mc-Si PV modules drops to almost zero for $\lambda < 400$ nm, where absorption by the glass and the EVA encapsulation material becomes dominant [24]. The c-Si solar cells exhibit a better performance for the region of 400 nm $< \lambda <$ 500 nm. However, their performance at module level is also significantly reduced for $\lambda < 400$ nm, when reflectance from the AR-coating and absorption by the glass and the encapsulant are again increasing. These reasons make mc-Si devices a good

candidate for applying the LDS technology, whereas c-Si devices are not expected to benefit as much. Having said this, the sharp decrease in EQE for $\lambda < 400$ nm justifies investigation of the LDS technology for c-Si devices as well, since there is still a maximum of 1.4 mA / cm^2 to be harnessed in the region of $\lambda < 400$ nm for the AM1.5G spectrum. Table 7 reports the existing short-circuit current density (J_{SC}) content in different bandwidths of the short-λ fraction of the solar spectrum, as calculated from equation (8) (see 3.6) for an ideal solar cell of broadband unity EQE.

Table 7: Existing J_{SC} content in different bandwidths of the short-λ fraction of the solar spectrum.

Start λ (nm)	End λ (nm)	J_{SC} content (mA/cm^2)
300	325	0.1
300	350	0.4
300	375	0.8
300	400	1.4
300	425	2.3
300	450	3.5
300	475	4.9
300	500	6.5

The LDS technology has been investigated for Si wafer-based devices by many research groups the recent three decades. A large number of theoretical calculations and simulation-based estimations as well as experimental attempts to exhibit the potential of the method have been reported. An overview of these works is given in Tables 8 and 9, summarising the overall results and the experimental choices that the various researchers made regarding the luminescent and host materials as well as of the illuminating spectrum. Details for the properties of the materials and the PV devices that were used can be found in the references provided. Table 8 is a summary of works on mc-Si devices and Table 9 on c-Si.

The first comment that can be made from the lot of these works is that there is a great disparity between the final reported results. This is due to both the large variety of materials that have been investigated by the various researchers, as well as the different approaches in where and how to introduce the LDS layer in the architecture of a PV module.

Table 8: Review of reported works on the LDS technology for mc-Si devices.

Luminescent Material	Host Material	Performance Difference	Illuminating Spectrum	Reference
MPI-(503C)	Paint thinner	+29 % ① †	Xe arc lamp	[52]
MPI-(505C and 503C)	Paint thinner	+30% ① † *	Xe arc lamp	[51]
MPI-(505C and 507C)	Paint thinner	+6% ① †	Xe arc lamp	[50]
Acrylite & Sumipex (range of dyes)	PMMA	+3% ① † *	AM1.5G	[39]
Bis-MSB, Stilben 189, Uvitex OB, Lumogen (range of dyes), Coumarin 307, Fluorescence Yellow CRS 040	PMMA	+1.8% ① *	AM1.5G	[30]
Eu^{3+}	Porous glass	-2-3% ①	Undefined	[44]
CdSe QDs	Ideal plastic	+30-40% ②	AM1.5G	[56, 58]
		+10% ④		
		+28.6% ③	AM1.5d	[57]
		+6.3% ③	AM1.5D	
		+9.6% ③	AM1.5G	
Lumogen (570, 083, 240 and 300)	PMMA	+0.3% ③	AM1.5G	[24]
		(+0.8 mA/cm^2) ③		
Lumogen (570, 083 and 300)	PMMA	+0.37 mA/cm^2 ②	AM1.5G	[65]
		+0.56 mA/cm^2 ②	AMO	
		+0.27 mA/cm^2 ②	AM1.5D	
Lumogen (570, 083, 240 and 300)	PMMA	+1.2% in J_{SC} ① *	AM1.5G	[80]
Eu^{3+}	Glass	+2-3% ① *	1 – 5 suns	[46]
Ideal‡	Ideal‡	+0.7% ③	AM1.5G	[81]

① Experimental result, ② Calculated through experimental data, ③ Modeling/simulation, ④ Estimation, † No prior AR-coating, * Best result among a series, ‡ as defined by the authors.

Table 9: Review of reported works on the LDS technology for c-Si devices.

Luminescent Material	Host Material	Performance Difference	Illuminating Spectrum	Reference
Organic dye	Undefined	< 1 mA/cm^2 ③	Undefined	[59]
Cr^{3+}	Al_2O_3	+1-2% ④	AM0	[32]
Eu^{3+}	ORMOSIL	+18% ① † (+7 mA/cm^2)	AM1.5	[47, 48]
Rhodamine (6G), Lumogen (241 & 339)	PMMA	+48% ① † *	Xe arc lamp	[63]
Uvitex OB, Hostasol (8G)	PMMA	+22-27% ① +35% ①	AM1D AM1d	[62]
Silicon nanocrystals	Spin-on glass	+2.5 mA/cm^2 ① † +2 mA/cm^2 ③	Undefined	[45]
Ag	Phosphate glass	+1.6% ① *	AM0	[82]
Large range of laser dyes (not photostable)	EMA, BMA, MMA	+5-20% ①	Specific λ	[64]
Alq_3, TPD, Gaq_2Cl	Alq_3, TPD, Gaq_2Cl	≈+10% ③ † (at λ=530nm)	Xe arc lamp	[83, 84]
Eu^{3+}	PVA	+0.8-1% ①	AM0	[41]
Eu^{3+}	PVA, EVA	+0.5%①, +2.9%①	AM1.5	[42, 68]
Eu^{3+}	SiO_2	+9.5%① *	AM1.5G	[85]
QDs (CdS)	SiO_2	+4% in J_{SC}①	AM1.5G	[86]
QDs (Si)	None	+3.7%*	Undefined	[87]
Eu^{3+}	Acryl resin	+1 mA/cm^2 ①	AM1.5G	[88]
Eu^{3+}	PVA	0.3% ①	AM1.5G	[89]

① Experimental result, ② Calculated through experimental data, ③ Modeling/simulation, ④ Estimation, † No prior AR-coating, * Best result among a series. Acronyms: ethyl methacrylate (EMA), methyl methacrylate (MMA), butyl methacrylate (BMA), Tris (8-hydroxyquinolinato) aluminium (Alq_3), N,N'-diphenyl-N,N'-(3-methylphenyl)-1,1'-biphenyl-4,4'-diamine (TPD), bis-(8-hydroxyquinoline)-chlorogallium (Gaq_2Cl), europium ion (Eu^{3+}) and silicon dioxide (SiO_2).

Many theoretical calculations have been reported, all agreeing on the existing potential of improvement for Si wafer-based PV devices via LDS. To a large degree, the initial analysis of Hovel *et al.* [32] is valid and the basis for all future works. The differences that are found in more recent works originate from the improved properties that more modern materials exhibit. Modelling tools are useful for exploring the wide range of available materials and the configuration of module layers in a fast and simple manner.

The first model in the literature is reported in [45]. This was a simplified model that assumed ideal broadband absorption in the region of 300–500 nm and down-shifting to 680 nm with a PLQY of 100 % in order to determine the modified spectrum. Solar cell parameters were input to an one-dimensional standard tool for predicting crystalline silicon solar cell performance (PC-1D) and the output of a solar cell was determined with and without the LDS layer. This model predicted a maximum possible gain in photocurrent of 2 mA / cm^2 for an one-to-one photon process, which would equate to a 1.2 % absolute efficiency improvement for c-Si devices.

A second modeling tool was developed in [56, 58]. However, this tool investigated the LDS technology under ideal conditions as well and included a large number of implicit assumptions to determine the modified spectrum (PLQY of the luminescent species, profile of its emission spectra, zero re-absorption events, minimum transmission losses, ideal properties of host material, ideal synergistic operation of luminescent species and host material, molar extinction coefficient relationship to particle size). Once the modified spectrum was determined, the authors used standard tools (PC-1D for mc-Si and ASA for a-Si) to evaluate the impact of the LDS layers for mc-Si and a-Si solar cells. However, due to the many assumptions of the method, qualitative results that could not be explained were reached and the authors lowered their quantitative estimations about the possible efficiency enhancement from the most impressive values in Tables 8 and 9 of 30–40 % to a more moderate but arbitrary 10 % for mc-Si solar cells, and no benefit for a-Si.

The third modeling tool in the literature is the in-house ray-tracer already referred to in this thesis, *RAYLENE* (see 3.7 and [24, 40]). Again, this tool makes some implicit assumptions (ideal interfaces and isotropic profile of emission). However, it is using as inputs experimentally obtained values for the properties of the luminescent species (absorption and emission profiles in specific hosts and PLQY) and the devices under investigation,

before calculating its output results through ray tracing and standard optical laws. The qualitative difference of *RAYLENE* compared with the two previous models is that by using experimental data as inputs, it was possible to achieve relatively good agreement between simulation [24] and experimental results [65] on LDS. Finally, recent detailed balance modeling suggested that the theoretical maximum efficiency improvement that can be achieved with the use of an ideal LDS layer in a mc-Si module is 0.7 %, with most of this improvement originating from the re-optimisation of the AR-coating to better match the modified spectrum [81].

In the experimental field, a large range of materials and methods were investigated with a great disparity among the reported results. The absence of a common standard for reporting results on the LDS technology complicates the comparative evaluation of different experiments. This is simply impossible in certain cases, due to lack of knowledge of critical experimental conditions.

Two major sources of complexity in the analysis of reported experimental results are, firstly, the use of different illuminating spectra (see 2.4) and secondly, the use of solar cells equipped with different or at times no AR-coating. A bare silicon wafer will reflect more than 30 % of the incident light if left uncoated [75]. It is for this reason that there is no PV device in a real application without an AR-coating. Several reports of large efficiency improvements via application of LDS layers onto cells not equipped with an AR-coating can be found in the literature [39, 45, 48, 50-52, 63]. In these cases however, the reduction of front surface reflection losses due to the addition of an intermediate refractive index material between air and the silicon wafer, has played a significant part in the reported efficiency improvement [27, 30, 80]. Correct estimation of the impact of LDS to the devices' performance requires the resolution of the two distinct mechanisms that contribute to it. The actual improvement due to LDS only will be significantly less than what was initially reported, if this resolution takes place. When this task was carried out in one of the works in the literature, the initial reported value of 30 % overall relative improvement in cell efficiency compared with an uncoated cell, was revised to a 5 % increase due to LDS alone [51]. The correct resolution of the reduced reflection from the LDS impact is also essential for any considerations regarding the re-optimisation of the AR-coating to better

match the modified spectrum, which is an action that can yield additional gains in terms of overall device efficiency [24, 48, 81, 82].

It is evident from the review of these results that a more standardised protocol for reporting results in the future would make the comparative analysis of the various works simpler. It is most informative for the evaluation of the LDS technology when a result is presented in comparison to a coated device with a non-luminescent layer of the same material. It is in this way only that the impact of LDS alone can be accurately determined. The use of standard spectra would again simplify the analysis of results. However, the exact matching of the incident spectrum is not always possible in different laboratories, since even a solar simulator with a ‘‘class A’’ match to the AM1.5G solar spectrum is allowed a tolerance of ±25 %, while there is no requirement at all for the content in the region of 300-400 nm that is the primary focus of LDS [90]. Reporting the measured spectral distribution of the incident spectrum is one way to overcome these difficulties that complicate the comparative analysis of results.

To evaluate the existing potential of the LDS technologies for Si PV devices, the reported results that included a suitable non-luminescent layer from the same materials as the LDS layer are considered [41, 42, 62, 65, 80, 82, 86]. In all these cases 0.5–3 % relative efficiency improvement was reported. Further gains through re-optimisation of the AR-coating for the modified spectrum have been predicted [24, 82], however, this has not been realised yet experimentally.

There are additional benefits that can be pursued via the introduction of the LDS technology to Si PV modules. UV absorbers and stabilisers are commonly used in Si PV modules to prevent UV-induced photodegradation of the EVA encapsulant [54]. In this way, the energy of these photons are wasted from the point of view of power generation. If long-term photostable luminescent materials are utilised to absorb high energy photons, the protection of the encapsulant can be achieved by converting their energy content to electricity, while eliminating the need to use the UV absorbers and stabilisers. LDS can also reduce the electron-hole pair thermalisation losses occurring in the semiconducting material of Si PV devices when high energy photons are absorbed, since the excess energy of such photons will be partially spent in the process of luminescence before they reach the solar cell. Decoupling thermalisation losses from the solar cells can potentially decrease

slightly their operational temperature, thus, slightly increase their overall performance [91]. Finally, the use of visible emitting luminescent materials can introduce an aesthetical result for PV modules, through emission of luminescence to all directions. This is an important aspect of LDS if emerging markets where colour is a requirement for further deployment of PV products are considered, such as building-integrated PV (BIPV) [92, 93].

The introduction of the LDS technology to Si wafer-based PV devices is possible to be achieved at relatively low cost, which is important for any method with a prospect of commercialisation. The efficiency improvements reported in [62, 65, 80] have been achieved with the use of polymeric host materials and organic dyes, both of which represent the most cost-effective options in their area. An additional challenge in the prospect of commercialisation of the LDS technology is to invent a methodology that can be applied on an industrial scale without adding significant complication in the well established manufacturing process of Si PV modules. To this direction, two distinctive approaches that proposed the use of an existing layer in a Si PV module architecture as the host material for the luminescent species are highlighted. The first is the use of the front glass cover, which is present at the top of a Si PV module to protect the device from environmental factors. This has been realised in practice [44-46, 82] with varying results for the reasons discussed previously. The second is the use as host material the EVA encapsulant, which is already widely used in commercial Si PV modules [54]. This was proposed in [53, 65, 80], but there were no reports of experiments having used the EVA copolymer as host material before the experimental work presented in this thesis. This approach is further discussed in 2.11 and focused on experimentally in chapters 4, 5 and 6.

2.7 GaAs Devices

Some early experiments on the LDS technology were performed using GaAs PV devices, since these devices also exhibit worse EQE for short-λ light (see Figure 6 (a)). The poor short-λ response of GaAs PV devices is primarily because GaAs is a direct bandgap semiconductor, which means that electron–hole pairs are generated by high-energy photons very close to the front surface of the devices, where recombination of charge carriers is fast [94]. In addition to fast surface recombination, short-λ photons are lost due to absorption by the AlGaAs window layer of GaAs devices [32, 94]. These early results on GaAs PV devices were mixed, as can be seen in Table 10. Recent work however, has not focused on

this technology. The enhancement of the short- λ response of GaAs PV devices has come from the development of triple-junction GaAs cells, for which there is very little room for any improvement, given their very good response at short λ [95].

It is worth noting that for the case of GaAs devices used in space applications, it is a standard technique since the1970s to include a 5 % of cerium oxide (ceria) in the front cover glass [96]. Ceria-doped glass exhibits strong absorption in the UV region of sunlight (240—380 nm) and luminescence from the trivalent cerium ion (Ce^{3+}) in the blue (380—500 nm) [97, 98]. The motivation, however, for its inclusion in the special cover glass used for space applications is not driven by any potential for short-λ response enhancement due to LDS, but by the additional protection it affords to the glass and the encapsulation material against the damaging cosmic rays that are present in space [96, 99]. This is a good example of how a luminescent material can be introduced to PV modules based on merits that are not related to the devices' electrical performance. Hence, indicates that LDS can be also considered based on alternative benefits than a potential short-λ response enhancement exclusively.

Table 10: Review of recorded applications of the LDS method for GaAs devices.

Luminescent Material	Host Material	Performance Difference	Illuminating Spectrum	Reference
Roehm-Haas 2154, Coumarin 540, Rhodamine 6G	PMMA	+17% ① *	AM0	[32]
Cr^{3+}	Al_2O_3	+3% ①	AM0	[32]
ZnSe	ZnSe	0% ①	Undefined	[94]

① Experimental result, * Best result among a series. Symbols: chromium ion (Cr^{3+}) and zinc selenide (ZnSe).

2.8 CdTe Devices

Considering the EQE curves presented in Figure 6, CdTe-based devices appear to be the most promising candidate PV technology for achieving significant performance enhancement via LDS. This is mainly because of the sharp cut-off in the EQE curves of CdTe PV devices for λ < 520 nm, which is a result of parasitic absorption by the CdS buffer layer with an energy band gap of ~ 2.4 eV [26]. To improve the response of CdTe devices to short-λ photons, attempts have been made to either reduce the thickness of this

layer, or even completely eliminate it, but these efforts resulted in lower cell efficiencies [100]. Given the relatively low E_g of CdS for high efficiency PV applications, there is clearly potential for significant efficiency gains in the case of CdTe PV devices via LDS.

The summary of works on the LDS technology for CdTe devices is given in Table 11. Comparative analysis of these results is relatively simplified in this case, as all works reported results under the standard AM1.5G spectrum, although data obtained under day-light and white-light spectra were also used in [60, 61]. Also, organic luminescent dyes were the choice of researchers in all works except one, where samarium ions (Sm^{3+}) were added to a potassium magnesium fluoride ($KMgF_3$) crystal [101].

Table 11: Review of recorded applications of the LDS method for CdTe-based devices.

Luminescent Material	Host Material	Performance Difference	Illuminating Spectrum	Reference
Rhodamine (6G)	PMMA	Negative effect ①	AM1.5	[102]
	PVB	+11% ①		
Sm^{3+}	$KMgF_3$ crystal	+5% ①	AM1.5	[101]
MPI- (505M)	paint thinner	+11% ②	AM1.5	[61]
Lumogen (083)	PMMA	+33% ②	AM1.5D	[60]
Lumogen (570 + 083 + 240)	PMMA	+17% ③	AM1.5G	[40]
Lumogen (570 + 083)	PMMA	+1.9 mA/cm^2 ①	AM1.5G	[103]
Lumogen (570 + 083)	PMMA	+9% in J_{SC} ①	AM1.5G	[104]

① Experimental result, ② Calculated through experimental data, ③ Modeling/simulation.
Acronym: poly-(vinyl butyral) (PVB).

The application of LDS layers to CdTe devices has demonstrated that efficiency increases of up to 33 % relative can be achieved for a solar cell that exhibits nearly no response to photons of $\lambda < 510$ nm [60]. The theoretically maximum possible efficiency increase for such a device is in the scale of 40 % relative, assuming the use of a luminescent material with unity PLQY [60]. The review of these results indicates that organic dyes seem a promising candidate to perform LDS for CdTe devices, with the best two results achieved with the use of Lumogen dyes hosted in PMMA [40, 60]. The simulation results of [40] indicate that multiple-dye mixtures can produce better results than a single dye, suggesting

that the cell used in [60] could be improved beyond the reported 33 % relative increase in efficiency. This approach was recently realised experimentally, resulting in a more modest reported efficiency improvements of ~10 % relative [103, 104]. It must be noted however, that it is reasonable to expect more recent studies that utilise modern better performing solar cells to result in lower efficiency improvements than the impressive figures quoted in earlier studies of 2001 [60, 61], given the advances in CdTe devices in recent years.

The most popular choice of materials by the researchers was PMMA host and organic dyes. PVB was also investigated comparatively to PMMA in [102] with the Rhodamine 6G dye being the chosen luminescent species. The PLQY of this dye was found to be significantly higher in the PVB host (90 %) compared with PMMA (40 %), which lead to an efficiency improvement of 11 % relative in the former case and a negative impact in the latter. However, no other experiments have been reported to use Rhodamine dyes since then. Lumogen dyes were the most popular choice of researchers, with no report of adverse effects in PMMA host in terms of optical performance.

While LDS appears very promising to afford a significant efficiency improvement for CdTe-based PV devices, there are three notes of caution. Firstly, the CdS buffer layer in CdTe cells may be negatively affected by the absence of short-λ light, as a result of the light modulated barrier height of the CdS buffer layer [105, 106]. The absence of high-energy photons, which lowers the CdS conduction band height and reduces the barrier for electron transport [107], can potentially result in slightly reduced FF and J_{SC}, and thus efficiency, for cells under LDS layers. This issue, however, does not seem to have inhibited significant efficiency improvements to be achieved for CdTe devices with the use of LDS layers, as can be seen in Table 11. Secondly, modern CdTe PV devices exhibit better performance compared to those used in the first experiments of Table 11 that reported very impressive values of possible improvement [60, 61, 101, 102]. In addition, high-efficiency laboratory-scale CdTe cells exhibit a significantly better response than large-scale production modules in the blue region of the spectrum and these achievements will gradually be passed on to the commercial modules with time. Both these arguments indicate that the true potential for efficiency improvement via LDS is not as high as the highest values of Table 11, although a significant enhancement is still possible. Finally, since the CdS and CdTe layers are commonly grown on a TCO-coated glass superstrate, the

major challenge lies in the approach of where and how to introduce an LDS layer to the architecture of a CdTe PV module. The obvious solution is on top of the glass superstrate, which is what all works reported in Table 11 have done. However, this would mean that the LDS layer would neither be protected from the environment nor would exhibit adequate mechanical resistance in a real application. Hence, an intelligent design that will satisfy these necessary requirements must first be invented in order to consider introducing the LDS technology in a commercial CdTe module.

2.9 a-Si Devices

The review of works on LDS for thin-film a-Si devices is given in Table 12. The majority of the researchers focused their efforts on using rare-earth ions (Eu^{3+} and terbium (Tb^{3+})) to perform LDS, hosted in a wide range of materials. Thin-film a-Si devices were investigated from the first study in the field of LDS by Hovel *et al.*, but no overall efficiency increase was achieved, as the increase of the EQE in the UV region was cancelled out by a decrease in EQE for longer wavelengths [32]. More recent modelling of QDs in an ideal plastic also indicated that there is no potential for efficiency enhancement via LDS for a-Si devices [56, 58], similar to the conclusion of another modeling study for Tb^{3+}-doped glass [108]. In contrast to these studies that did not identify any potential of LDS for a-Si devices, other researchers reported significant improvements [43, 44, 46-48, 66, 67, 108].

Table 12: Review of recorded applications of the LDS method for a-Si devices.

Luminescent Material	Host Material	Performance Difference	Illuminating Spectrum	Reference
Roehm-Haas (2154)	PMMA	0% ①	AM0	[32]
Eu^{2+}	CaF_2 and CaF_2:SrF_2	+50% ① †	AM1.5	[43, 44, 66]
Eu^{3+}, Tb^{3+}	Glass (R7, G9)	+2% ① *	1 – 5 suns	[46]
Eu^{3+}, Tb^{3+}	ORMOSIL	+8% ① *	AM1.5	[47, 48, 67]
QDs	Ideal plastic	No benefit ③	AM1.5G	[56, 58]
Tb^{3+}	Glass	+0.1%	AM1.5	[108]

① Experimental result, ③ Modeling/simulation result, * Best result among a series, † No prior AR-coating.

To understand this qualitative discrepancy of the reported results, normalised EQE curves of the cells used in different studies are plotted in Figure 11. It is shown that the cells used in these studies exhibited a significantly different EQE profile at short-λ, which means that there is different potential for an improvement of performance via LDS. The variance of the EQE profiles is a result of the different properties of the cells. For example, the thin solar cell used by Sark *et al.* [56, 58] will respond better to shorter-λ photons and the potential for improvement via LDS is inhibited. This consideration is a good example of how the EQE profile of different devices is a critical aspect that will define certain choices for the LDS layers and eventually, what one can expect from the introduction of the LDS technology to PV devices. This issue is highlighted in chapter 6, where CIGS solar cells with different EQE profiles due to the different thickness of the CdS buffer layer are studied. The most impressive result of 50 % relative efficiency improvement reported in [44, 66] was achieved in the absence of an AR-coating prior to applying the LDS layers.

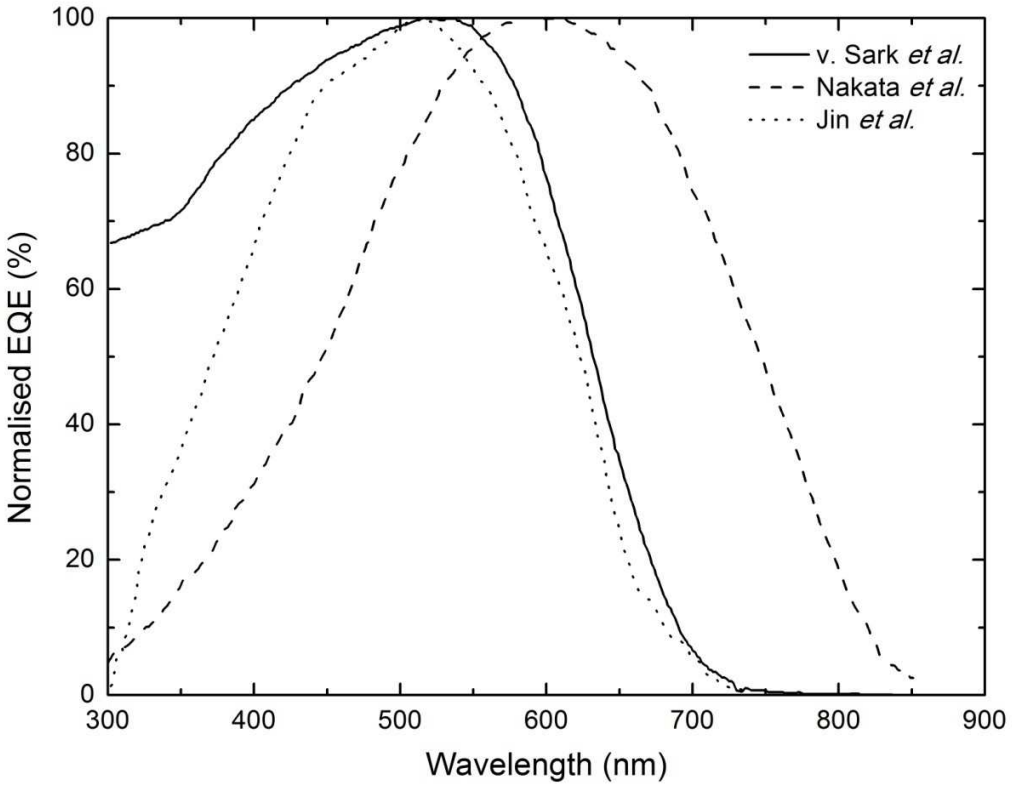

Figure 11: Comparison of different a-Si cells, data from: Jin [47, 48, 67], Nakata [43, 44, 66] and van Sark [56, 58].

2.10 CIGS Devices

CIGS PV devices exhibit poor response to short-λ photons, mainly due to absorption by the TCO window and buffer layers. As in the case of CdTe devices, the most commonly used buffer material is CdS ($E_g \approx 2.4$ eV), which absorbs light of $\lambda < 520$ nm. Zinc oxide (ZnO) ($E_g \approx 3.3$ eV) is the most common material to form the TCO window layer and will strongly absorb photons of $\lambda < 375$nm. A more thorough discussion of the optical losses occurring in CIGS devices can be found in chapter 6, which focuses on this PV technology.

There had been only two experiments reported in the literature for CIGS devices before the work conducted for this thesis. They reported similar final improvements of 4 % [27] and 3% [55], as can be seen in Table 13, even though they used different materials and methods to apply the LDS layers.

Table 13: Review of recorded applications of the LDS method for CIGS devices.

Luminescent Material	Host Material	Performance Difference	Illuminating Spectrum	Reference
Lumogen (570, 083)	PMMA	+0.62 mA/cm^2 ① *	Undefined	[27]
	varnish	+0.75 mA/cm^2 ① ‡ +1 mA/cm^2 ① *		
QDs (CdS nano-particles)	ILGAR-ZnO/$Zn(OH)_2$	+2.8 mA/cm^2 ① † ‡	AM1.5	[55]

① Experimental result, † No prior ARC, ‡ 0.5 cm^2 area solar cells, * 54 cm^2 area mini-modules. Symbol: zinc hydroxide ($Zn(OH)_2$).

Several combinations of host materials, organic dyes, solar cells and mini-modules were investigated in [27]. An important aspect of results on the LDS technology was highlighted. That is the importance of PV device versus LDS layer dimensions. This issue played a significant role in the different improvement achieved by PMMA and varnish hosted dyes, due to the significantly different magnitude of edge losses. A second important note made in the same work was that part of the observed improvement was due to the impact of the LDS layers to the reflection properties of the devices, although the distinction between the two mechanisms of improvement was not accurately determined in all cases, as was also the case in [55]. Resolving the contribution of the two mechanisms is one experimental direction that is focused on in chapter 6. A reduction of plasma

absorption by the ZnO-window due to lower free electrons concentration, thus lower front contact conductivity as well, were also observed in [55]. These effects were due to the deposition process of the LDS layer and resulted to slightly increased EQE for NIR photons, but also to a small increase in series resistance of the device. The impact of both these effects, however, was not accurately quantified and no results were given for a cell coated in a control non-luminescent layer in [55].

One important note to be made for CIGS devices is that they also rely on front-side encapsulation for protection against the environment, often using similar materials and methods as Si-based PV modules. However, no experiment has been recorded in the literature where researchers investigated the opportunity to use the encapsulation layer for hosting the luminescent species.

2.11 Emerging Technologies: DSSCs and Polymer-Based Devices

The work conducted on DSSCs is summarised in Table 14. While initially it might seem unlikely that LDS layers would result in an improvement for DSSCs, given their relatively good EQE at short λ, this is not necessarily the case. Liu *et al.* [109] noted that LDS layers of some form could be used to replace the UV blocking layer that is currently needed for long-term stabilisation of DSSCs, since UV blocking additives and LDS species both target to absorb the high energy photons of the solar spectrum. They showed that while a cell with LDS layer exhibited an 8 % relative lower efficiency than a bare cell, its lifetime was greatly improved and its efficiency was 23 % relatively higher than a cell with a UV blocking layer. However, no improvement at all was observed in the case of the more standard polymeric LDS layer doped with a wide range of organic dyes [30].

There was only one study conducted for OPVs, with a notable improvement achieved [30]. A wide range of organic dyes were tested in PMMA host, as shown in Table 15. Stilben189 resulted in the best result of 2 % relative efficiency increase. A promising research direction would be the investigation of dye mixtures, as suggested for other PV technologies [24, 27, 40]. Another interesting possibility for OPV would be to utilise the front-side encapsulation layer to host the luminescent species, since it is necessary to encapsulate them for protection from the environment.

Table 14: Review of recorded applications of the LDS method for DSSCs.

Luminescent Material	Host Material	Performance Difference	Illuminating Spectrum	Reference
Dy^{3+}	$LaVO_4$	+23% ① * -8% ① ‡	Undefined	[109]
Bis-MSB, Stilben (189), Uvitex OB, Lumogen (range of dyes), Coumarin (307), CRS (040)	PMMA	No benefits ① †	AM1.5G	[30]

① Experimental result, † No prior AR-coating, * compared with a UV blocking-coated device, ‡ compared with a bare cell. Symbols: dysprosium ion (Dy^{+3}) and lanthanum vanadate ($LaVO_4$).

Table 15: Review of reported LDS experiments for polymer-based PV devices.

Luminescent Material	Host Material	Performance Difference	Illuminating Spectrum	Reference
Bis-MSB	PMMA	+0.9% ① †	AM1.5G	[30]
Stilben (189)		+1.9% ① †		
Uvitex OB		+1.2% ① †		
Lumogen F (570)		+1.2% ① †		
Coumarin (307)		+0.7% ① †		
CRS (040)		-4% ① †		
Lumogen F (083)		-5% ① †		
Lumogen F (170)		-28% ① †		

① Experimental result, † No prior AR-coating.

2.12 The Opportunity to Use the Encapsulation Layer as Host

Following the review of the previous applications of the LDS technology to PV devices, an opportunity was identified on how to introduce the technology to commercial PV modules with a production-feasible methodology. This can be achieved by utilising an existing layer of a PV module as host material for the luminescent species. The first direct consequence of this approach is that there will be no added layer(s) to the module's architecture. This is a positive attribute for a mature PV technology with a well established manufacturing methodology, such Si wafer-based modules, since any manufacturer will be skeptical to

introduce radical changes to a production line that produces highly reliable products with long-term performance guarantees. As it was noted in 2.5, researchers have investigated the possibility to utilise the front glass cover of Si PV modules with results shown in Tables 8 and 9. It has also been suggested that the EVA encapsulation layer of these modules could host the luminescent species [53, 65, 80]. However, there had been no experimental works to this direction prior to the work presented in this thesis.

The approach of utilising the EVA encapsulation layer of Si PV modules to host the luminescent species offers certain additional advantages on top of not adding any layer(s) to the module's architecture. Firstly, there is no requirement, in principle, for any modification to the processes involved in module manufacturing, since the doping of the encapsulant can take place independently from device fabrication. From the point of view of a Si PV module manufacturer, the only change would be to order the encapsulation sheet already doped with the luminescent species. The process of doping would be undertaken either by the EVA resin supplier or the sheet manufacturer. In either case, it does not constitute a major challenge, since, as will be described in chapter 3, EVA can be doped without the need of highly sophisticated apparatus and/or methodology, and sheets with uniform thickness can be produced via standard extrusion. This means that the LDS technology could be relatively simply introduced to any existing production line of Si PV modules in the not so distant future.

Secondly, EVA is a well-known and proven material for the PV industry, which fulfills all the criteria that are required for fabrication of highly reliable commercial PV modules. This includes optical performance, mechanical strength, resistance to heat and humidity as well as long-term stability (with the use of suitable UV absorbers and stabilisers, as noted in 2.1). Provided that the doping of EVA does not impair any of these properties, doped EVA encapsulation sheets can be directly implanted to the production of Si PV modules.

Finally, the fact that EVA sheet and PV cell manufacturing do not interfere with each other at all, can afford the optimisation of certain solar cell properties to exhibit higher overall performance under the modified incident spectrum. This would most importantly include the thickness and the refractive index of the AR-coating that commercial devices are commonly equipped with, so that it better performs under the modified, red-shifted spectrum. The impact of this action has at least once been identified as the most significant

implication that LDS can have for Si PV devices [81]. In addition, the absence of short-λ photons, may allow the re-configuration of certain layers for more robust manufacturing, or utilisation of materials that would otherwise waste too much energy contained in UV and blue parts of the spectrum. Such potentially positive modifications in the design of solar cells, which are driven by the red-shift of the incident spectrum via LDS, will be highlighted in the next chapters on a PV technology-specific basis.

The PV technologies of mc-Si and CIGS that both rely on encapsulation for protection from the environment are focused on in the experimental chapters of this thesis, as it is in these cases that the LDS technology can be introduced with the advantages listed here. CdTe devices were not experimentally focused on for the purposes of this thesis, although they are the ones with the best potential for significant efficiency enhancement, since they do not rely on front side encapsulation. An additional motivation however, to investigate at least one thin-film PV technology, that being CIGS, was the possibility to use a light-weight flexible cover material, instead of rigid glass. This direction is becoming increasingly interesting for the thin-film PV industry, since light-weight and flexibility are two properties that can afford niche applications for PV that are not possible to envisage with heavy rigid devices.

CHAPTER 3 – MATERIALS AND METHODS

This chapter presents the materials used in the experiments performed for this thesis, including relative properties and a brief explanation on the motivation of the particular choices. It also describes the methods and the apparatus used to obtain results.

3.1 Luminescent Materials

There were two types of luminescent materials used in the experiments of this work: i) four commercially available visible fluorescent organic dyes; and ii) a novel ligand sensitised complex based on emission from the Eu^{3+}. The motivation for their inclusion in this series of experiments and certain properties of these luminescent materials are given in the 3.1.1 and 3.1.2.

3.1.1 Lumogen organic dyes

Four visible fluorescent organic dyes from the Lumogen-F series by BASF (Germany) were included in the series of experiments presented in this thesis. All four are commercially available and they were chosen based on a series of desirable properties for successful LDS. Other researchers have also identified the potential of these dyes for performing LDS and they have included them in a number of previous experiments on the LDS technology, as shown in chapter 2, although they are currently not in use in any commercial PV application.

The four Lumogen dyes exhibit very high PLQYs in solution and in PMMA [70, 110], which is a fundamental property for successful LDS. They exhibit good solubility in a wide range of organic solvents and polymeric matrices [110], with PMMA described by the manufacturer as the optimal polymeric host material [70]. This is a positive indication for investigating their compatibility with EVA matrix and PLQY results from the literature in PMMA can be used as a good reference for comparison.

Lumogen dyes also exhibit relatively high mass absorptivity (ε) ($dm^3g^{-1}cm^{-1}$), shown in Table 16, which allow high optical densities to be achieved by using relatively low concentrations [111]. The OD is defined for a material as the negative logarithm of its internal transmittance (T) through equation (6), whereas the T is given by equation (7):

$$OD(\lambda) = -\log_{10} T(\lambda) \qquad \text{and} \qquad (6)$$

$$T(\lambda) = \frac{I}{I_0} = 10^{-\varepsilon(\lambda)Lc\rho} \qquad , \qquad (7)$$

where, L is the optical path or thickness for the light (cm), I the transmitted irradiance (W / cm^2), I_0 is the incident irradiance (W / cm^2), c the concentration of the luminescent material (g / Kg) and ρ the density of the host (Kg / dm^3). Additional information about the four chosen Lumogen dyes are given in Table 16, including their abbreviated symbols that will be used in the remainder of this thesis. The molecular absorption and emission profiles of the dyes are plotted in Figure 12 (data taken from [111, 112]), presenting the common feature for organic dyes of the emission band being the mirror image of the absorption.

Table 16: Properties of the Lumogen dyes used in this thesis in PMMA host [70, 110-114].

Dye	Structural type	Density (g/cm^3)	Molecular weight (g/mol)	Peak ab. λ (nm)	$\varepsilon(\lambda)$ ($dm^3g^{-1}cm^{-1}$)	Peak em. λ (nm)
V	Naphthali-mide	1.28	370	375	48.0	434
Y_{083}	Perylene	1.27	503	474	88.8	513
Y_{170}	Perylene	1.31	507	502	88.5	551
O	Perylene	1.36	711	526	118.8	561

Abbreviations: absorption (ab.), emission (em.), violet 570 dye (V), yellow 083 dye (Y_{083}), yellow 170 dye (Y_{170}) and orange 240 dye (O).

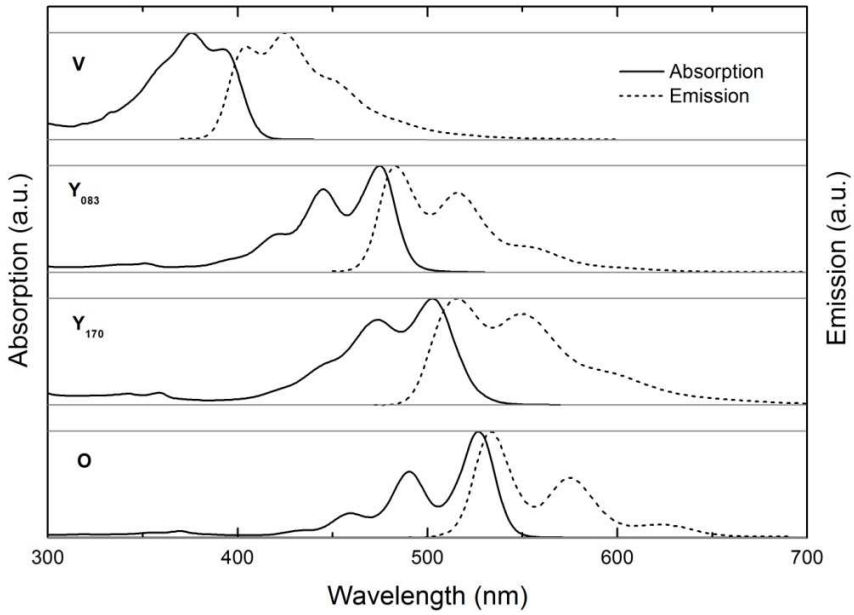

Figure 12: Molecular absorption and emission profiles of the four Lumogen dyes used in this work.

There are two sources of concern regarding the suitability of these dyes for successful LDS. The first is the overlap of their absorption and emission bands, which will result in re-absorption events. If the frequency of these events is high, then the optical losses occurring due to the LDS layer will be significantly higher [74]. This issue is further discussed in 4.3.1. Finally, if attention is paid to the direction of commercial application of the LDS technology, the adequate photostability of LDS layers is a requirement that must be satisfied. The Lumogen dyes exhibit excellent photostability in the absence of very short wavelength photons ($\lambda < 345$ nm) [70]. However, they exhibit much faster degradation under sunlight that contains such photons, with the V exhibiting inferior stability than the other three [110]. Nevertheless, the important question in respect of the LDS technology is not whether the dyes can satisfy the strict requirements for inclusion in PV products, but whether PV products that include the dyes can satisfy the long-term guarantees of 20—25 years that PV modules manufacturers offer to their customers. There is a subtle difference in these two questions, which can potentially result in different answers. The issue of photostability is further discussed in 4.5.

3.1.2 Europium ion based complex

A novel, ligand-sensitised, rare-earth complex that is based on emission from the Eu^{3+} was also included in some of the experiments presented in this thesis. The complex was

synthesized by the group of Prof. Neil Robertson from the department of Chemistry of Edinburgh University [115]. The motivation for including it in this work lies primarily in the near ideal emission profile of the Eu^{3+}, with its main emission peak centered at 614 nm, very close to the peak of most PV technologies' EQE profile. In addition, Eu^{3+}-based complexes exhibit a large Stoke-shift with no overlap between the absorption and emission bands. The latter means that there are no re-absorption events that will increase the optical losses in a LDS layer containing such a complex. For these reasons, the potential of using such complexes for LDS has been acknowledged in the literature in recent years [41, 42, 85, 88, 89].

The disadvantage of the Eu^{3+} as a LDS material for PV applications is that the rare-earth series of ions typically exhibit weak absorption. However, it has been demonstrated in the literature that this can be overcome by coordination to an organic ligand that contains energy harvesting antenna chromophores, which then transfer the energy across to the Eu^{3+} ion [73, 116, 117]. The efficiency of this process must be very high to afford an also very high overall PLQY for the complex, as is necessary for successful LDS. The complex of this type that was included in the experiments presented in this thesis was previously shown to exhibit very high overall PLQY in solution and in PMMA [115]. Its successful inclusion in PMMA matrix was encouraging for investigating the compatibility with other polymeric hosts, including EVA. The use of EVA as host material for the complex can allow the encapsulation of mc-Si solar cells using the complex as LDS material in a standard mc-Si PV module.

3.2 Doping of EVA and Manufacturing of Encapsulation Sheets

The starting material for the manufacturing of the encapsulation sheets of this work were commercially available EVA pellets (Elvax PV 1650, DuPont). Elvax PV 1650 has a vinyl acetate content of 33 % w/w, which is the standard for PV device encapsulation to provide high transmittance of light as well as good adhesion and mechanical properties [54]. Its nominal density is 0.96 g / cm^3 and has a melting point of 61 °C. It must also be noted that the formulation used in this work does not contain any UV-stabilising additives, but only an antioxidant to avoid oxidation during transport and storage. The stabilisation of EVA sheets against prolonged exposure to sunlight is usually performed by the sheet suppliers of

the PV industry. The reader that is interested in more details on the physical and chemical properties of EVA should refer to the very informative review of Czanderna and Pern [54].

There were two different methodologies used for the fabrication of both doped and undoped EVA encapsulation sheets during this work. The first had its focus on feasibility for mass-production and a batch of sheets was produced using standard industrial techniques only. Up to three Lumogen dyes were added in the EVA matrix using a high-shear mechanical mixer with heated rolls. The processing temperature should be greater than the melting point of EVA (61 °C) to aid mixing, but less than 130 °C to avoid premature cross-linking of the copolymer. There are no degradation issues with the Lumogen dyes in this temperature range, as they are suitable for injection-moulding and resistant to at least 300 °C of processing temperature [113, 114]. Encapsulation sheets of 0.5 mm uniform thickness were achieved by standard extrusion. Sheets were left to passively cool down to ambient temperature. This procedure was carried out by BASF and the sheets were provided for application to PV devices. Sheets containing the V, Y_{170}, O and mixtures thereof were produced using this mechanical mixing and extrusion-based methodology. The concentrations used were 0.13 % w/w, 0.07 % w/w and 0.05 % w/w, respectively, in order to achieve an OD of 3 at peak absorption λ of each dye for sheet thickness of 0.5 mm.

An alternative in-house method for producing smaller quantity / area of EVA sheets was developed at later stage of this work. The luminescent materials were first dissolved in toluene (analytical grade 99.98+ % purity, Fischer Scientific). They were then added to EVA pellets also diluted in toluene (~25 % v/v) and heated to a temperature above the EVA softening point (~90 °C). The resulting EVA : luminescent material(s) : toluene mixtures were stirred on a hotplate for 1 h to achieve uniform solution of the luminescent material(s) and to allow partial evaporation of the solvent. Subsequently, the mixtures were poured into a flat container to increase the surface exposed to the environment and placed in a vacuum oven at 60 °C under 0.2 Pa absolute pressure for 3 h in order to extract the solvent residue. Sheets of 0.5 mm uniform thickness were produced with the use of an Al mould between two polished Al plates and a heated hydraulic press. The moulds were pressed under 2×10^9 Pa pressure at plate temperature of 100 °C for 1 min and were then kept under pressure for 1 min more, while actively cooling the plates down to 10 °C.

However, sheets containing the Eu^{3+} complex resulted in significant light scattering, due to its insufficient solubility in toluene. For this material, the solvent was switched to dichloromethane (DCM) and scatter-free EVA sheets were achieved.

Sheets containing the V, the Y_{083}, the Eu^{3+} complex and mixtures thereof were produced using this solution-based methodology. The concentrations used for the V were 0.04 % w/w, 0.13 % w/w, and 0.26 % w/w, leading to design ODs of 1, 3, and 6 at peak absorption λ and sheet thickness of 0.5 mm, respectively. The concentrations for the Y_{083} and the Eu^{3+} complex were 0.07 % w/w and 0.31 % w/w respectively, both leading to OD of 3 at peak absorption λ and sheet thickness of 0.5 mm.

It should be emphasised that reference sheets of undoped EVA were produced with exactly the same methodology as the doped ones for each separate batch of sheets. This is a necessary precaution in order to eliminate any impact to the reported results due to the different processing of different EVA sheet batches. A comparative evaluation of the two different methodologies to manufacture EVA encapsulation sheets is presented in 5.4.

3.3 Characterisation of EVA Sheets and Luminescent Species in EVA Host

The characterisation techniques of the EVA sheets manufactured for this work and the luminescent species in this host included determination of PLQY via emission and transmission measurements, absorption-emission spectroscopy, photoluminescent excitation (PLE) spectra, transmission measurements and polarised light microscopy. The PLQYs of the luminescent materials in EVA were determined via transmission and emission measurements in a spectrofluorometer (Edinburgh Instruments FS920), using the integrating sphere method described in [112, 118]. It should be noted that for the dye mixtures studied in chapters 5 and 6, the PLQY describes the efficiency of multiple luminescent processes that take place in a sheet, with light being absorbed by the externally excited dye only. For such a measurement, a dye must be excited at a wavelength where the absorption of any other dye present in the same sample is insignificant. The uncertainty of all PLQY results presented in this thesis is ±10 % relative, as quoted by the calibration certificate of the instrument. The emission spectra of the luminescent materials in EVA host were also obtained during the PLQY emission measurements. PLE spectra of the luminescent materials in EVA host were also obtained using the spectrofluorometer. Absorption of the luminescent materials in EVA host and transmission measurements were

carried out using a UV / vis / NIR spectrophotometer (Perkin Elmer Lambda 950), with a relative uncertainty of < 0.5 %, as quoted by the calibration certificate of the instrument. Absorption, emission and PLE results for the luminescent materials in EVA host were obtained by using an undoped EVA sample as baseline in these measurements. Polarised microscopy of EVA sheets was carried out using a compound polarised incident-light microscope (Leica DMRX). The sheets were illuminated from the back with linearly polarised light of a halogen lamp and they were observed from the top through a second polariser with variable orientation in the x-y plane. In this way, a so-called bright position can be defined when the axis of the second polariser is parallel to the axis of the first (thus the incident light will be transmitted through the sample and the second polariser). In contrast, a dark position is defined when the second polariser has its axis rotated 90° from that of the first (thus no light is transmitted through the second polariser). Amorphous materials will appear isotropically bright or totally dark in the respective positions, whereas crystalline materials will be anisotropic and will present birefringent patterns. Finally, note that transmission measurements were made through the outer areas of glass : EVA : glass laminates (see 4.2 and Figure 17) rather than through EVA sheets only. This choice was made to avoid the random impact of surface roughness and the resulting haze that the EVA sheets exhibited after manufacture and before lamination to the flat surface of the glass.

3.4 Solar Cells

Production-line screen-printed mc-Si solar cells (E-Ton Solar, Taiwan) were used in the work presented in chapters 4 and 5 of this thesis. Although the commercial standard size of these cells is 155 mm × 155 mm, they were cut into quarters of ~59 cm^2 active area using a high repetition rate neodymium-doped yttrium vanadate ($Nd:YVO_4$) pulsed laser (Newport Spectra-Physics Inazuma) operating at 355 nm.

The CIGS solar cells studied in chapter 6 of this thesis were manufactured at EMPA-Thin Films and PV Laboratory (Swiss Federal Laboratories for Materials Science and Technology). They were manufactured on four soda-lime glass substrates (dimensions 5 cm × 5 cm × 1 mm), coated with 1 μm of direct current-sputtered molybdenum (Mo) back contact. The CIGS absorber layer had a thickness of ~1.7 μm and was deposited using the three stage process of elemental co-evaporation described in [119]. To realize the heterojunction, buffer layers of CdS were applied via chemical bath deposition. For cells

on the first two substrates, the CdS thickness was ~50 nm and for the second ~100 nm. Front contacts consisting of a 50-nm-thick intrinsic (*i*)-ZnO and 270-nm-thick ZnO : Al bi-layer were deposited via radio frequency sputtering. To enhance current collection, a metal grid consisting of 50 nm of nickel (Ni) and 2 μm of Al was finally evaporated on to the samples. Two different grid designs were deposited on each pair of substrates. There were 12 cells on each glass substrate. All cells had an aperture area of 1 cm^2.

3.5 Application of EVA Sheets and Lamination of Solar Cells

The mc-Si solar cells were encapsulated between a symmetrical sandwich of EVA and borosilicate float glass (Schott BF33). Although the PV industry commonly uses white Tedlar backing sheets, glass was utilized here in order to allow for transmission measurements through the final laminates. This type of glass was chosen to maximise the gains from LDS, since it is more transparent to short-λ photons compared with low-iron soda-lime glass that is usually used in commercial Si PV modules [120]. A large-area vacuum laminator (EETS PVLAM 1.0) was used for the encapsulation of the devices using the extruded EVA sheets (chapter 4) and a small-area vacuum laminator (EETS PVLAM 0.25) was used for the remainder of the devices (chapters 5 and 6). Separate control mini-modules using undoped EVA were included in each set of samples that used EVA sheets manufactured with different method. The encapsulation cycle in all cases was 155 °C for 5 min under vacuum and no external pressure and 5 min under vacuum and atmospheric pressure from the top, resulting in bubble-free samples.

EVA sheets were applied onto CIGS solar cells for the initial screen-testing presented in 6.4 using glycerine as optical matching medium. The latter is required for applying EVA sheets onto bare cells to avoid interface reflection losses that will occur if a layer of air is between the EVA sheets and the cells. Glycerine was chosen here because it has a refractive index of 1.47 for visible wavelengths and 25 °C temperature, which is very close to the value for EVA in this spectral region (n_{EVA} = 1.48 for λ = 600 nm [121]), thus, minimising the reflection losses at the interface of the two materials.

Following the initial screening of the available luminescent EVA sheets, CIGS solar cells were encapsulated in the optimal EVA sheets for each CdS thickness and covered by a highly transparent fluorinated ethylene propylene (FEP) sheet of 50 μm thickness and n = 1.34 for visible λ (DuPont [122]). FEP sheets were used here instead of glass so that

LDS could be experimentally pursued for light-weight flexible CIGS devices. In addition, the lower *n* of the FEP material compared with that of glass ($n_{glass} \approx 1.5$) can reduce optical losses occurring at the interfaces of the module shown in Figure 13. Each sample (glass substrate with 12 solar cells) was encapsulated using two pieces of EVA, as shown in Figure 13. A piece of luminescent EVA was used for part of each sample and undoped EVA for the remainder. The interface between the two pieces of EVA, where a partial mixing of the two EVAs would most likely occur during the lamination process, was over the centre of two cells, to ensure that cells further away from the interface were covered by one type of EVA only. The cells under this interface were rejected from the measurements. The separation of samples to two parts was made so that to allow for at least two control cells (encapsulated under undoped EVA) from each sample. The small area vacuum laminator was used for the encapsulation with a cycle of 150 °C for 5 min under vacuum and no external pressure and 4 min under vacuum and atmospheric pressure from the top, resulting in bubble-free samples.

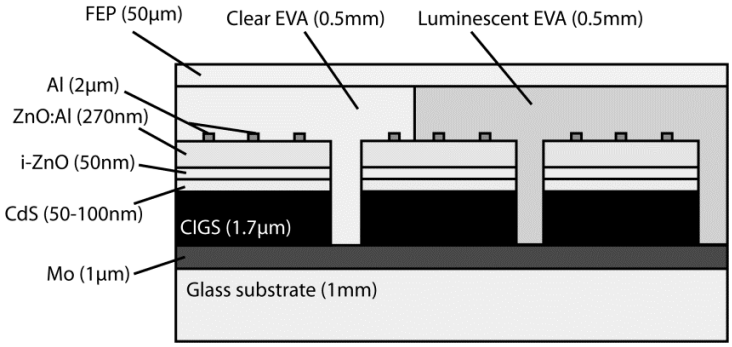

Figure 13: Schematic (not to scale) of a sample encapsulated using doped (luminescent) and undoped (clear) EVA, separating the sample into two parts. Cells located near the interface of the two EVA types were not included for measurements.

3.6 Characterisation of PV Devices

Characterisation of PV devices included EQE and current—voltage (*I*—*V*) curve measurements. EQE curves were obtained using a custom-built monochromator-based SR system (Bentham) under one-sun bias from a halogen lamp (biased area 12.5 cm^2). The monochromatic beam area was 0.4 cm^2 when measuring mc-Si solar cells and 0.1 cm^2 for CIGS. A number of measurements (usually four) were always taken and the results were averaged resulting in a standard deviation (σ) of < 1 % relative in all cases.

I—V curves were measured using a custom-built flash solar simulator (ATS) for the devices using EVA sheets that were produced via mechanical mixing and extrusion and the corresponding cells prior to encapsulation. A continuous solar simulator (ABET Technologies Sun 2000) was used for the devices using EVA sheets produced via solution-based mixing and pressure moulding and the corresponding cells prior to encapsulation. Both set-ups were class A rated for their spectral match to the AM1.5G standard spectrum. However, the continuous system, which was equipped with quartz optics, provided a better match in the region of 300–400 nm. This is of great interest in experiments on LDS, but there are no requirements for matching the standard spectrum in order to achieve the class A rating, as per the International Electrotechnical Commission (IEC) standard 61215 [90]. All devices were masked during *I—V* curve measurements so that only light directly incident to the active area reaches the cells, in accordance with [123]. Light intensity was set to one-sun (1000 W / m^2). For mc-Si devices, the temperature was actively regulated to 25 °C using a temperature-controlled base, whereas in the case of CIGS devices, the temperature was passively monitored using a thermocouple attached to the back of the glass substrate of the cells and measurements were taken at 25 °C. Again, a number of measurements were taken for each sample, with $\sigma < 0.2$ % relative in all sets of data.

In all sets of electrical measurements — both EQE as well as *I—V* curves — the relative uncertainty of the instruments' calibration, as quoted in the calibration certificates from the manufacturers, was higher than the σ between measurements; hence, is quoted as the experimental error of the measurement. For EQE curve measurements, this is ±6 % for the region of 300–370 nm and ±4 % for 370–700 nm, due to the greater uncertainty in calibration for the UV region, and for *I—V* curve measurements < ±2 %.

The J_{SC} of PV devices can be determined directly by the corresponding EQE curve with the use of equation (8):

$$J_{SC} = q \int_{\lambda_1}^{\lambda_2} \varphi(\lambda) EQE(\lambda) d\lambda \qquad (8)$$

where $\varphi(\lambda)$ is the photon flux of the incident spectrum and λ_1 and λ_2 define the region of the spectrum for which the J_{SC} is to be determined. This method for determining the J_{SC} of PV devices is particularly useful and practical when a study is focused on a narrow bandwidth only, as is the case of experiments on the LDS technology. This is because by setting the

desirable values for the λ_1 and λ_2, the spectral region of interest can be focused on, avoiding the impact of photons out of the specified bandwidth.

3.7 *RAYLENE* Ray-Tracing Software

The simulation results already presented in 2.3 and 2.4 as well as those in 4.3.1 were obtained using the in-house Visual Basic-based ray-tracer *RAYLENE*. *RAYLENE* tracks the position, direction, intensity and wavelength of rays as they pass through a PV device and determines the optical losses associated with absorption in all layers and reflection at all interfaces using standard optical laws. It continues to do so until the intensity of each ray decreases below a user-defined limit, which was set in all simulations presented in this thesis at 0.1 %. The incident rays are perpendicular to the front surface of the device and all interfaces are assumed planar, parallel and specular. The LDS species absorbs direct as well as diffuse light and does not exhibit an angular dependence. Emission is modeled as isotropic. In the case of mc-Si solar cells, a broadband reflectance of 5 % is added to the EVA : AR-coating interface to account for reflection from the metal grid. Reflection from the solar cells is modeled as Lambertian.

Input values for the materials and the solar cells can be either drawn from the literature and/or the manufacturers' data sheets, or experimentally determined. For the simulations presented in 2.3 and 2.4, PMMA data were obtained experimentally at the Australian National University from cast sheets made by Rohm and Haas and can be found in [65]; absorption, emission and PLQY data for the Lumogen dyes were taken from the manufacturer's datasheets [37, 110, 113, 114]; and the solar cell characteristics were measured at the Australian National University in the case of mc-Si (BP Solar) and taken from [26] for CdTe. For the simulations presented in 4.3.1, mc-Si solar cell (E-Ton Solar) data were supplied by the manufacturer and confirmed in-house. These are the same data presented for mc-Si solar cells in Chapters 4 and 5 of this thesis. Absorption, emission and PLQY of the Lumogen dyes in EVA were measured in-house as described in 3.3 and presented in Chapter 4; and EVA data were taken from [121].

CHAPTER 4 – IMPROVING THE SHORT-WAVELENGTH RESPONSE OF mc-Si PV MODULES VIA LDS

This chapter first introduces in more detail the motivation to apply the LDS technology to mc-Si devices. It then reports the results of characterisation of EVA sheets doped with a single organic dye. These EVA sheets are used to encapsulate mc-Si solar cells, thus producing single-cell mini-modules. The results of their characterisation are reported and the impact of LDS is determined. Suggestions are made on how to further increase these results. Also, a cost estimate for the introduction of this approach to production is presented. Finally, the aspect of LDS to colour the PV devices is highlighted and the photostability of this design is discussed.

This chapter expands on material from the following publications:

E. Klampaftis and B. S. Richards, Improvement in multi-crystalline silicon solar cell efficiency via addition of luminescent material to ENA encapsulation layer, Progress in Photovoltaics: Research and Applications 19 (3) (2011) 345—351.

E. Klampaftis and B.S. Richards, Improvement in multi-crystalline photovoltaic efficiency using luminescent encapsulation layers, Proceedings of 25th EUPVSEC / 5th World Conference on Photovoltaic Energy Conversion, Valencia, Spain, 2010, pp. 251—254 (Oral Presentation).

4.1 Background

Commercial screen-printed mc-Si PV modules exhibit significantly worse response for UV and blue wavelengths compared with longer-wavelength visible light (see Figure 6 (a)). The most dominant optical loss mechanisms that collectively result in this poor short-λ performance are:

i) Reflection and absorption by the front cover (most commonly glass);
ii) Absorption by the EVA encapsulation material;
iii) Reflection and absorption by the AR-coating (most commonly silicon nitride), which is optimised for longer visible wavelengths; and
iv) High surface recombination velocities in the heavily doped emitter and at the Si : AR-coating interface.

Reflection losses at the glass : EVA interface and from the metallic contact grid have been omitted from this list, because the former are very small due to the very similar refractive indices of glass and EVA, and the latter are broadband.

The conventional way of reducing these losses is to continuously optimise the optical and electronic properties of mc-Si devices using more advanced techniques in manufacturing and/or novel materials when they can afford a performance benefit. However, progress in this field for a mature technology, such as mc-Si PV modules, can be slow; and even when achieved, it can be resource intensive, challenging and costly to implement at production scale.

LDS, using the EVA encapsulation layer to host the luminescent species, is a production-ready alternative approach to improve the poor short-λ response of mc-Si PV modules that requires no modification to their well-established manufacturing process [124]. This approach affords the advantages listed in 2.11, including the no-need to add an additional layer to host the luminescent species, the use of a well-known and proven material for PV applications to act as host for the luminescent species (provided that an adequate compatibility is exhibited) and the possibility to independently re-optimise the solar cells to perform optimally under the modified spectrum.

The potential of LDS to offer short-λ response enhancement to mc-Si PV modules is visualised in Figure 14, where the absorption and emission profiles of an organic fluorescent dye (V) are plotted against the sum of optical losses occurring in a mc-Si module and its consequent EQE profile. If the dye is hosted in the EVA encapsulation layer, LDS will not reduce the losses occurring at the front glass cover. It will, however, have a positive impact on the other three loss mechanisms described previously:

- Absorption by the EVA will be reduced, as short-λ photons will travel shorter distances on average in the copolymer before being absorbed by the luminescent species;
- Absorption and reflection by the AR-coating will also be reduced, since the resulting red-shifted incident spectrum better matches the properties of this layer; and
- Recombination at the front surface of the cell will be reduced because the longer-λ emitted photons are more likely to be absorbed deeper into the device.

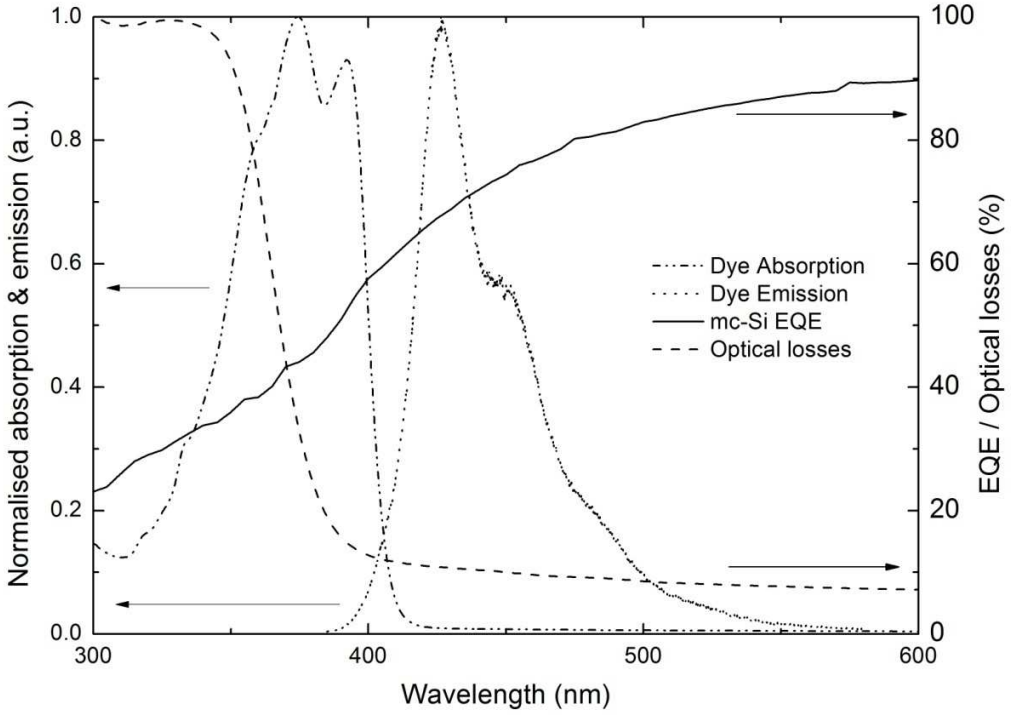

Figure 14: Absorption and emission profiles of a fluorescent dye (V) in EVA, together with the EQE of a standard screen-printed mc-Si mini-module to give the reader an appreciation of the dye activity in relation to the device's spectral response. Also plotted, the optical losses occurring before light reaches the solar cell, due to reflection to the air : glass and glass : EVA interfaces as well as absorption and scattering by the glass and EVA.

Figure 15 shows a cross-section of the upper part of a mc-Si PV module using doped EVA as encapsulant, highlighting the possible optical paths that a photon can follow when travelling through this layer. Some of these constitute new optical loss mechanisms for a mc-Si PV module due to the introduction of the luminescent material in the EVA encapsulation layer. This aspect of the LDS technology was briefly discussed in 1.5 and a

number of loss mechanisms were identified for the generic module design of Figure 9. In the case of mc-Si modules and the approach of doping the encapsulant, the added optical losses are due to multidirectional luminescence and less than unity PLQY. Both these losses will be greater if the absorption and emission bands of the luminescent species overlap, due to the appearance of re-absorption events [74]. In addition, if high doping concentrations are used, luminescence quenching may occur and the potential for performance enhancement will be inhibited. The optical loss mechanisms (iv) and (v) listed in 1.5 are not relative here, since using the EVA layer to host the luminescent species means there is no added layer in the design of the module. The overall impact of the LDS technology to mc-Si PV modules will be determined by the net result in the trade-off between the better response of the solar cell to the modified spectrum and the reduced incident photon-flux due to the added optical losses.

The answers for two principal research questions are experimentally pursued in this chapter. The first is whether Lumogen dyes can be incorporated in the EVA material, while retaining the high PLQY values they exhibit in solution and PMMA, and without impairing the optical performance of the encapsulant. The second is whether such doped EVA layers can enhance the short-λ response and offer an overall efficiency increase for mc-Si PV modules.

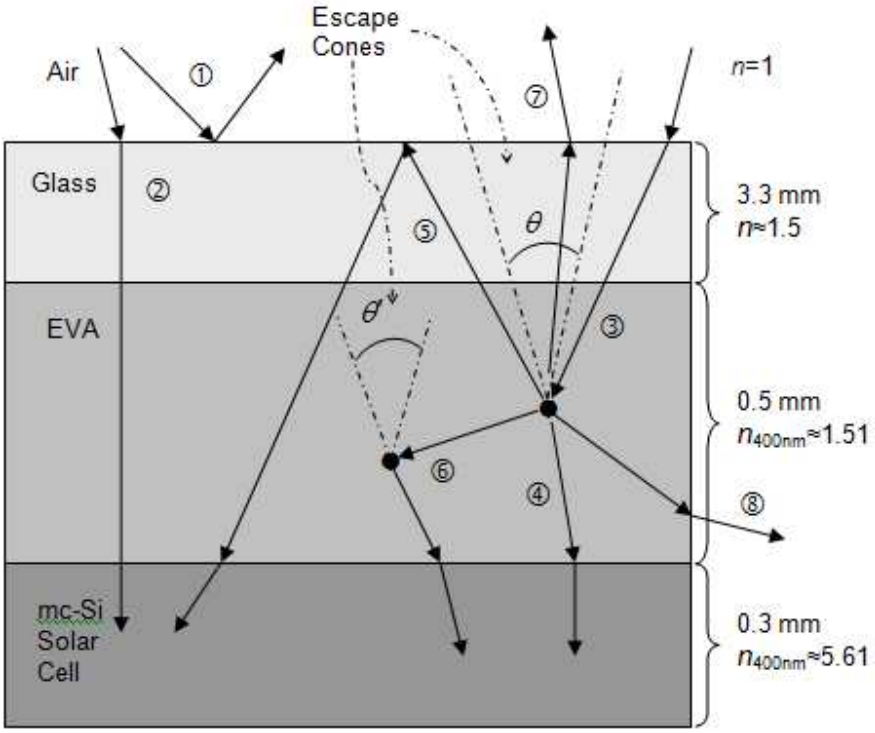

Figure 15: Cross-section of the upper part of a mc-Si (n_{Si} [125]) module encapsulated in doped EVA. The incident light will be partially (4%) reflected by the front glass surface ①. Longer-λ light entering the module is transmitted to the cell without any dye interaction ②, whilst short-λ light (within the absorption band of the luminescent species) will be absorbed ③ and re-emitted at longer λ. The majority of the emitted light will reach the cell, either directly ④, or after internal reflection to the air : module interface ⑤, or via re-absorption and re-emission by another luminescent species ⑥. A smaller proportion of the light will be emitted out of the module through the top plane escape cones ⑦ or through the sides ⑧. Certain optical losses have been omitted for the sake of clarity, including reflection at the glass : EVA and EVA : AR-coating interfaces, as well as absorption in the glass and EVA.

4.2 Characterisation of Luminescent EVA Sheets

The absorption and emission profiles of the dyes in the EVA sheets prepared for this experiment are shown in Figure 16. The emission profiles of the doped EVA sheets are not mirror images of their absorption bands, as is the case for the molecular spectra shown in [111, 112]. This is because the much higher concentrations used here to reach ODs of three at peak absorption λ of each dye nearly eliminated emission within the dyes' absorption bands. The motivation for using such a high doping concentration in this work was that to

perform meaningful LDS, it is desirable to absorb a high fraction of the incoming photons within the absorption band of the luminescent species. This is not the case when fundamentally studying the optical properties of luminescent materials, where it is common practice to use very low concentrations to obtain a good approximation of molecular spectra.

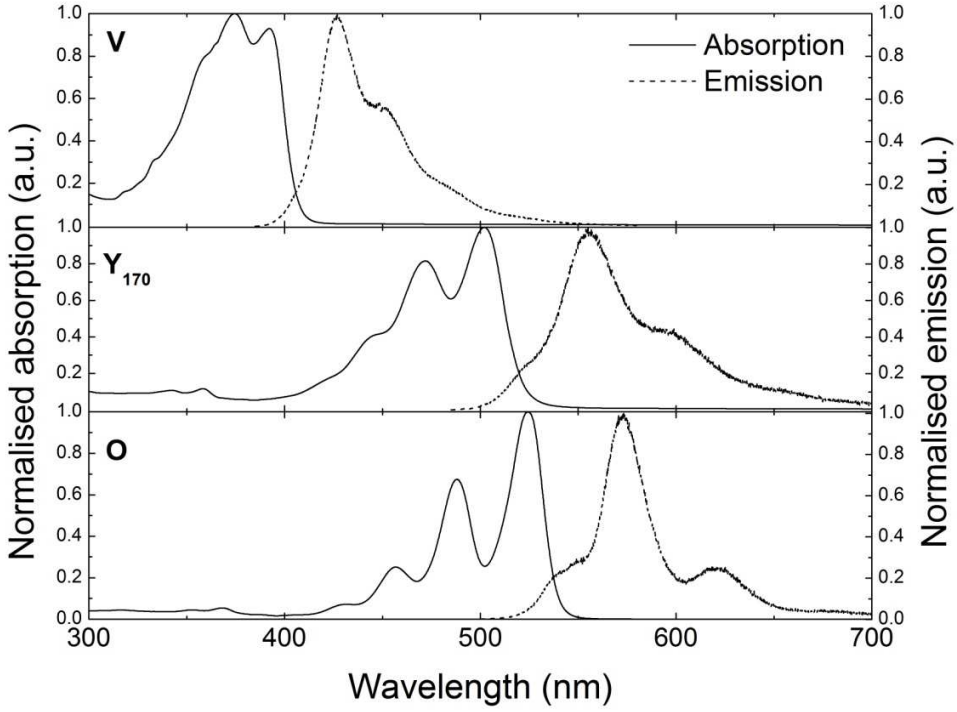

Figure 16: Absorption and emission spectra of the V, Y_{170} and O Lumogen dyes in EVA host.

The PLQY results of the three Lumogen dyes chosen for this experiment in EVA are shown in Table 17. These are very high values indeed and in good agreement with those in PMMA [112], which is quoted by the manufacturer as the optimal host for these dyes [70]. The relative difference in the value for the Y_{170}, although within the error margin for these measurements, is very likely due to the much higher concentration that was used in the EVA sheets. Higher doping concentration results in higher frequency of re-absorption events and for each absorption–emission event, there are additional losses if the actual PLQY is anything less than 100 %. Hence, high doping concentrations will reduce the measured PLQY when the actual PLQY is not exactly 100 % [112]. The measured 100 % PLQYs for the violet and orange dyes in these high concentrations imply that their actual PLQYs are very close to unity [112].

The PLQY of the dyes was calculated for several samples across the doped EVA sheets. The relatively uniform values that were obtained for all samples indicate that the dye molecules are fine dispersed and homogeneously distributed in the EVA matrix. This should result in very low — ideally zero added — scattering of light due to the presence of the dye molecules, which is essential for achieving a net benefit in current generation by the underlying solar cell. This is particularly important when referring to longer wavelengths than the end of each dye's absorption band, where the dyes should ideally have no impact at all. To confirm that no additional scattering of light is introduced due to the presence of the dye molecules, transmission measurements were made through several points of the outer areas of the mini-modules, as shown in the schematic of Figure 17. For clarity, averaged transmission curves are plotted in Figure 17.

Table 17**:** Measured PLQY of the V, Y_{170} and O in EVA and PMMA matrices.

Dye	PLQY (%) in EVA	PLQY (%) in PMMA [112]
V	100±10*	100
Y_{170}	88±9*	98
O	100±10*	100

* Uncertainties are as quoted by the calibration certificate of the instrument.

These results show no significant difference for the region where the dyes do not absorb (described as region 2 in Figure 17). The difference here is confined within the absorption band of the relative dye in each case (region 1 in Figure 17). Hence, the performance of the underlying solar cells is not expected to be affected by the doping of the encapsulant for wavelengths that the dyes do not absorb, and the impact of LDS is anticipated within the regions where each dye absorbs, as is the original intention. Note that transmission through the outer areas of the mini-modules drops to < 1 % for λ < 350 nm even when using undoped EVA. This is due to absorption from the two pieces of glass and the thick EVA layer that has filled that area with total thicknesses of 6.6 mm and 1.2 mm respectively. This is an experimental weakness if trying to measure how much light will arrive to the front surface of a solar cell in a standard PV module where only one piece of glass and a thinner EVA layer (thicknesses of 3.3 mm and 0.5 mm respectively) would precede the solar cell. This is particularly so for very short-λ photons with λ < 370 nm where EVA absorption is very strong. However, this is not a major issue for the purpose of

investigating the impact of the EVA doping to the visible and NIR regions of the solar spectrum, which was the purpose of these measurements.

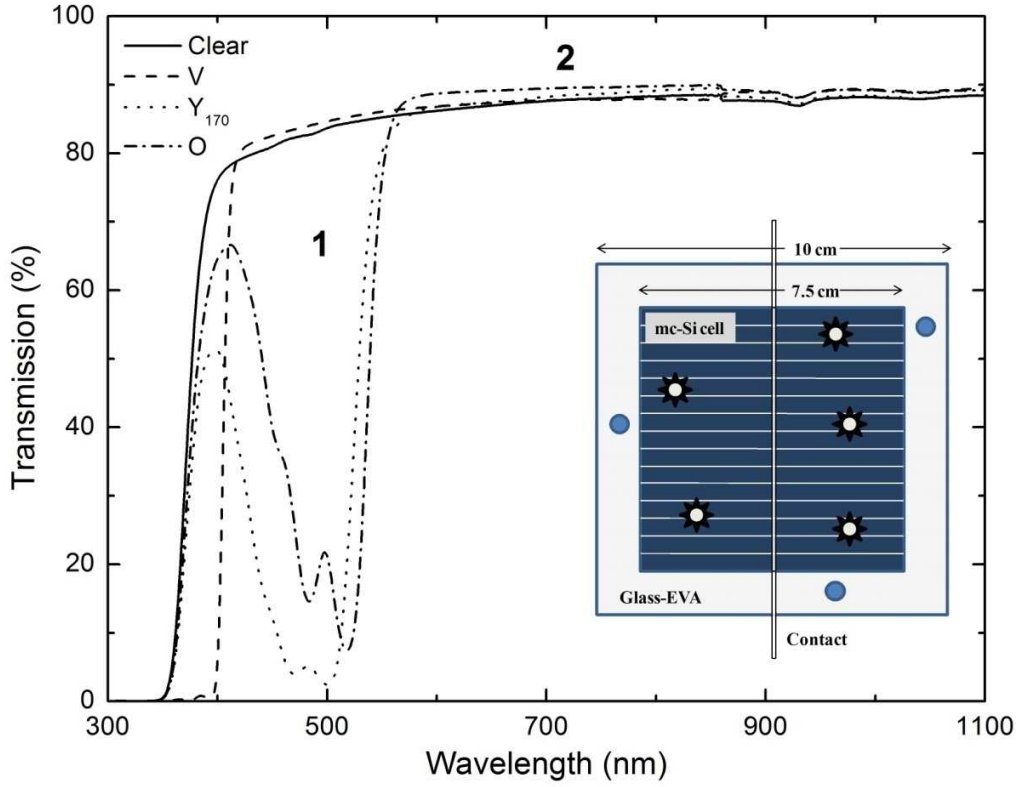

Figure 17: Averaged transmission curves through the outer areas of the mini-modules at three different points for each sample. Note that these measurements refer to transmission through two pieces of cover glass and a layer of EVA with total thicknesses of 6.6 mm and 1.2 mm respectively. In the inset, a schematic of a mc-Si mini-module prepared for this work, where the approximate positions of EQE (with bias light not shown here) and transmission measurements are shown.

4.3 Impact of LDS to mc-Si PV Devices

The impact of LDS to mc-Si PV devices was assessed by comparing the EQE curves of single-cell mini-modules using luminescent EVA encapsulation to a control device encapsulated in standard undoped EVA. Several measurements were made onto various random points of the devices (as shown in the schematic of Figure 17 and with bias light not shown in the schematic) to account for the non-uniform nature of the multi-crystalline material and any localised discrepancies this could introduce. The variation between results for the same mini-module was in all cases less than 4 % absolute for a certain

wavelength. For clarity, averaged EQE curves for each sample are shown in Figure 18. Five EQE curves for the devices encapsulated in violet-doped and undoped EVA are shown in Figure 19 (see paragraph 4.3.1) to exhibit the influence of the multi-crystalline material on the EQE curves of the devices.

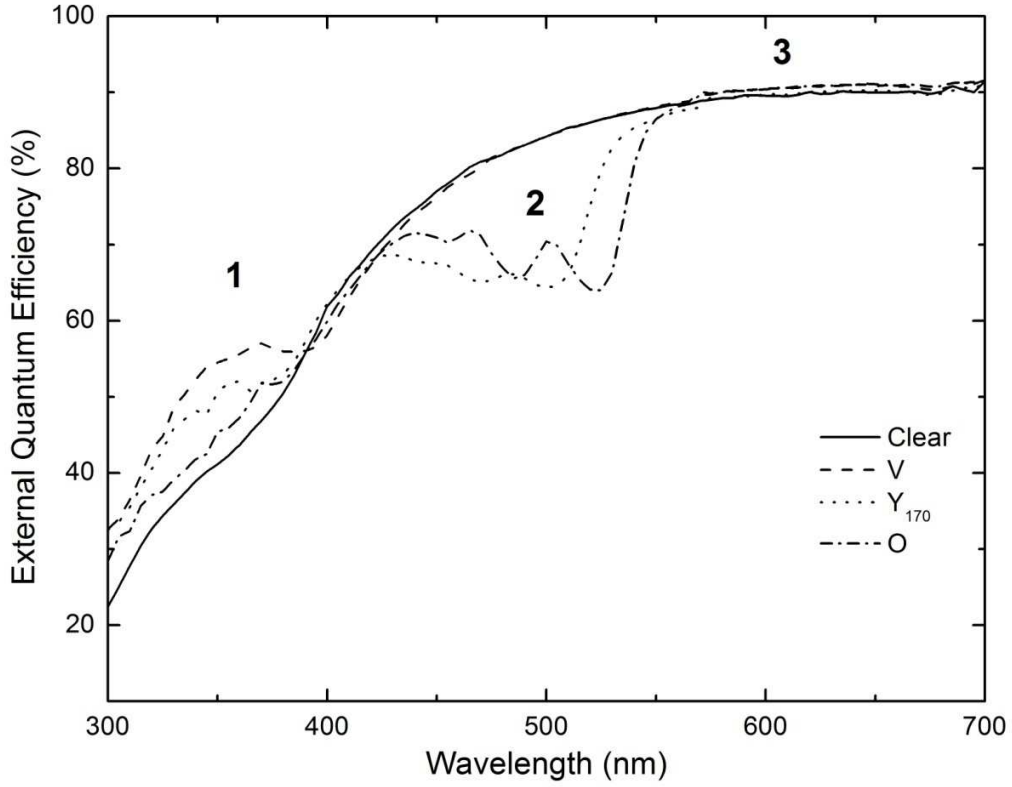

Figure 18: EQE curves for the four mc-Si mini-modules to exhibit the impact of LDS on the spectral response of the devices.

The dye activity has a clear visible impact on the EQE profile of each device for the regions where the dyes absorb light (highlighted as regions 1 and 2 in Figure 18). Where the dye absorption ends in each case, the EQE curve of the corresponding sample lies on top of that of the control sample encapsulated in undoped EVA (region 3 in Figure 18). All three mini-modules using doped EVA exhibit higher EQE than the control device for $\lambda < 400$ nm (region 1 in Figure 18). Naturally, the increase in EQE in this region is higher when the dye's absorption is stronger. Hence, the Y_{170} results in higher improvement than the O, and the V higher than both. The V-doped-EVA mini-module exhibits an increase of 10–20% in EQE in the range of 300–400 nm, achieving a net benefit in the optical trade-off discussed earlier for this region.

Figure 18 also shows, however, that only the EQE curve of the V-doped EVA mini-module overlaps with the EQE curve of the control device for $\lambda > 400$ nm. The devices with the Y_{170}- and O-doped EVA sheets exhibit a decrease in EQE for the region of $400 \text{ nm} < \lambda < 550 \text{ nm}$ (region 2 in Figure 18). Although these two dyes emit light at wavelengths near the peak of the mc-Si solar cells' EQE curves, the overall trade-off with the added optical losses due to LDS is negative for this region. This is because a mc-Si solar cell exhibits already very high EQE for these wavelengths (> 65 %) for LDS to afford an improvement. Note, that the photon flux of sunlight is significantly higher in the region of $400 \text{ nm} < \lambda < 550$ nm compared with the $300 \text{ nm} < \lambda < 400$ nm, which means that the Y_{170} and O will overall reduce the photocurrent of the corresponding devices.

The electrical performance of the mc-Si devices was determined via *I—V* curve measurements. These results are given in Table 18. Note that LDS is not expected to have a significant impact to the V_{OC} and FF of the devices, since it does not change anything to their electronic and/or electrical properties. However, a change in J_{SC} will have a small impact to the V_{OC} of a PV device, which can be calculated via the equation (2) (see 1.3). The V_{OC} is expected to increase by ~1 mV in the case of the two devices that exhibited an increase in J_{SC} of > 1 mA / cm^2, and to have a non-significant change for the other two due to the small change in their J_{SC}. The results shown in Table 18 are in very close agreement to these expectations. However, in the case of the devices' FF there is a consistent small drop of 2.1—3.6 % for all four samples post lamination (and this is also the case for the samples presented later in 5.2 and Table 23). This behavior is not attributed to LDS, but to a small increase in series resistance that has most likely occurred at the points where the contact wiring was soldered onto the cells, due to manual handling and possibly stress during lamination. This discrepancy will introduce a small systematic error in the calculations regarding the efficiency of encapsulated devices.

To determine the impact of LDS, the J_{SC} and η results for the mini-modules are compared to the values for the corresponding cells prior to encapsulation, rather than directly to each other. This approach is followed here to avoid the error that would be introduced in a direct comparison due to the slightly different initial performance of the cells, which is in the order of the impact of LDS. The benefit directly attributed to the LDS is calculated by the difference between the values for the same device prior and post lamination, assuming an

equal impact of encapsulation to the reflection profiles of all devices. The results are given in Table 19.

Table 18: Electrical performance of mc-Si devices based on *I—V* curve measurements.

EVA Type	Bare cell				Encapsulated mini-module			
	J_{SC} (mA/cm^2)	V_{OC} (V)	FF (%)	η (% ab.)	J_{SC} (mA/cm^2)	V_{OC} (V)	FF (%)	η (% ab.)
Clear	32.6	0.607	75.5	14.9	33.8	0.609	73.0	15
V	32.5	0.607	76.5	15.1	33.9	0.609	74.4	15.4
Y_{170}	32.4	0.607	75.4	14.8	32.6	0.607	73.0	14.4
O	32.3	0.607	76.6	15.0	32.2	0.607	73.0	14.3

Table 19: The overall impact of encapsulation and that of LDS to mc-Si devices.

EVA Type	Overall encapsulation impact		LDS impact	
	ΔJ_{SC} (mA/cm^2)	$\Delta\eta$ (%)	ΔJ_{SC} (mA/cm^2)	$\Delta\eta$ (%)
Clear	+1.2	+0.1	n/a	n/a
V	+1.4	+0.3	+0.2	+0.2
Y_{170}	+0.2	-0.4	-1.0	-0.5
O	-0.1	-0.7	-1.3	-0.8

These results show that there is an increase in J_{SC} when going from a bare cell to an encapsulated mini-module, which is 1.2 mA / cm^2 for the undoped-EVA encapsulated mini-module. This is a result of the trade-off between improved coupling of light into the cell, due to the introduction of two $n \approx 1.5$ layers between air and AR-coated cell, and the parasitic absorption resulting from the glass and the EVA. This trade-off will be very similar for all devices irrespectively of the EVA doping, thus, the assumption of equal encapsulation impact to the reflection profiles of the devices is not expected to introduce a significant error to what is attributed to LDS. For the violet-doped EVA mini-module, an increase in J_{SC} of 0.2 mA / cm^2 is directly attributed to LDS, which translates to an absolute efficiency enhancement of 0.2 %. The other two dyes, however, have a negative impact on the performance of the devices, reducing their ΔJ_{SC} by 0.4 and 0.7 mA / cm^2 respectively. This is due to the decrease in EQE in the region of 400 nm < λ < 550 nm, which has a greater impact in the overall J_{SC} of a PV device than the gains for λ < 400 nm, due to the

higher photon flux of sunlight in the former case. The Y_{170}- and O-doped EVA encapsulation results in an efficiency loss for these devices, of 0.5 % and 0.8 % respectively.

The performance enhancement when using the V may be further increased if certain optimisation techniques are realized for the LDS layer. There are more photons in the region of 300–400 nm to be absorbed. This can be achieved by further increasing the dye concentration or by broadening the absorption bandwidth of the LDS layer. Furthermore, higher gains can be achieved if a luminescent species with larger Stokes shift is utilised, since it will emit at longer more favourable wavelengths than the violet dye. Better separation of the absorption and emission bands of the luminescent species can also offer a benefit, since there will be no re-absorption events and the losses from luminescence outwards the PV module through the top and side planes will be reduced. To these directions, suitable dye mixtures can be used as well as inorganic luminescent materials and organo-lanthanide complexes. Finally, controlling the direction of emission, which is a technique that has been applied for the technology of LSCs [126, 127], can potentially offer a reduction of the losses due to luminescence through the top and side planes of the module.

Some further gains can be pursued by modifying the solar cell itself to perform optimally under the modified incident spectrum. For example, the optimisation of the AR-coating for mc-Si modules equipped with a LDS layer does not need to take into consideration reflection losses for short-λ photons, since they will be down-shifted to longer wavelengths. Thus, the thickness and refractive index of the AR-coating can be slightly modified to afford a further efficiency increase of ~0.2 % [24, 81]. Also, the absence of UV light arriving at the cell will reduce the recombination losses at the heavily doped emitter of a mc-Si solar cell, since lower energy photons will be absorbed deeper into the device. This may allow slightly higher doping levels for the emitter, which can lead to a more robust manufacturing process of mc-Si PV modules [24]. Finally, it has to be noted that the down-shifting of high energy photons may result in slightly higher field performance of mc-Si PV modules, due to a likely reduction of lattice thermalisation for the semi-conducting material of the devices. This is because the excess energy of the down-shifted short-λ photons will be partially spent during the luminescence process, which occurs

outside the solar cell. Preliminary results for two mini-modules with a thermocouple embedded at the back of the cells indicate a different profile of device temperature increase under continuous illumination. However, no conclusive results were possible to be included in this thesis on this matter, which remains for the present an open research direction for future experimentation.

The Y_{170} and O do not exhibit suitable absorption-emission profiles to offer an overall efficiency enhancement to mc-Si PV modules. This is due to absorption extending to wavelengths where the devices exhibit a relatively high response, as discussed previously, and despite their emission profiles being almost ideal within a range where mc-Si PV devices exhibit peak response. The latter can be exploited by mixing these two dyes with the violet (or another luminescent material) that will absorb shorter wavelength photons than they do and will emit within their absorption band. In this case, the wavelength shift that the violet dye can offer alone can be increased through cascade absorption–emission events, whilst a broader overall absorption band can be also achieved. This direction was indeed experimentally pursued and the results are presented in 5.2.

4.3.1 Focus on the violet dye

The mini-modules using undoped and V-doped EVA are focused on in Figure 19, to exhibit the influence of the multi-crystalline material in EQE measurements. Data for $\lambda > 360$ nm are plotted in the inset for the cells prior to encapsulation. They are included here to exhibit the very similar initial performance of these two solar cells. It can be seen in Figure 19 that the multi-crystalline material introduces a small variation in EQE curves as measured across the length or width of a device; however, this variation does not exceed the mark of 4% for any given wavelength.

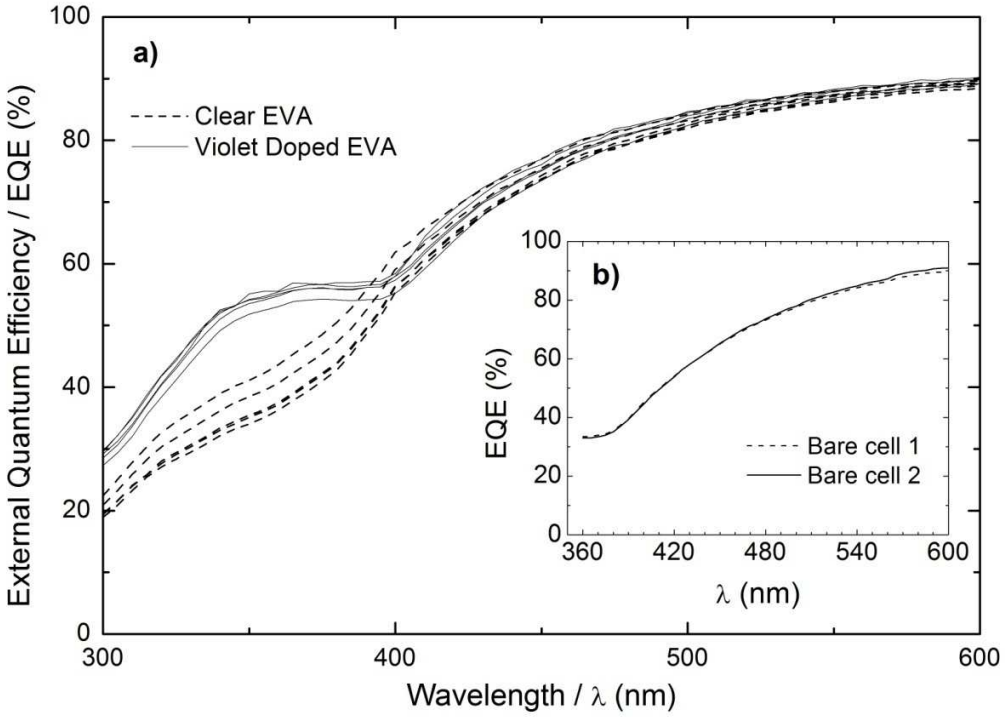

Figure 19: Five EQE curves for two mc-Si mini-modules encapsulated in violet-doped and undoped EVA respectively to exhibit the variation between EQE measurements due to the nature of the multi-crystalline material. The inset shows data for the same solar cells prior to encapsulation.

To better understand the new optical losses that are introduced in a mc-Si PV module due to the introduction of the luminescent material in the encapsulation layer, ray-tracing simulations were made using *RAYLENE*. Simulations were made for three concentrations of the V in order to investigate the impact of increasing concentration and to estimate an optimum value for future experimentation. The results of these simulations are given in Table 20.

Absorption by the front glass is expected to increase slightly with the introduction of the dye and with increasing concentration, due to luminescence emitted through the top plane escape cone of the module (see Figure 15). Absorption by the EVA is expected to decrease significantly, as short-λ photons travel less distance on average in the EVA before they are absorbed by the dye and then emitted at longer wavelengths where EVA absorption is weaker. Losses through the top and side planes are present for the undoped-EVA encapsulated mini-module as well, due to reflection from the textured surface of the cell. They will increase significantly upon introduction of the dye and with increasing dye

concentration in this range. Note that the side losses are strongly dependent on the module's dimensions and are higher for smaller dimensions, as discussed in 2.3. The top and side plane losses will not increase greatly due to the overlap of the absorption and emission bands and the consequent re-absorption events, since the frequency of these events for this sheet thickness and range of concentrations is low (< 1) (the first absorption event in the results of Table 20 does not count as re-absorption event). Overall, the sum of the optical losses for the doped EVA with dye concentration leading to OD = 3 is 0.2 % of the incident power lower than when using the undoped EVA, which translates to an increase in J_{SC} of 0.04 mA / cm^2. These simulations show very little difference for this range of concentrations and this do not allow a confident prediction of the optimal value. This issue is experimentally investigated in 5.3.

Table 20: Ray-tracing predicted breakdown of the LDS effect in the optical losses occurring in the mc-Si module shown in Figure 15. Reflection at the front glass surface and glass : EVA interface are omitted because the refractive indices of the two layers are not affected from the doping of EVA. Losses are shown as percentages of the incident power (0.1 W/cm^2, AM1.5G).

EVA Type	OD (-)	Glass ab. (%)	EVA ab. (%)	Top plane Em. (%)	Side planes Em. (%)	No of dye absorption interactions
Clear	n/a	10.8	4.2	3.7	2.2	n/a
V	1	11.0	3.4	3.9	2.7	1.22
V	3	11.0	2.8	4.0	2.9	1.31
V	6	11.1	2.5	4.0	3.0	1.39

Abbreviations: absorption (ab.) and emission (em.)

4.3.2 Cost estimate

A cost estimate was first made for the transfer of the LDS technology to production in 2010. The quantity of dye needed to achieve specific OD can be calculated from equations (6) and (7) (see 3.1.1). To manufacture a 1 m^2 EVA sheet of 0.5 mm thickness doped with the violet dye at concentration that leads to OD = 3 at peak absorption λ (375 nm), approximately 625 mg of dye are required. Lumogen dyes were commercially available in bulk quantities at about €7000 – 9000 / kg [128]. Thus, the additional cost of materials for a 1 m^2 active area module is ≈ €5. This is very small in comparison to the factory-gate

price of ≈ €360 / m^2 in 2008 for European manufacturers of mc-Si PV modules [129]. The reported efficiency improvement of 1.3 % relative was very similar to the increase in the cost of the module due to the cost of the dye, thus, there was no impact to the price of power generation (≈ €2.4 / watt-peak (W_p) in Europe for 2008 [129]). This analysis assumes no added cost for the doping of the encapsulant, which is a process that can be undertaken by an EVA sheet supplier with no major hurdles.

However, the factory-gate price of mc-Si PV modules in 2011 was nearly half of that in 2008 [130] and the cost of dyes had dropped by a factor of 10—20 % [131]. If these most recent costs are taken into consideration, then a small increase in the range of ~1 % in cost of power generation will result from the introduction of this LDS layer to a commercial mc-Si PV module. It has to be noted here that prices continue to rapidly decrease in these fields in recent years, thus any attempt to accurately determine the cost of introducing LDS to commercial mc-Si modules will be quickly outdated. What can be said as a qualitative conclusion that will stand for the foreseeable future is that he cost of dyes will always be a small fraction of the overall cost to manufacture a mc-Si module. This was 1.4 % in 2008 and increased to 2.2 % in 2011 with half the price of a commercial mc-Si module. It cannot become a much more significant fraction even if commercial modules continue to become much cheaper to manufacture if we also consider that the cost of the dye will continue to decrease with time as well. Hence, the overall conclusion is that to introduce this LDS layer to a commercial PV module will add a small cost to power generation. Here, small is defined as few percentage units in the range of 1–3 %.

4.4 Colouration of Devices due to LDS

An interesting effect of the LDS process, which is not related to electrical performance, is that it results in colouration of mc-Si PV devices that utilise doped EVA. The dyes used in this work absorb short-λ photons and emit light of visible λ at all directions. This has been already described previously as top and side plane losses, which reduce the J_{SC} gains that can be achieved via LDS. However, this lost luminescence introduces an aesthetical result, which can be exploited for PV applications where colour is a desirable property.

A good example is the emerging market of BIPV, where colour is one of the main requests to the PV industry from architects [92, 93]. The usually black or dark blue colour of high efficient PV devices does not encourage their further uptake for architectural purposes. The

colour of mc-Si PV modules can be changed by modifying the thickness of their AR-coating [132]. However, this comes with a significant reduction to their efficiencies of up to 4.6 % absolute in the worst case scenario of green finish [133], which will raise the cost of solar power in BIPV applications and increase the pay-back times. The glass-to-glass mini-modules that were fabricated for this work exhibited either a small increase in overall efficiency or a decrease of < 1 % absolute, even in the worst case scenario of orange colour. The measured efficiencies of differently coloured PV devices due to the two different methodologies to achieve the aesthetical result (LDS and modification of AR-coating) are given in Table 21. The colourful mc-Si mini-modules that were manufactured for this work can be seen in Figure 20.

Table 21: A comparison of efficiencies for PV devices exhibiting different colours due to either LDS or modification of the AR-coating thickness.

Colour	LDS mini-module η (%)	Modified AR-coating thickness solar cell η (%) [133]
Reference (clear EVA) / Black (highest efficiency)	15	15
Violet / dark blue	15.4	14.7
Yellow / Gold	14.4	12.9
— / Green	—	10.4
Orange / —	14.3	—

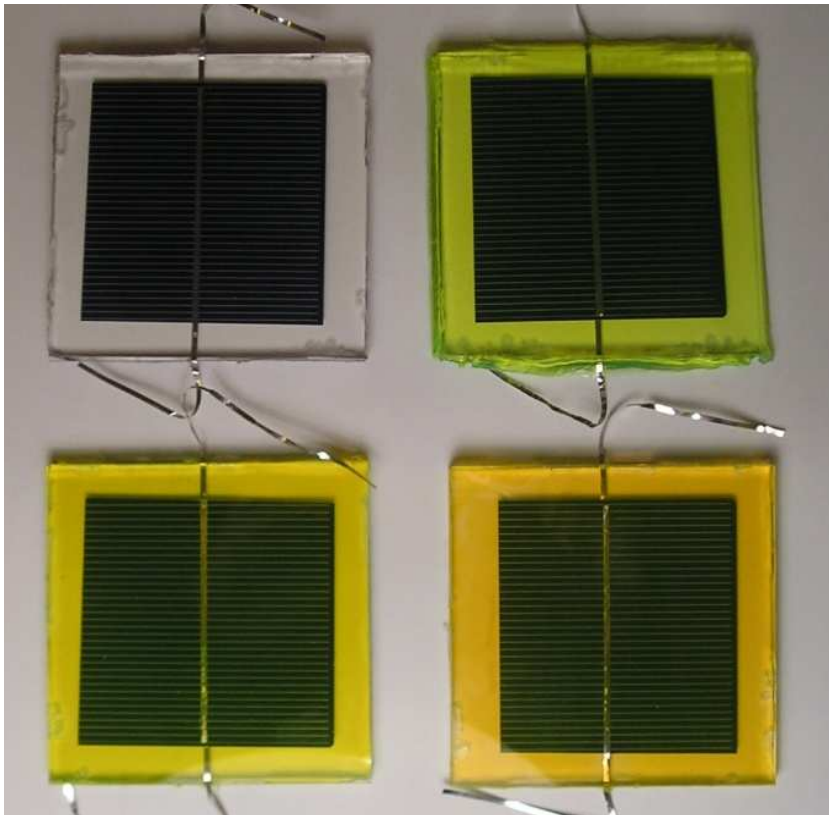

Figure 20: Coloured mc-Si mini-modules due to multi-directional luminescence.

4.5 Photostability Considerations

One important factor that must be also considered is the photostability of the doped EVA encapsulant. Manufacturers of mc-Si PV modules typically guarantee a minimum performance of their products over an extended period of 20—25 years and any change in their products must comply with this strict requirement.

EVA exhibits inherently inadequate photostability upon exposure to UV light [54]. The requirement for the 20—25 years guarantee is satisfied only by inclusion of suitable UV-absorbing and stabilising additives that protect the copolymer. The Lumogen dyes exhibit long-term stability in an ideal host matrix and are described by the manufacturer as suitable for PV applications, although they were also reported to photodegrade under irradiation with photons of $\lambda < 345$ nm [70]. The V in particular has been shown to exhibit up to 50 % reduced emission after exposure to sunlight for $\approx$ 2 years in experiments with a PMMA host [134] and is characterised by the manufacturer as less stable than the other Lumogen dyes [110]. However, it is has been also reported in the literature that the observed photodegradation of Lumogen dyes in polymeric matrices is strongly dependent on the

matrix itself as well as on impurities and additives present in the usually PMMA host, such as residue monomer and initiator [70, 134-136].

The important question that must be answered experimentally for the doped EVA encapsulation sheets presented here is not whether the copolymer and/or the dyes exhibit adequate photostability as separate components. It is whether a mc-Si PV module encapsulated in doped EVA can satisfy the long-term stability requirements. All the aforementioned studies focusing on the performance of Lumogen dyes refer to the LSC technology, hence, to direct exposure of doped PMMA to either sunlight or simulated UV test conditions. In the case of the suggested module design using doped EVA encapsulant, this layer is beneath the glass cover of a mc-Si PV module, and the glass will strongly absorb light of $\lambda < 340$ nm [24]. The cover glass and the UV-absorbing additives that must be included in the EVA for stabilisation will afford additional UV protection for the module. However, there has been no study to-date to determine the lifetime of either EVA sheets doped with these dyes, or of a PV module using this encapsulant. This research direction is an on-going effort of the author's research group. Finally, it must be noted that the purpose of the work presented in this thesis is not to support that the materials that were used are the absolute best candidates to perform LDS. The intention is to demonstrate that efficiency gains can be achieved via LDS, using the existing encapsulation layer of mc-Si PV modules so that it is not required to add a new layer to mc-Si PV modules. This is an approach that can be readily reproduced for a wide range of encapsulation and luminescent materials, if novel or existing ones are shown to afford higher efficiency gains and/or better photostability than EVA and Lumogen dyes.

CHAPTER 5 – OPTIMISATION OF LDS EVA SHEETS FOR mc-Si PV DEVICES

This chapter builds on the previous findings for mc-Si devices and investigates certain suggestions made in order to further increase the impact of LDS for mc-Si devices. EVA sheets doped with organic dye mixtures are characterised. Two different methods to manufacture LDS EVA sheets are also compared. An optimisation study for the concentration of the most promising luminescent species is performed. Finally, the suitability of an organolanthanide complex to perform LDS is investigated.

This chapter expands on material from the following publications:

E. Klampaftis, M. Congiu, N. Robertson and B.S. Richards, Luminescent Ethylene Vinyl Acetate Encapsulation Layers for Enhancing the Short Wavelength Spectral Response and Efficiency of Silicon Photovoltaic Modules, IEEE Journal of Photovoltaics 1(1) (2011) 29—36.

E. Klampaftis and B. S. Richards, Optimisation of luminescent EVA encapsulation layers for silicon PV modules, Proceedings of 26th EUPVSEC, Hamburg, Germany, 2011, pp. 517—521.

E. Klampaftis, D. Ross, S. Seyrling, J. Perrenoud, A. N. Tiwari and B. S. Richards, Luminescent down-shifting for improving the efficiency of photovoltaic modules, Proceedings of PV-SAT-7, Edinburgh, UK, 2011, pp. 5—8.

5.1 Background

The results presented in the previous chapter showed that it is possible to achieve a short-λ performance enhancement for mc-Si PV modules via LDS, with the violet dye leading to an overall efficiency improvement. The next research question that is the core of this chapter

is whether these results can be further improved. Certain suggestions towards this direction that were made in the literature and the previous chapter, including mixing luminescent materials in the same layer, optimising the concentration of the luminescent species and investigating a novel organolanthanide complex, were pursued experimentally.

The use of LDS layers doped with suitable dye mixtures is one way to possibly increase the efficiency gains that can be achieved via LDS. The first consequence of using multiple dyes in the same sheet is that the overall absorption bandwidth will be broadened, since the absorption bands of different dyes are centered to different wavelength ranges. The second consequence is that longer wavelength shifts can in principle be achieved with suitable choice of dyes. For the simplest case of a sheet doped with only two dyes, this is possible if the absorption band of the second (second meaning that it absorbs longer wavelength photons than the first) overlaps with the emission band of the first. This can lead to cascade absorption-emission events, since photons emitted by the first dye are likely to be absorbed by the second before exiting the sheet, and will then be re-emitted at even longer wavelengths. However, it must be noted that the top and side plane losses will increase for each additional absorption event, similarly to what has been discussed for the case of re-absorption events by the same dye. There is no apparent reason to limit the number of dyes that can be used in the same sheet, other than the necessary requirement to not impair the transmittance of the encapsulant for wavelengths that the dyes do not absorb. However, if multiple dyes are to be used in the same sheet, it is the overall PLQY of all the luminescent processes that must be considered for photons involved in more than one absorption events. If there is no non-radiative pathway for the transfer of energy from one dye to another, the overall PLQY for multiple absorption events by several dyes will be the product of the PLQY values of the individual dyes involved. This means that the already highly desirable property of high PLQY for the luminescent materials to be used for LDS becomes increasingly important when multiple dyes are used. EVA sheets doped with two and three Lumogen dyes were experimentally tested for their performance and impact onto mc-Si PV mini-modules.

Another approach to increase the gains via LDS is to optimise the concentration of the V, which was shown in the previous chapter to offer a positive overall result. This was experimentally investigated for three different concentrations leading to nominal ODs of 1,

3 and 6. Given that EVA sheets for this experiment were manufactured using a different methodology than the ones used in the previous experiments (see 3.2 for details of both methods), a comparative evaluation of the two methodologies was performed using EVA sheets of the same type.

Finally, the compatibility of the novel Eu^{3+} complex described in 3.1.2 was investigated in terms of compatibility to be hosted in EVA matrix and applicability to perform LDS for mc-Si PV devices. The potential to mix the Eu^{3+} complex with the V in the same sheet was also investigated, since these two materials combined can result in broadband UV absorption.

5.2 EVA Sheets Doped with Dye Mixtures and Impact on mc-Si PV Devices

The PLQY results for EVA sheets doped with two- and three-dye mixtures are given in Table 22. Rows 2 and 3 show the PLQY values when directly exciting the V only, whereas rows 4 and 5 when directly exciting the Y_{170} only. Note that it was not possible to excite the O only in these sheets, since its absorption band overlaps for the most part with that of the Y_{170}. These PLQY results show that the dyes retain their high PLQY values when present in mixtures, with values very similar to those in single-dye-doped EVA sheets. The Y_{170} exhibits the same (within the experimental error) value when measured alone and when in mixture with the V. The PLQY results that refer to cascade absorption-emission events (rows 2 and 3 by directly exciting the V and measuring emission from the Y_{170} and O respectively, as well as row 5 by exciting the Y_{170} and measuring emission from the O) are equal with good approximation to the products of the PLQYs of the individual dyes involved in each case. This indicates the absence of a non-radiative pathway for the transfer of energy from one dye to another, unless this transfer has a near unity efficiency like the radiative process. In that is the case, it is not a matter of concern.

Table 22: Measured PLQYs for dyes in two- and three-dye mixtures in EVA host. All dye concentrations corresponded to nominal OD = 3.

Luminescent species	Dye excited	Excitation λ (nm)	PLQY (%)
VY_{170}	V	375	94
$VY_{170}O$	V	375	91
VY_{170}	Y_{170}	460	89
$VY_{170}O$	Y_{170}	420	90

The absorption and emission profiles of the dyes in two- and three-dye doped EVA sheets are plotted in Figure 21, together with those of the three individual dye-doped EVA sheets shown in Figure 16 for comparison. In this case absorption has not been normalised to show the experimental versus the design OD for these sheets.

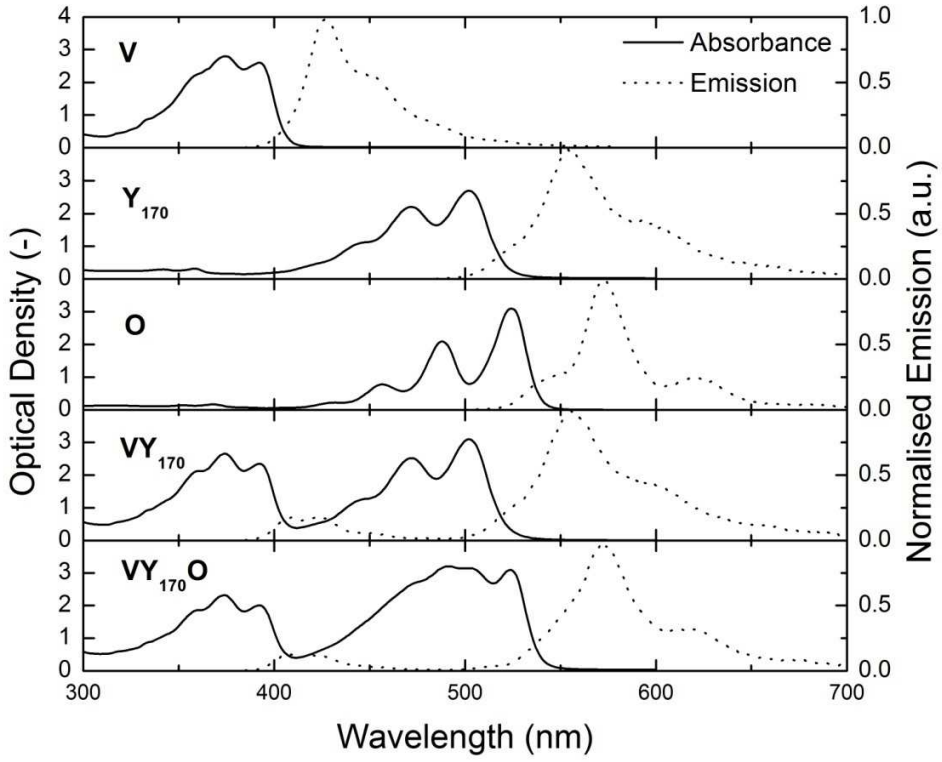

Figure 21: Measured ODs and normalised emission spectra for the doped EVA sheets. The concentrations of the dyes corresponded to nominal OD of three in all cases.

These results show that the absorption bandwidth has been successfully broadened with the use of more than one dye in one sheet. In addition, they show that the predicted cascade absorption by the longer-λ absorbing dye(s) has indeed taken place and emission from the shorter-λ emitting dye(s) has been nearly eliminated. Given that this process happens with the high efficiencies of Table 22, it is expected that the two- and three-dye doped EVA sheets will result in a higher short-λ response enhancement compared to single-dye-doped EVA sheets.

The last remaining consideration regarding the optical performance of these sheets is their transmittance. These results are shown in Figure 22, again together with the control and the single-dye-doped EVA sheets for comparison. As concluded in the previous chapter, the

inclusion of the dyes in the EVA encapsulant does not impair the performance of the encapsulant for wavelengths out of the dyes' absorption bands and thus, it is not expected to have any impact to the performance of the underlying solar cells. This is now shown to be true for the case of dye mixtures as well.

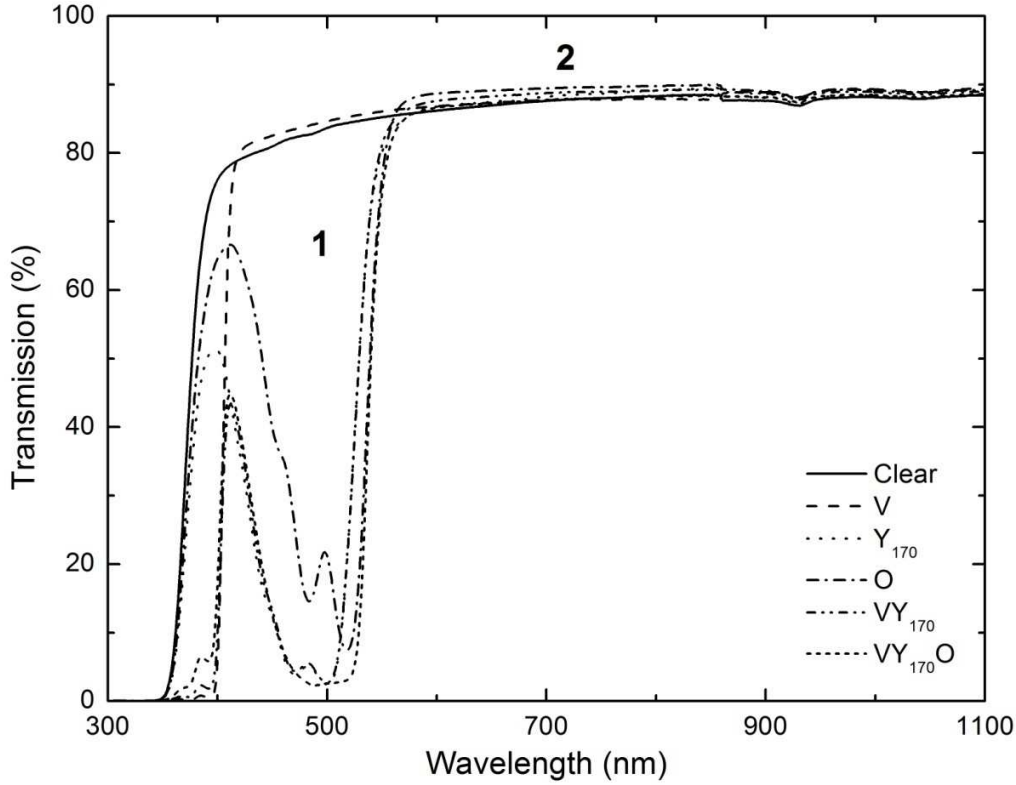

Figure 22: Transmission results through the outer areas of the mc-Si mini-modules. Note that these measurements refer to transmission through two pieces of cover glass and a layer of EVA with total thicknesses of 6.6 mm and 1.2 mm respectively.

The impact of these EVA sheets to the performance of mc-Si mini-modules was assessed via EQE curve measurements, shown in Figure 23. The corresponding curves for the mini-modules using the single-dye doped sheets are also included in Figure 23 for comparison. In all cases, the dye activity has a clear impact on the EQE profile of the mc-Si devices for the region where the dyes are active in each case. For the samples using the dye mixtures, the impact is strong for the whole UV and blue regions of the spectrum, since their absorption bands is broader compared with single dyes. The EQE curve of each sample lies on top of that of the control when the dye absorption ends. The mini-modules using dye mixtures exhibit a greater EQE increase for $\lambda < 400$ nm compared to single dyes. This is

because of light absorbed by the V being emitted at longer wavelengths by the Y_{170} and O, following the previously described cascade absorption-emission events, where it is more favorably converted into electron-hole pairs by the underlying mc-Si solar cell. The EQE increase is significantly higher for the sample using the three-dye mixture, since the wavelength shift is maximised. The EQE increase is up to 20 % compared to the control sample in this case. However, both samples using the two- and three-dye mixtures have a negative impact in the region of 400 nm < λ < 550 nm, due to the Y_{170} and O absorbing light that was already very efficiently utilised by the solar cells (EQE > 65 %).

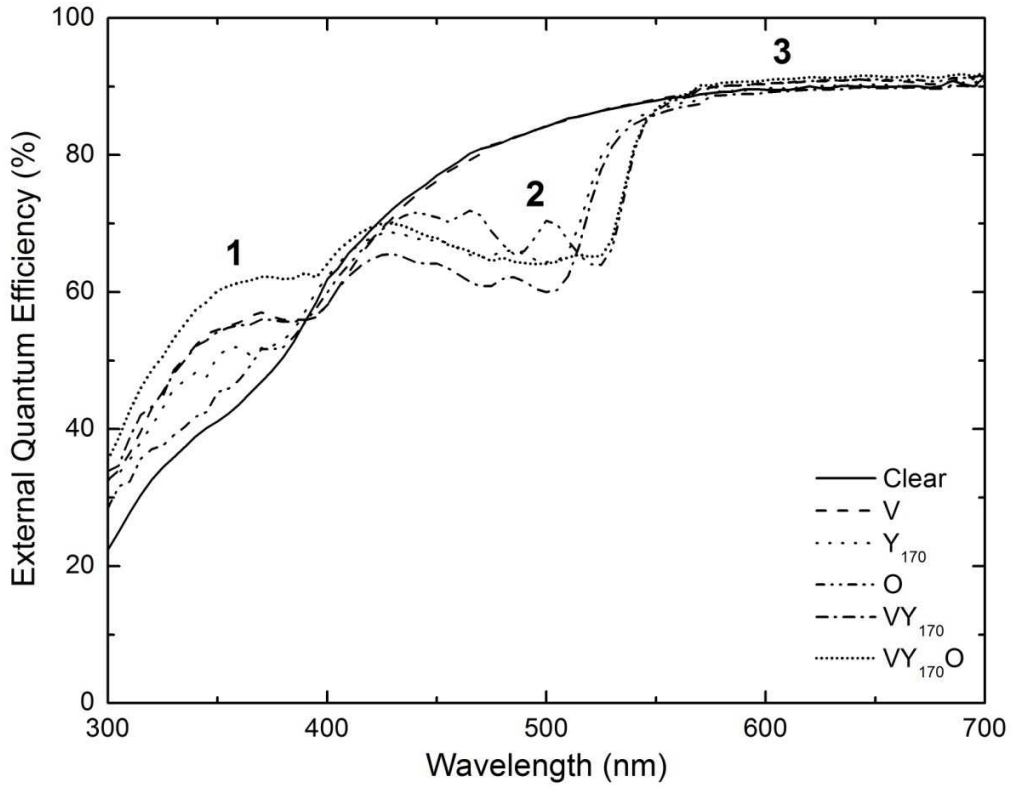

Figure 23: EQE curves of the mini-modules encapsulated in clear and luminescent EVA sheets. For λ < 400 nm (region 1), the EQE of all samples has improved in comparison with the control sample. The mixture-doped sheets lead to higher improvement compared with single-dye doped. However, there are also losses for 400 nm < λ < 550 nm (region 2) in all cases except for the violet dye. Where absorption ends in each case (region 3), all curves follow the EQE curve of the control sample.

The electrical performance of the devices was determined via *I—V* curve measurements and the results are given in Tables 23 and 24. As described in the previous chapter, to determine the impact of LDS the parameters for the mini-modules are compared to those

corresponding to the same devices prior to encapsulation and assuming an equal impact of encapsulation to the reflection profiles of the devices. The small differences in V_{OC} and FF are not attributed to LDS (see relative discussion in 4.3).

Table 23: Impact of dye-mixture-doped EVA sheets on mc-Si mini-module efficiency, determined by *I—V* curve analysis.

EVA Type	Bare cell				Encapsulated mini-module			
	J_{SC} (mA/cm^2)	V_{OC} (V)	FF (%)	η (% ab.)	J_{SC} (mA/cm^2)	V_{OC} (V)	FF (%)	η (% ab.)
Clear	32.6	0.607	75.5	14.9	33.8	0.609	73.0	15.0
VY_{170}	32.2	0.610	75.8	14.9	32.3	0.611	75.5	14.7
$VY_{170}O$	32.7	0.612	76.4	15.3	32.9	0.611	74.9	15.1

Table 24: The overall impact of encapsulation and LDS to mc-Si devices.

EVA Type	Overall encapsulation impact		LDS impact	
	ΔJ_{SC} (mA/cm^2)	$\Delta\eta$ (%)	ΔJ_{SC} (mA/cm^2)	$\Delta\eta$ (%)
Clear	+1.2	+0.1	n/a	n/a
VY_{170}	+0.1	-0.2	-1.1	-0.3
$VY_{170}O$	+0.2	-0.2	-1.0	-0.3

These results show that despite the significant performance enhancement for the region of $\lambda < 400$ nm, the decrease of EQE in the region of 400 nm $< \lambda <$ 550 nm, where the photon flux of the spectrum is significantly higher, results in an overall decrease of efficiency for both devices using the dye mixtures. However, it must be noted that the use of the Y_{170} and O in mixture with the V results in smaller J_{SC} and η decrease compared to when these two dyes are used alone (see Table 19). This is an interesting result when considering applications where colour is the primary objective, but the associated efficiency loss must be kept at the minimum possible level.

These results are in agreement with the conclusion of the previous chapter that the Y_{170} and O do not exhibit suitable absorption-emission profiles for affording an overall efficiency increase for mc-Si PV devices. However, they are a positive contribution to the direction of understanding the optical behavior of dye mixtures hosted in the same layer. The mixing of dyes does not impair their performance in terms of PLQY. The objectives of broadening

the absorption bandwidth and pursuing a greater wavelength shift for UV photons through cascade absorption-emission events were successfully achieved. These EVA sheets have a greater potential to offer efficiency improvement for other PV technologies that exhibit worse response in the range of 400 nm < λ < 500—550 nm, such as heterojunction CdS/CdTe [40]. This direction was recently pursued with positive results for rigid CdTe devices [103, 104, 137]. A particular opportunity to achieve furthermore significant efficiency gains that has not yet been realised is presented by CdTe devices grown on low-weight and flexible polyimide superstrate, which introduces very high optical losses for λ < 500nm [138].

5.3 Optimisation of Concentration for the Violet Dye

Following the results obtained with the use of EVA sheets doped with single and multiple dyes, an optimisation study for the concentration of the violet dye, which offered the best overall result for mc-Si devices, was performed. Three different concentrations were studied, leading to nominal ODs of 1, 3 and 6 respectively. The measured PLQYs for these samples did not reveal any decrease with increasing concentration over this range of concentrations. This is in agreement with results obtained in PMMA host, which showed that much higher concentrations of the violet dye can be used before luminescence quenching becomes an issue [111]. The absorption and emission spectra of the dye in the EVA sheets manufactured for this study are shown in Figure 24.

These results show that more light is absorbed in the region of 300 nm < λ < 410 nm with increasing dye concentration. Note that the design ODs of 1, 3, and 6 at peak absorption λ have not been achieved accurately in practice, especially the high ODs of 3 and 6. This is because the concentration calculations to determine the dye quantity needed to achieve a certain OD were made by considering the whole thickness of the EVA sheet as optical path for the absorption of the dye. However, in practice some photons are absorbed by the EVA before they reach the rear of the sheet, thus reducing the measured in practice OD of the dye in an EVA sheet. Nevertheless, more than 99 % of the photons (OD = 2) are absorbed by both samples at peak absorption λ. The impact of increasing concentration is more pronounced for shorter (300–370 nm) and slightly less so for longer (390–410 nm) wavelengths than that of peak absorption. This is because the increase in dye concentration will have a greater impact when the OD has a lower value compared to those for peak

absorption, since in the latter case some absorption by the EVA is unavoidable and it will impose an upper limit for the fraction of photons that the dye will absorb. This different increase in OD for different wavelengths when varying the dye concentration results in an altered fine structure of the absorption band around the peak absorption λ, which becomes nearly flat for the high concentration leading to OD = 6. The small red-shift of the absorption tail with increasing concentration will additionally give rise to a slightly higher frequency of re-absorption events. This was predicted by ray-tracing simulations (see 4.3.1 and Table 20) and is also expressed in Figure 24 in the form of the small red-shift of the dye's emission spectra with increasing concentration. The impact of these EVA sheets to the spectral response of mc-Si mini-modules was assessed via EQE curve measurements, shown in Figure 25.

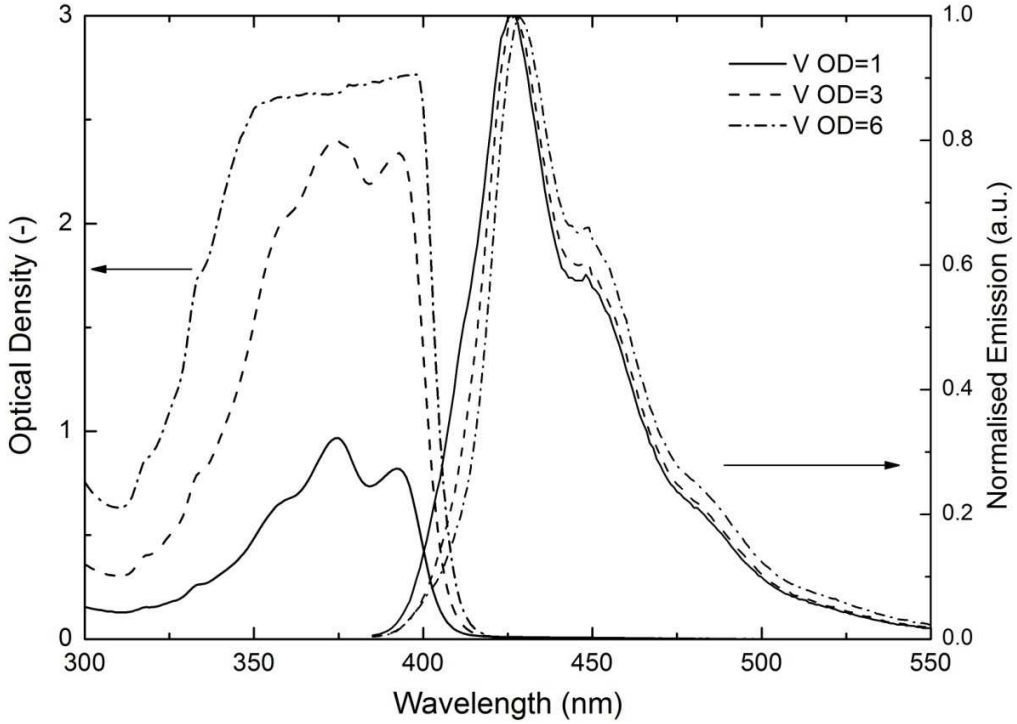

Figure 24: Impact of different violet dye concentration on its experimental OD and emission spectrum in EVA host.

These results show that that there is a slightly higher short-λ response enhancement with increasing concentration in the region of 300–370 nm, as a result of the stronger absorption shown in Figure 24. The slightly more frequent re-absorption events with increasing concentration are also evident in the EQE profiles of the mini-modules, where a slight

decrease in EQE occurs for wavelengths within the tail of the dye's absorption band (390–430 nm).

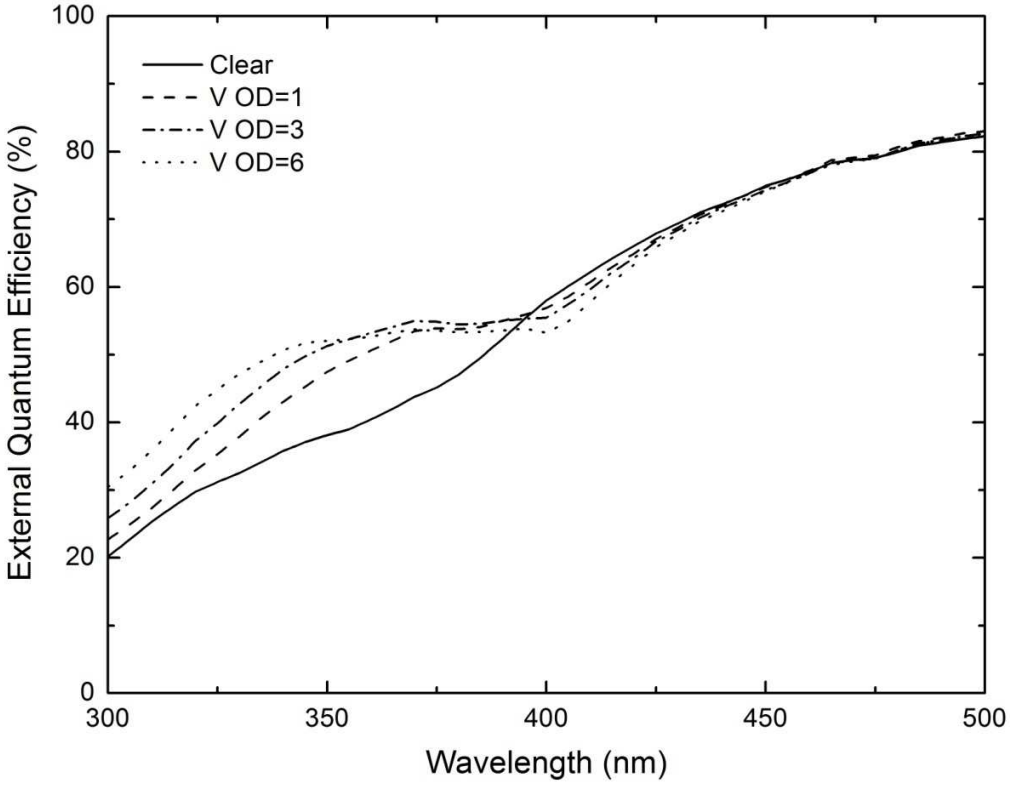

Figure 25: Impact of different violet dye concentration on the EQE profiles of mc-Si mini-modules.

The impact of LDS to the photocurrent of the devices was determined from their EQE curves with the use of equation (8) (see 3.6) and the standard spectrum AM1.5G. The EQE curves were integrated for up to $\lambda_2 = 450$ nm only, as for longer wavelengths the dye is inactive and the EQE curves of the devices almost overlap with each other. This method avoids the error associated with small differences in cell performance for wavelengths longer than the absorption band of the dye, which can be significant when trying to accurately determine a small fraction of the overall J_{SC} of a PV device. The results of these calculations are given in Table 25.

These results are in agreement with the ray-tracing-based prediction in 4.3.1 and show that there is little difference resulting by the variation of the violet dye's concentration within this range. In all cases a small increase in J_{SC} of ~0.1 mA / cm^2 is achieved. However, it must be noted that the layer OD = 1 uses only one third of dye compared to the OD = 3.

This is an important balance when considering the cost associated with transferring the LDS technology to production (see 4.3.2). It means that if a very similar gain can be achieved with using lesser quantity of dye, the LDS technology can become more cost effective. Also, using lesser quantity of dye may be advantageous in terms of achieving adequate and faster dispersion in a polymer matrix. This was not an inhibitive factor for the concentrations used in this work and there was no segregation and/or quenching of luminescence observed. However, it could become an issue of concern when mixing several luminescent materials in high concentrations in order to achieve either a performance enhancement or a specific aesthetical result.

Table 25: Impact of LDS to the J_{SC} of mc-Si mini-modules for the region of 300 nm < λ < 450 nm for different violet dye concentrations.

EVA Type	OD (-)	J_{SC} (mA/cm^2)	LDS Impact (mA/cm^2)
Clear	n/a	2.0	n/a
V	1	2.1	+0.1
V	3	2.1	+0.1
V	6	2.1	+0.1

The electrical performance of the mini-modules was also tested via *I—V* curve measurements and the results are given in Table 26. They show that there is no major difference with varying the dye concentration, which is in agreement with the conclusions from the EQE-based analysis. However, these *I—V* measurements have resulted in slightly higher J_{SC} values for the mc-Si devices used in this experiment compared to those in chapter 4 and 5.2, as well as slightly lower V_{OC} and FF. These differences are due to the different *I—V* set-ups that were used to obtain these sets of data. For obtaining the results presented in Tables 18 and 23, a well-optimised flash tester with an operating temperature control facility was used, whereas for obtaining the results shown in Table 26, a newly purchased continuous solar simulator was used. The temperature control apparatus of the continuous system was not yet installed during these measurements. Measurements for the bare cells were taken under ambient temperature, whereas for the mini-modules it was pursued to make measurements that would match the V_{OC} of the corresponding bare cell. The latter non-standard technique was forced due to the absence of an active temperature control facility and it was based on the assumption that the encapsulation of the devices,

either in doped or undoped EVA, would not introduce any change to the V_{OC} of the devices. This means that measuring the same V_{OC} before and after encapsulation is an indication that the devices were measured having the same temperature, which is the remaining factor that can have an impact on this property of the devices. However, the significantly lower V_{OC} values measured for the devices of Table 26 compared to those in Tables 18 and 23 (all devices came from the same manufacturer and batch) indicate that the cells were measured in a higher temperature when using the continuous system. This error was carried in the measurements for the encapsulated devices as well, due to the approach followed in these measurements. The very likely higher temperature of the devices also resulted in lower measured FF values. The slightly higher measured J_{SC} is most likely due to a small difference in the calibration of the two instruments. The operation of the continuous system was later improved in our laboratory; however, it was not possible to repeat these measurements, since the solar cells had already been encapsulated.

Table 26: Impact of dye-mixture-doped EVA sheets on mc-Si mini-module efficiency, determined by *I—V* curve analysis.

EVA Type	OD (-)	Bare cell				Encapsulated mini-module			
		J_{SC} (mA/cm^2)	V_{OC} (V)	FF (%)	η (%)	J_{SC} (mA/cm^2)	V_{OC} (V)	FF (%)	η (%)
Clear	n/a	33.7	0.593	71.7	14.3	33.1	0.597	73.1	14.4
V	1	33.9	0.597	72.2	14.6	34.5	0.597	72.5	14.9
V	3	33.5	0.597	71.3	14.3	33.8	0.597	72.7	14.7
V	6	33.4	0.592	71.6	14.2	33.3	0.597	72.1	14.3

5.4 Comparison between EVA Sheets Manufactured with Different Methods

The optical performance of EVA sheets manufactured with the two different techniques described in 3.2 was comparatively evaluated. Transmission measurements through the outer areas of two pairs of mini-modules using undoped and V-doped EVA sheets respectively were made and the results are shown in Figure 26. These plots show that for EVA sheets made with the first method (mechanical mixing and extrusion), a fraction of photons with $\lambda < 600$ nm are not transmitted through compared with sheets made with the second (solution-based mixing and pressure moulding). The doping of the EVA material

does not influence this performance, given the similar trends of undoped and doped EVA sheets manufactured with the same method. Hence, the origins of this performance difference for the region of $\lambda < 600$ nm must be looked for within the possible consequences of the two manufacturing methodologies.

If the processing details are carefully considered, the optical band gap and the refractive index of the EVA material are not likely to have been altered. Thus, reflection and parasitic absorption losses will be very similar in EVA sheets irrespectively of which of the two manufacturing methodologies was followed. However, the slower cooling rate of the sheets after extrusion (passive cooling to ambient temperature) compared with during pressure moulding (active cooling down to 10 °C) can give rise to crystallite formation in the ideally amorphous copolymer, which can potentially result to added scattering of light [54, 139, 140]. The presence of crystallite formations that will interact with visible light was investigated via polarised light microscopy. These results are shown in Figure 27. The sample manufactured via pressure moulding and active cooling exhibited a totally dark image in the dark position of observation (see 3.3. for definitions of bright and dark positions) and an isotropic image in the bright position (Figure 27 a) and b) respectively). This is what is expected from an amorphous material in the absence of crystallite formations that interact with visible light. On the contrary, the corresponding images from the sample manufactured via extrusion and passive cooling are anisotropic and reveal evidence of birefringence (Figure 27 c) and d)), which indicate the presence of crystallite formations that interact with visible light. In addition, there seems to be a broadly mono-axial orientation of crystallites in the extruded sample, which can be explained by the directionality of extrusion.

The scattering of the fraction of the incident photons in the case of extruded sheets does not necessarily lead to loss of their energy. Reflection from the underlying solar cell is high only for very small angles of incidence at $\lambda > 370$ and $\lambda > 390$ nm, where absorption from the EVA and the V, respectively, become dominant anyway. Thus, the fraction of the scattered photons that will reach the solar cell in suitable angles to not be reflected will be absorbed. However, a fraction of the scattered photons will be lost and naturally, the faster cooling rate methodology to manufacture EVA sheets is concluded to result in slightly superior performance, as seen in Figure 26.

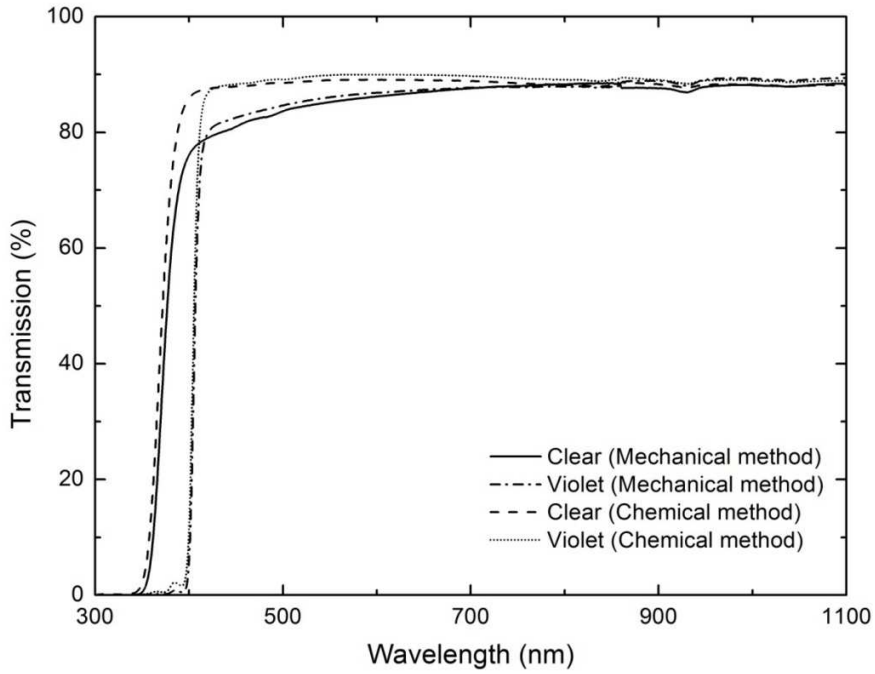

Figure 26: Transmission spectra through the outer areas of two pairs of mini-modules encapsulated in EVA sheets manufactured with two different techniques. Note that these measurements refer to transmission through two pieces of cover glass and a layer of EVA with total thicknesses of 6.6 mm and 1.2 mm respectively.

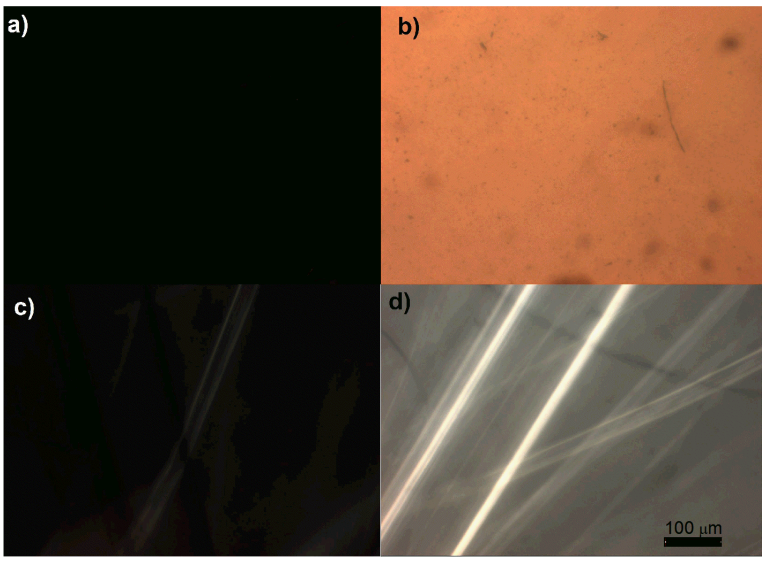

Figure 27: Images of EVA samples obtained via polarised light microscopy: a) dark image in dark position for EVA actively cooled during pressure-moulding; b) isotropic image in bright position for EVA actively cooled during pressure-moulding; c) image with birefringent patterns in black and white contrast for EVA passively cooled after extrusion; and d) the same as c) with the sample and the observation polariser rotated 45°.

5.5 The Eu^{3+} Complex as LDS Material

The PLQY of the Eu^{3+} complex in EVA was measured to be 88 % (excited at 340 nm), which is very similar to the values of 76 % and 85 % in the literature for in-solution and PMMA host [115]. This means that the complex is compatible with EVA matrix and that it satisfies the fundamental requirement for very high PLQY in order to afford a performance enhancement to PV devices. The absorption, emission and PLE profiles of the Eu^{3+} complex in EVA matrix are shown in Figure 28. The results of transmission measurements for the glass-EVA-glass sandwiches for EVA sheets doped with the complex, both alone as well in mixture with the V, are given in Figure 29.

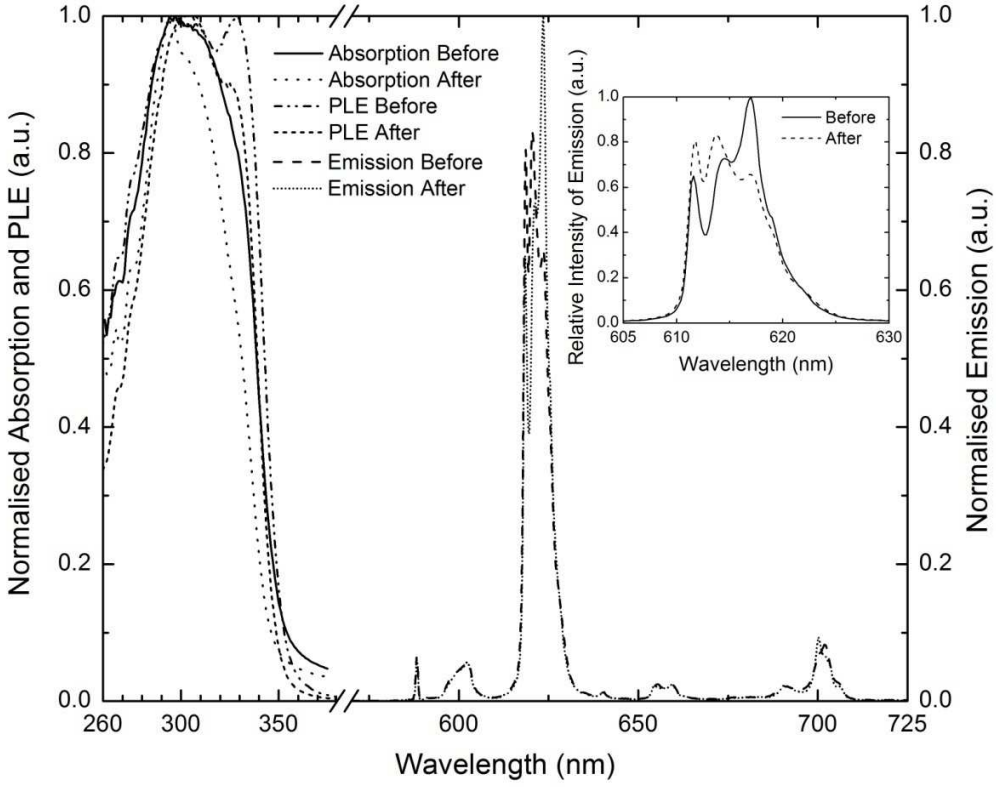

Figure 28: Absorption, PLE and emission spectra for the Eu^{3+} complex in EVA before and after lamination. The emission spectra have been scaled so that the areas under the 594 nm peak are equal. The fine structure of the main emission peak is highlighted in the inset.

The characterisation results for the EVA sheets containing the Eu^{3+} complex are very promising, since the complex absorbs light in a wavelength region where the mc-Si devices exhibit very poor response and offers a large wavelength shift to a region near the peak of

the devices' EQE curve. However, the impact of these EVA sheets was negative to the EQE of the mc-Si mini-modules, as can be seen in Figure 30.

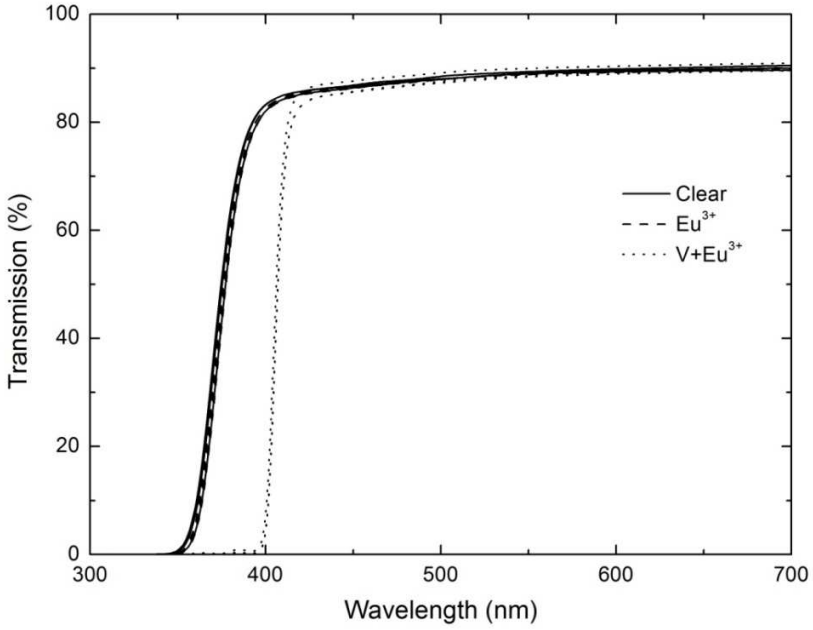

Figure 29: Transmission through the outer areas of mini-modules using EVA sheets that were undoped and doped with the Eu^{3+} complex alone and mixed with the violet dye. Note that these measurements refer to transmission through two pieces of cover glass and a layer of EVA with total thicknesses of 6.6 mm and 1.2 mm respectively.

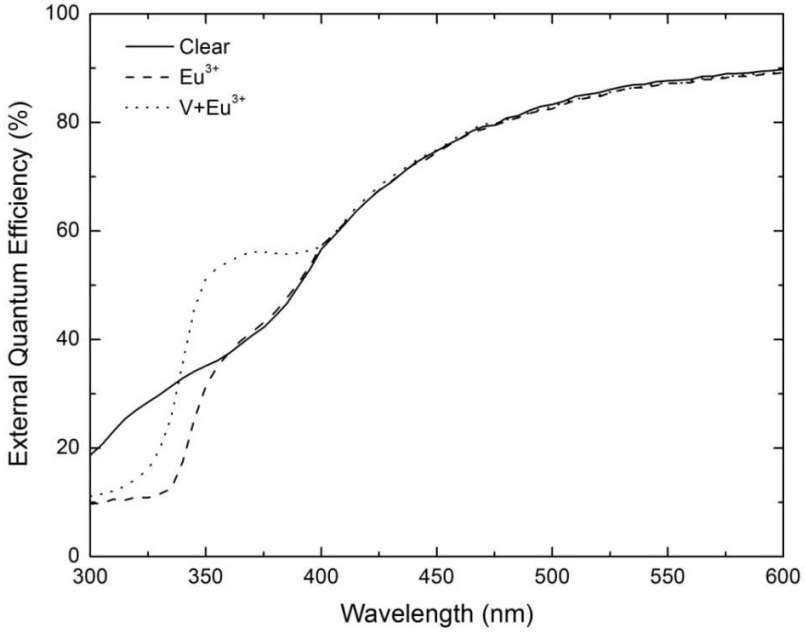

Figure 30: EQE results for the mini-modules encapsulated in undoped EVA sheets and ones containing the Eu^{3+} complex alone and in mixture with the V.

The origin of this negative result was investigated. Further absorption, PLE and emission measurements were performed on pieces of EVA that were recovered from the mini-modules after the lamination process, both doped with the Eu^{3+} complex and undoped. These measurements are also included in Figure 28, enabling a comparison with the same sheets prior to lamination. The emission spectra of the complex before and after the lamination step have been scaled so that the area under the peak centered at 594 nm is equal for both curves. This peak is a result of the only permitted magnetic dipole transition for the Eu^{3+} ion and the rate of this radiative decay pathway is independent from the ion's surroundings [141]. This means that it can be used as means of internal reference for the emission spectrum of Eu^{3+} complexes [142].

The results in Figure 28 show that the highest peak of emission (centered at 614 nm) has lost a significant part of its intensity post lamination, compared with the peak at 594 nm, while also exhibiting a different fine structure, as shown in the inset. These are both indications of a change in the symmetry of the ion's surroundings [142, 143]. The PLQY of the complex post lamination was found to have decreased from 88% to 56%. These findings imply that the complex has survived the lamination conditions, but a partial inhibition of the electronic transition that corresponds to the primary peak of emission from the Eu^{3+} (this is the transition $^5D_0 \rightarrow {}^7F_2$; for a full diagram of electronic transitions for the Eu^{3+} see [142]) has occurred due to a change in the ion's surroundings. Consistent with this, the PLE spectra show no major changes before and after lamination, suggesting no loss of ligands from the primary coordination sphere. While the exact mechanism of this performance degradation is not yet perfectly understood, two potential sources of change of the ion's surroundings are identified: first, the thermal and mechanical stress during the lamination process, which could have an impact to the organic component of the complex, and second, the cross-linking of EVA that can be considered to be the extensive surroundings of the ion, which also play a significant role in the luminescence characteristics of the complex [144].

Finally, it has to be noted that the V did not appear to be adversely affected by the presence of the Eu^{3+} complex, if the sample containing both luminescent materials is considered. In fact, the V results in an enhancement of the device's response for the region of $340 \text{ nm} < \lambda < 400 \text{ nm}$, where the absorption of the Eu^{3+} complex is weak. The integration

of these EQE curves over the AM1.5G standard spectrum using equation (8) (see 3.6) shows that the Eu^{3+} complex results in a J_{SC} decrease of 0.04 mA/cm^2, whereas the complex and V mixture in an increase of 0.11 mA/cm^2. The fact that these two materials can be mixed is interesting if we consider that the Eu^{3+} complex absorbs photons in the region that is responsible for the reported photodegradation of the V ($\lambda < 345$ nm [70]) and of EVA. If the challenge of retaining performance post lamination is overcome and the Eu^{3+} complex exhibits adequate photostability, there is a potential opportunity to substitute the UV absorbers and stabilisers that are commonly used for stabilising the EVA (and could also protect the dye) with the complex. The beneficial impact of a suitable LDS layer to the photostability of the underlying PV devices has been exhibited at least once for the generally prone to fast degradation under UV irradiation DSSCs [109]. This direction means harnessing of the energy content of the very high energy photons instead of wasting it, as is the case when the UV additives are used.

CHAPTER 6 – IMPACT OF LDS EVA LAYERS TO CIGS DEVICES

This chapter investigates the impact of LDS EVA layers to CIGS devices. By experimenting with devices with two different buffer layer thicknesses of 50 nm and 100 nm respectively, it is shown that the EQE profile of the PV devices is crucial for the choice of the optimal luminescent material. A wide range of LDS EVA sheets are first applied externally to CIGS solar cells to determine the optimal luminescent species for each buffer layer thickness. The optimal choice is then used to encapsulate the solar cells and the impact of LDS is determined by resolving it from the impact of encapsulation to the reflection properties of the devices. Then, considerations are made on how the possibility to actively tailor the incident spectrum can have implications relative to certain parameters of the design of CIGS solar cells. The aspect of CIGS device colouration due to LDS is finally highlighted.

This chapter expands on material from the following publications:

E. Klampaftis, D. Ross, S. Seyrling, A.N. Tiwari and B.S. Richards, Increase in short-wavelength response of encapsulated CIGS devices by doping the encapsulation layer with luminescent material, Solar Energy Materials & Solar Cells 101 (2012) 62—67.

E. Klampaftis, D. Ross, S. Seyrling, A.N. Tiwari and B.S. Richards, Impact of luminescent down-shifting EVA layers onto CIGS solar cells, Proceedings of PV SAT-8, Newcastle, U.K., 2012, pp. 37—40.

E. Klampaftis, D. Ross, S. Seyrling, J. Perrenoud, A. N. Tiwari and B. S. Richards, Luminescent down-shifting for improving the efficiency of photovoltaic modules, Proceedings of PV SAT-7, Edinburgh, UK, 2011, pp. 5—8.

6.1 Background

Chalcopyrite solar cells are the fastest growing PV technology, with CIGS absorber solar cell production growing with an impressive 104 % in 2011 [79]. Recent progress in the

field of CIGS solar cell efficiency has resulted in the development of laboratory-scale devices exceeding the 20 % landmark [145]. However, there is still a large margin of improvement to be achieved towards the theoretical maximum efficiency of ~33 % for a semiconductor with $E_g \approx 1.15$ eV [22]. One of the reasons for this large disparity between world record device and the theoretical limit is the typical poor short-λ response that CIGS devices exhibit in practice, which reduces their J_{SC} [22, 146, 147].

The theoretically maximum J_{SC} that a single-junction solar cell with an absorber band gap of 1.15 eV can generate is 42.3 mA / cm^2 [22, 146]. However, there is a number of optical loss mechanisms that will reduce the J_{SC} of a CIGS solar cell to a lower value than the theoretical maximum:

- Shading by the contact grid;
- Reflection at the front planar surface;
- Absorption by the TCO window layer;
- Absorption by the buffer layer;
- Insufficient absorption and collection of low energy photons.

The former two optical loss mechanisms are broadband phenomena, whereas the latter will affect only the NIR response of CIGS solar cells. Absorption by the TCO window and buffer layers are the two mechanisms that dominate the short-λ performance of CIGS solar cells, which will further deteriorate at module level, due to reflection and absorption by the cover and encapsulation layers.

The most commonly used TCO window for CIGS solar cells is ZnO [148]. It has an E_g of ~3.3 eV and will strongly absorb photons of $\lambda < 375$ nm, reducing a cell's EQE to practically zero for very high energy photons. The most commonly used buffer material is CdS with a direct E_g of ~2.4 eV [148], which will absorb photons of $\lambda < 520$ nm. Significant research effort has been directed towards reducing these optical losses, including CdS layer thickness optimisation [149] and use of alternative buffer and TCO materials as well as methods for processing them [148, 150, 151]. The potential to mitigate these short-λ optical losses of CIGS solar cells via LDS is investigated in this chapter. CIGS solar cells with two different CdS thicknesses are tested, since this layer has a

significant impact on the EQE profile of the devices and thus, the choice of the most suitable luminescent species for maximising the photocurrent.

The in-principle potential of LDS to enhance the short-λ response of CIGS solar cells has been demonstrated in the two previous experimental attempts in the literature [27, 55]. These two first works investigated LDS layers placed or deposited onto CIGS solar cells with a single CdS layer thickness with positive results. However, the materials and/or methods used by the researchers cannot be readily transferred to production of CIGS PV modules. One step beyond the proof-of-concept stage can be made based on the approach of doping the encapsulation layer, since CIGS PV modules must be encapsulated for protection against moisture [147]. EVA being a well-known and proven material for the PV industry is one of the first obvious encapsulant candidates [147] and the choice of at least one major existing CIGS production-line [152]. This means that the PV module design that was applied to mc-Si mini-modules in the previous chapters can offer a production-ready solution for reducing the short-λ optical losses of CIGS devices as well. The use of the encapsulant to host the luminescent species for performing LDS offers the same significant advantage in the case of CIGS PV modules as for mc-Si devices. This is that there is not the need for any added layers and/or manufacturing processes to an existing production-line that already utilises EVA encapsulation. Having said that, the approach of doping the encapsulation layer can be, in principle, replicated using alternative materials that will become available in the future as encapsulants for thin-film PV technologies.

6.2 Characterisation of EVA Sheets

The PLQY values for the Y_{083} alone and in mixture with the V in EVA host are given in Table 27. The conclusion from these values is that this dye also exhibits very high PLQY, when either alone or in mixture with the V.

Table 27: PLQY for the Y_{083} alone and in mixture with the V in EVA host.

Luminescent species	Dye excited	Excitation λ (nm)	PLQY (%)
Y_{083}	Y_{083}	440	92
VY_{083}	V	375	89
VY_{083}	Y_{083}	440	92

Figure 31 shows the absorption and emission spectra of the V and the Y_{083} in EVA, together with the EQE curves of two CIGS solar cells with different CdS layer thickness to visualise the potential for short-λ response enhancement due to LDS from these materials. The violet absorbs light in a region where both solar cells exhibit very poor response, and emits where the cells exhibit an average response. The matching of the absorption band of the Y_{083} with the emission from the V is better than in the case of the Y_{170} used in the previous chapters. The Y_{083} emits at wavelengths very near to the peak response of both solar cells, similarly to the Y_{170}.

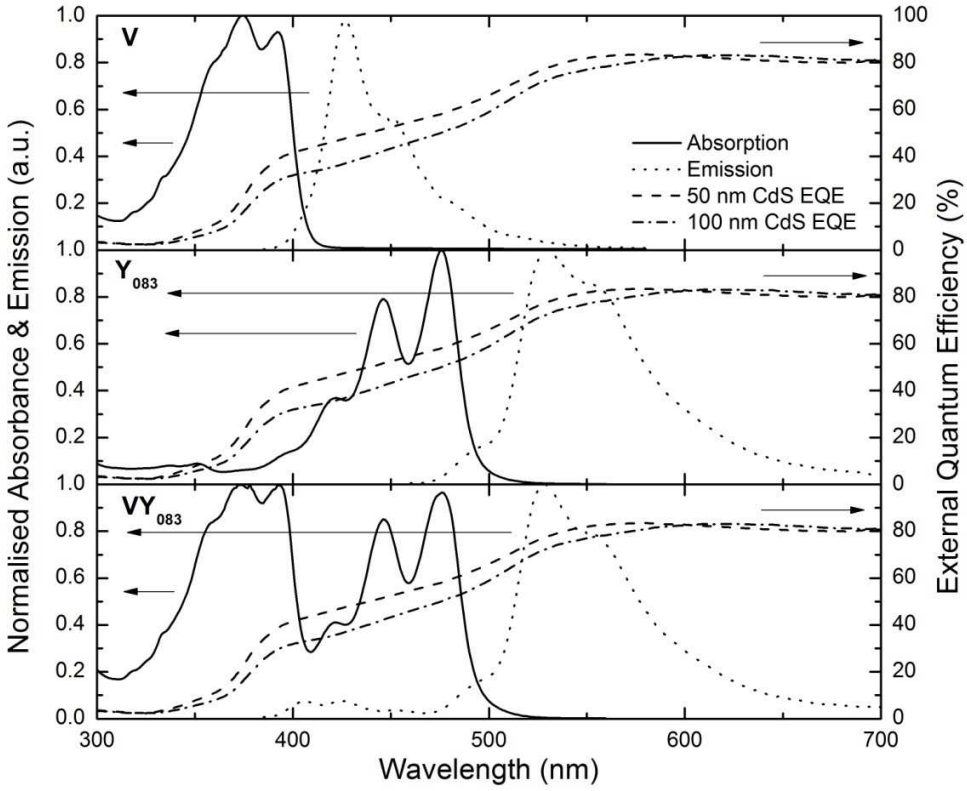

Figure 31: Absorption and emission spectra of the V and Y_{083} dyes alone and in mixture in EVA. Representative EQE curves of two cells with 50-nm- and 100-nm-thick CdS buffer layers, respectively, are also plotted.

6.3 The Impact of Different CdS Thickness on CIGS Solar Cell Performance

The EQE curves of all the solar cells manufactured for this work are shown in Figure 32. There are two points to be highlighted in this graph. The first is the impact of the different CdS thickness on the EQE profile of CIGS solar cells for the region of 350—550 nm. The second is the impact of the two different contact designs that were used in this work. The

grid that is commonly used in EMPA for manufacturing very high efficiency solar cells was not practical for tabbing the cells before encapsulation and without covering part of the active area with solder. Thus, a slightly larger pad was used for half of the devices to allow for tabbing and encapsulation, although this grid resulted in slightly lower EQE for visible wavelengths, due to the slightly higher resistive losses.

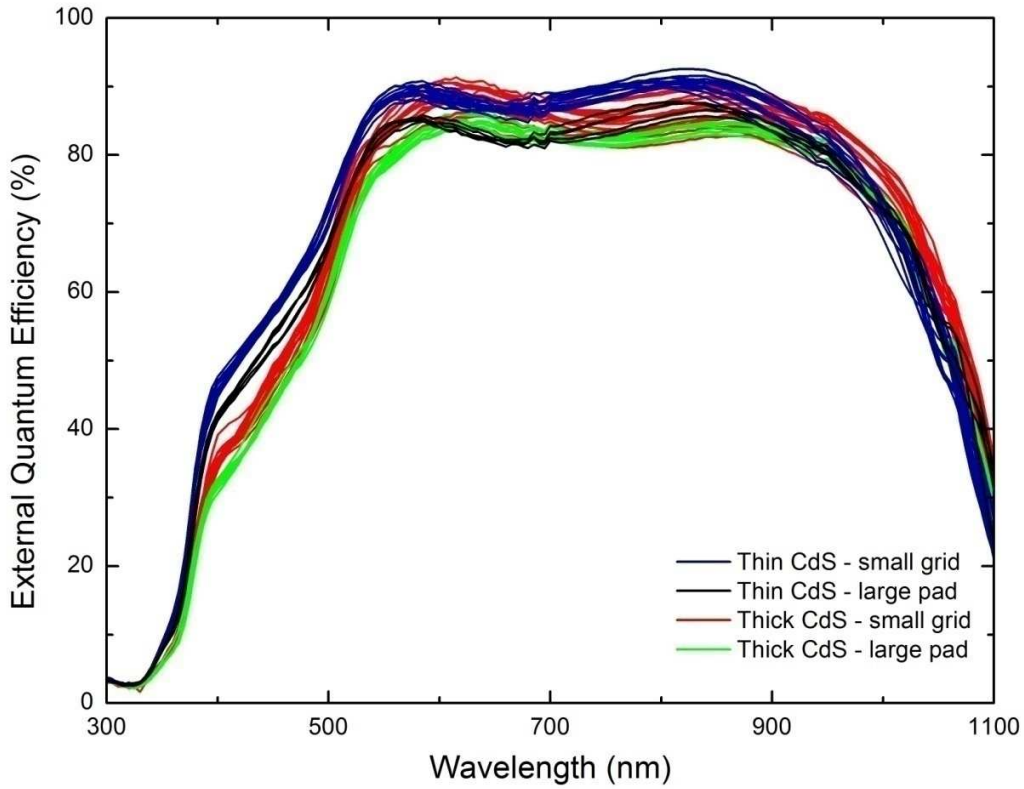

Figure 32: EQE curves for the CIGS solar cells used in this work.

Table 28 summarises the *I—V* characteristics of the cells of the two samples with the larger pad, which were used for encapsulation (see 6.4). There were five cells in the first sample with the 50-nm-thick CdS layer and six cells in the second sample with the 100-nm-thick CdS layer that exhibited a high J_{SC}. The cells of the first sample and two of the second also exhibited high V_{OC} and FF; however, four cells of the second sample were partially shunted during the scribing stage of fabrication, most likely via the formation of a low resistive connection between front and back contacts. As a result of the reduced shunt resistance, there is a reverse current flowing over the absorber when external voltage is applied, which mitigates the photocurrent and thus, reduces the V_{OC} and FF of these cells. Despite this short-coming, the J_{SC} of these cells can still be accurately determined via EQE curve

measurements and use of equation (8) (see 3.6), since the EQE measurements are performed under short-circuit conditions, hence, under no external voltage.

Table 28: *I—V* results for the solar cells of this work.

Cell	CdS layer thickness (nm)	J_{SC} (mA/cm^2)	V_{OC} (mV)	FF (%)	η (%)
1	50	33.8	656	67.4	15.1
2	50	34.9	656	63.4	14.7
3	50	33.6	664	70.9	15.9
4	50	35.1	661	64.9	15.2
5	50	34.5	664	67.7	15.7
6	100	33.4	576	43.3	8.4
7	100	32.9	588	44.6	8.7
8	100	33.2	652	68.4	14.9
9	100	32.9	636	65.5	13.8
10	100	32.9	562	47.0	8.8
11	100	32.9	366	43.0	5.2

The average J_{SC} for the cells of the first batch was 34.4 ± 0.7 mA / cm^2, whereas for the ones of the second batch it was 33.0 ± 0.2 mA / cm^2. This difference was mainly due to the better EQE of the cells with the 50 nm-thick CdS layer for photons in the region of 350 nm < λ < 550 nm. The EQE profiles of the cells were otherwise very similar, as can be seen in Figure 32. The impact of the different CdS thickness to the efficiency of the cells was in the range of ~1 % if we consider only the non-shunted cells. Small differences in efficiency are true even for cells with the same CdS thickness, primarily due to FF discrepancies that are a result of imperfect consistency in manufacturing.

6.4 Impact of LDS EVA Sheets Optically Coupled onto CIGS Solar Cells

The luminescent material with the potential to afford the highest performance enhancement for CIGS solar cells was determined in an initial screening test performed on two devices with different CdS layer thickness. EVA sheets doped with a wide range of the available luminescent materials and mixtures thereof as well as an undoped reference sheet were

applied onto the two solar cells using glycerine as optical matching medium. The EQE results of this experiment are given in Figures 33 and 34.

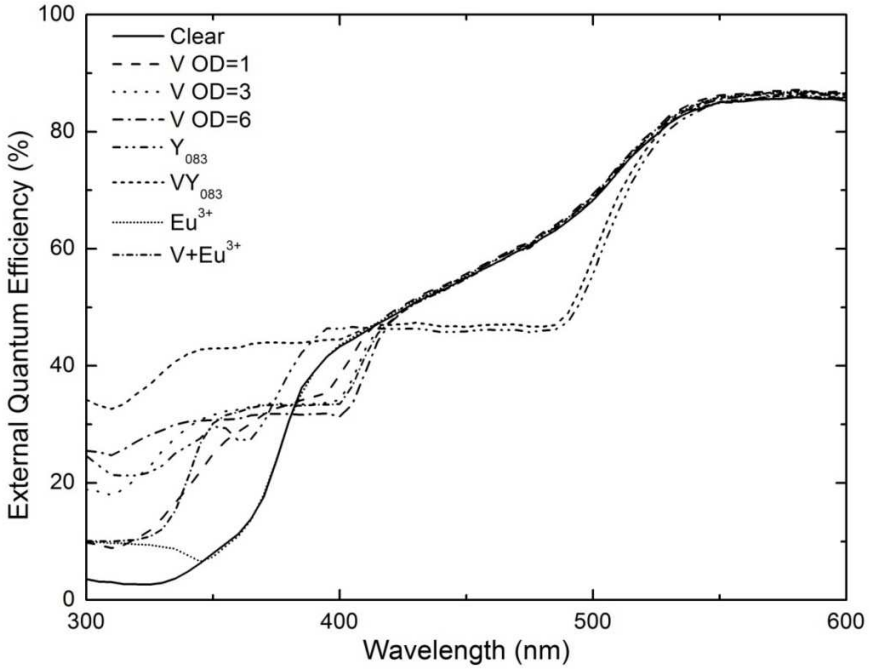

Figure 33: EQE curves for a CIGS solar cell with a 50nm-thick CdS layer under EVA sheets doped with a range of luminescent materials and mixtures thereof.

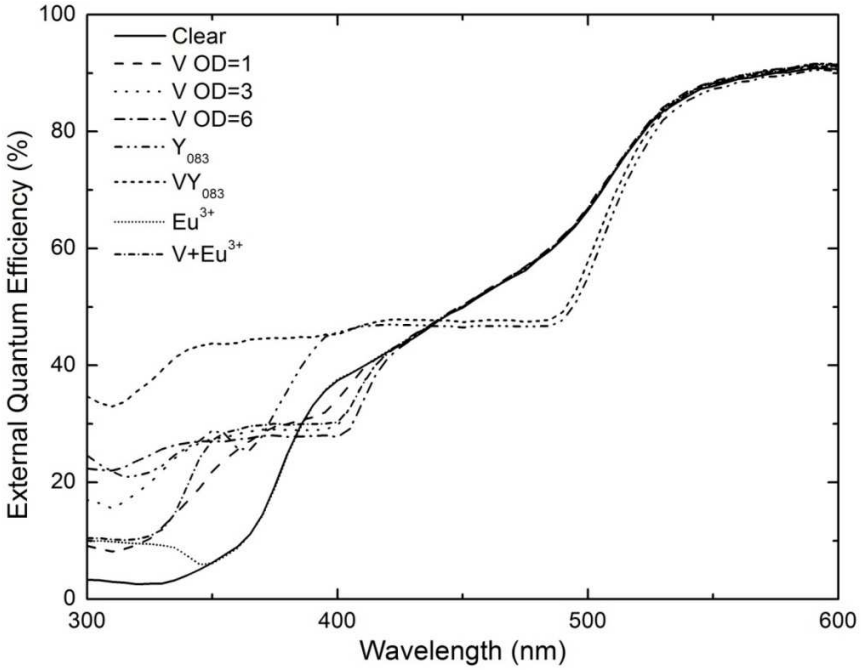

Figure 34: EQE curves for a CIGS solar cell with a 100nm-thick CdS layer under EVA sheets doped with a range of luminescent materials and mixtures thereof.

Figures 33 and 34 show that the short-λ response of both devices was improved in all cases of the investigated luminescent species. However, also for both devices there are regions of longer λ where the V and the Y_{083} dyes result in a decrease of EQE. As discussed in the case of mc-Si devices, these regions are critical for the overall result, due to the higher photon flux of sunlight in visible wavelengths. It can be seen in Figures 33 and 34 that the areas contained between the EQE curve corresponding to the clear and the doped EVA layers in each case are slightly different. This is a result of the initial slightly different EQE profiles of the two cells due to the different CdS layer thicknesses. Hence, the impact of the various LDS EVA layers is expected to be slightly different depending on the cell under investigation. The J_{SC} of the devices can be determined by integration of the EQE curves shown in Figures 33 and 34 with the use of equation (8) (see 3.6) and the AM1.5G photon flux. The results of these calculations are given in Tables 29 and 30.

Table 29: EQE-based J_{SC} results for a CIGS cell with a 50-nm-thick CdS buffer. J_{SC} is calculated for up to the wavelength where dye absorption ends in each case.

EVA type	λ_2 (nm)	J_{SC} (mA/cm^2)	LDS impact (mA/cm^2)
Clear	430	0.84	n/a
V1	430	0.94	0.10
V3	430	0.96	0.12
V6	430	0.93	0.09
V+Eu^{3+}	430	0.91	0.07
Clear	530	4.59	n/a
Y_{083}	530	4.18	-0.41
VY_{083}	530	4.38	-0.20
Clear	350	0.02	n/a
Eu^{3+}	350	0.03	0.01

Table 30: EQE-based J_{SC} results for a CIGS cell with a 100-nm-thick CdS buffer. J_{SC} is calculated for up to the wavelength where absorption ends in each case.

EVA type	λ_2 (nm)	J_{SC} (mA/cm^2)	LDS impact (mA/cm^2)
Clear	430	0.72	n/a
V1	430	0.82	0.10
V3	430	0.83	0.11
V6	430	0.81	0.09
V+Eu^{3+}	430	0.82	0.10
Clear	530	4.31	n/a
Y_{083}	530	4.18	-0.13
VY_{083}	530	4.43	0.12
Clear	350	0.01	n/a
Eu^{3+}	350	0.03	0.02

These results confirm that the impact of the LDS EVA sheets is slightly different for the two solar cells with different CdS layer thickness and EQE profiles. For the thinner CdS layer cell, the optical losses in the region of 350 nm < λ < 550 nm are slightly lower and an improvement can be achieved with the use of the V and the Eu^{3+} complex, which both absorb very short wavelengths of λ < 400 nm. However, by doubling the CdS layer thickness, the optical losses in the same spectral region are slightly higher and there is more potential for the use of the Y_{083}. The best result for the 50-nm-thick CdS cell is achieved using the V in concentration leading to OD = 3 at peak absorption λ, whereas for the 100-nm-thick CdS cell using the VY_{083} mixture (both dyes in concentrations leading to OD = 3 at peak absorption λ of each dye).

6.5 Encapsulated CIGS Devices Using LDS EVA Sheets and FEP Cover

The encapsulation of the CIGS solar cells was performed using the previously determined as optimal luminescent species for each CdS layer thickness based on the results shown in Tables 29 and 30. FEP cover was used instead of glass here in order to minimize reflection losses at the interfaces of the modules (see Figure 13 in 3.5) due to its lower refractive index compared to that of glass. In addition, flexible light-weight cover materials are

increasingly interesting for the thin-films PV industry, due to niche applications that make use of these two properties that rigid glass does not offer. Figures 35 and 36 show the EQE curves of CIGS devices before and after their encapsulation.

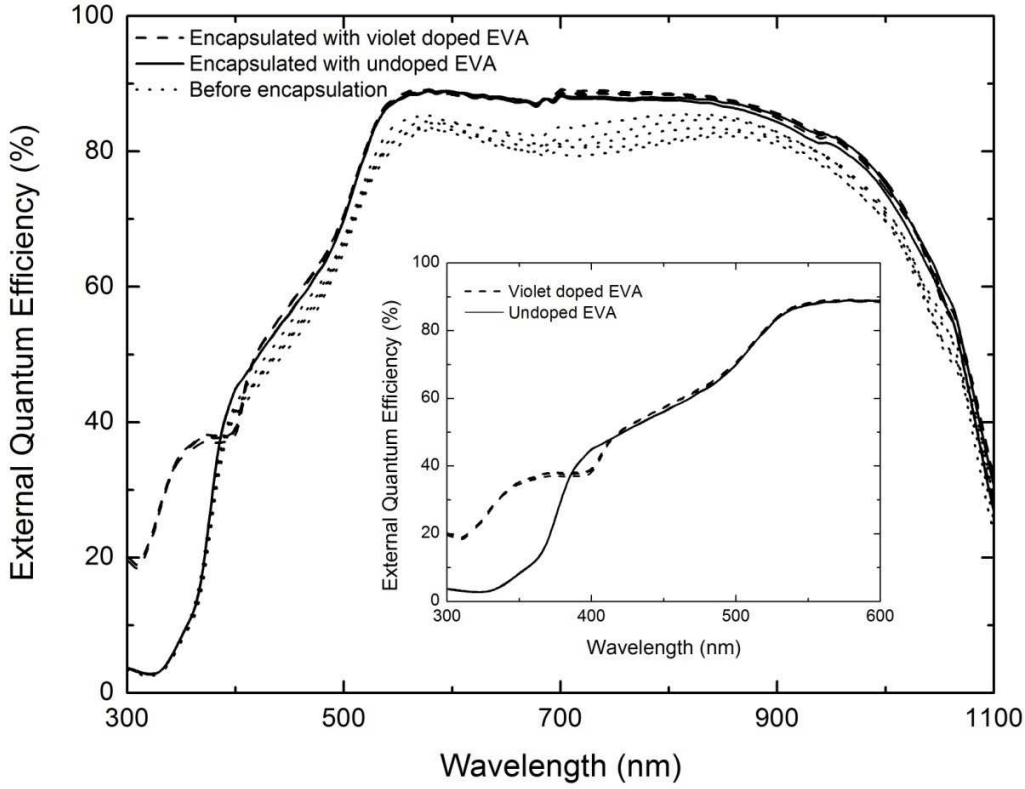

Figure 35: Comparison of EQE curves for the 50-nm-thick CdS CIGS solar cells before and after their encapsulation. Three cells were encapsulated with violet-doped EVA and two with undoped EVA. The encapsulation has a positive impact for all cells, while the impact of LDS is visible for wavelengths where the violet dye absorbs (expanded view for the encapsulated samples shown in the inset graph).

These results show that there are two distinct mechanisms present that both improve the performance of the devices, when going from a bare cell to an encapsulated device. These are, firstly, better optical coupling of light into the cells for encapsulated devices, due to the introduction of two polymeric layers of intermediate refractive indices (n_{FEP} = 1.34 [122] and n_{EVA} = 1.48 [121] for λ = 600 nm) between the air and the solar cells (shown as region 1 in Figure 36), and secondly, the impact of LDS at shorter-λ (shown as region 2 in Figure 36). The reduction in reflectance losses makes a greater contribution to the increased J_{SC} of the solar cells than LDS. This is because it improves the optical coupling for the whole region of 300—1100 nm, whereas the LDS mechanism is operating in the UV-blue region

of the solar spectrum only. Resolving the relevant contributions of these two mechanisms is essential for correct attribution of any overall benefit arising from LDS.

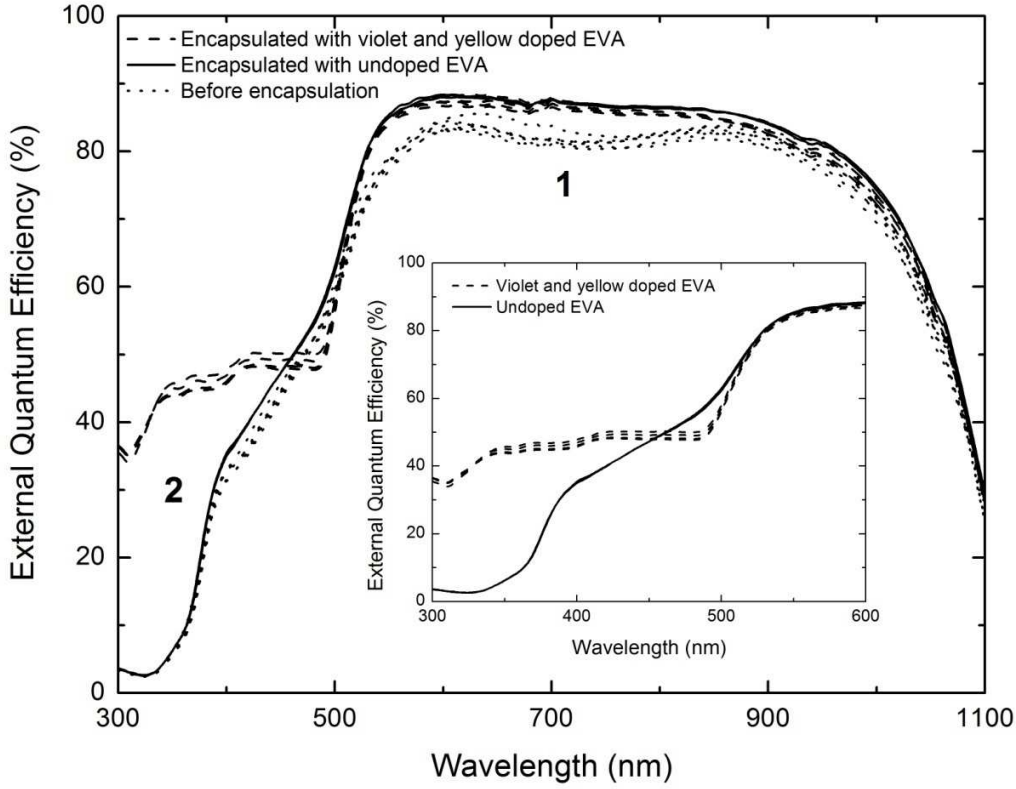

Figure 36: Comparison of EQE curves for the 100-nm-thick CdS CIGS solar cells before and after their encapsulation. Three cells were encapsulated with violet-doped EVA and two with undoped EVA. The encapsulation has a positive impact for all cells, while the impact of LDS is visible for wavelengths where the violet and the yellow dyes absorb (expanded view for the encapsulated samples shown in the inset graph).

Figures 35 and 36 also show that the encapsulation with doped EVA layers increases the short-λ EQE of all relative cells. This is true for $\lambda < 380$ nm in the case of devices with 50-nm-thick CdS using the V-doped EVA layer and for $\lambda < 460$ nm in the case of cells with 100-nm-thick CdS using the VY_{083}-doped EVA layer. In both cases, there is a narrow range of wavelengths near the tail of the absorption band of the dyes (380 – 410 nm for the V and 460 – 510 nm for the Y_{083}) where the EQE is reduced, as can be better seen in the insets of Figures 35 and 36. This is due to the dyes absorption extending out to wavelengths where the EQE of the device was already relatively high and for which the net benefit afforded by LDS becomes negative. The wavelength at which this transition occurs is defined by the EQE of the device, the absorption and emission profiles of the

luminescent species and its PLQY. To maximise the benefits that are possible through LDS, all photoactive layers above the absorber of a cell must be considered as a system. The small red-shift of the absorption tail and the emission spectrum of the luminescent species when varying the doping concentration can be used combined with fine-tuning the absorption properties of the buffer by modifying its thickness, to minimise the region where there is an EQE decrease.

Table 31 gives the impact of encapsulation for each cell and a quantification of the contribution of each mechanism that has an impact to the final EQE. These results were obtained by integrating the EQE curves of the cells using equation (8) (see 3.6) and the photon flux of the continuous solar simulator used for the *I—V* curve measurements. The latter was preferred over the AM1.5G here to pursue a better agreement between EQE and *I—V* based J_{SC} results. The method of calculating J_{SC} using equation (8) offers the possibility to do so for different regions of the spectrum, by altering the values of λ_1 and λ_2 in the equation, which allows calculating the contributions of each mechanism separately. The impact of improved optical coupling of light into the cells is calculated by comparing the total J_{SC} of the control cells, when going from a bare cell to an encapsulated device. The impact of LDS is calculated by comparing the J_{SC} of the cells that used doped EVA with the average J_{SC} of the two control cells from each sample, for the regions of the spectrum where LDS is relevant only (λ_1 = 300 nm in all cases, λ_2 = 410 nm for the 50-nm-thick CdS and V-doped EVA devices and λ_2 = 510 nm for the 100-nm-thick CdS and VY_{083}-doped EVA devices).

As mentioned previously, these results confirm that the gain in J_{SC} of the encapsulated devices due to better optical coupling of light into the cells is significantly higher than that due to LDS. This highlights the importance in experiments on the LDS technology to include suitable reference samples and to pursue the clear distinction between the reduction of reflection losses for a device and the impact of LDS. LDS has offered a gain in J_{SC}, which varies from 0.6 % for the 50-nm-thick CdS cells using the V-doped EVA, to up to 1.8 % for the 100-nm-thick CdS cells using the VY_{083} mixture, relative to the total J_{SC} of the corresponding encapsulated device.

Table 31: EQE-based J_{SC} results for the CIGS devices. There is no ΔJ_{SC} due to LDS for the undoped reference samples (n/a) and the impact of optical coupling is not calculated for the doped EVA samples (—).

Cell No	EVA type	EQE based J_{SC} (mA/cm^2)				
		Bare cell	Encapsulated device	ΔJ_{SC} total	ΔJ_{SC} due to optical coupling	ΔJsc due to LDS
1	Clear	33.2	36.4	3.2	3.2	n/a
2	Clear	33.6	36.1	2.5	2.5	n/a
3	V	34.8	36.6	1.8	—	0.2
4	V	34.4	36.8	2.4	—	0.2
5	V	33.9	36.7	2.8	—	0.2
6	Clear	33.6	35.3	1.7	1.7	n/a
7	Clear	33.3	35.3	2.0	2.0	n/a
8	VY_{083}	34.0	35.9	1.9	—	0.6
9	VY_{083}	33.2	35.5	2.3	—	0.5
10	VY_{083}	33.5	35.2	1.7	—	0.5
11	VY_{083}	33.2	35.2	2.0	—	0.4

The J_{SC} of the 50-nm-thick CdS layer cells was also determined via *I—V* curve measurements and the results are given in Table 32. The qualitative conclusions that can be drawn are in agreement with the EQE analysis already presented. The discrepancy in absolute values is due to the inherent difficulty in quantifying the impact of LDS via *I—V* curve analysis. This is because the LDS is focusing on a narrow region of the spectrum, where the photon flux is low and the relative current generation is a small fraction of the total output of a device. The impact of optical coupling is difficult to resolve when LDS is also present and hence it can only be determined for the control devices. Thus, the assumption of equal benefit due to optical coupling for all cells (used in the analysis of the results in Table 32) is another source of uncertainty when quantifying the impact of LDS via *I—V* curve analysis. Finally, for *I—V* measurements the whole area of a cell was illuminated including its contact grid, whereas for EQE measurements, only part of the active area of a cell was illuminated with the monochromatic beam. Hence, the reflection

properties of the same device are not exactly the same between the two sets of measurements.

Table 32: *I—V* curve-based J_{SC} results for the CIGS devices before and after encapsulation.

Cell No	EVA Type	*I—V* based J_{SC} (mA/cm^2)				
		Bare cell	Encapsulated device	ΔJ_{SC} total	ΔJ_{SC} due to optical coupling	ΔJsc due to LDS
1	Clear	33.8	—[a]	—[a]	—[a]	n/a
2	Clear	34.9	37.0	2.1	2.1	n/a
3	V	33.6	36.4	2.8	2.1[b]	0.7[c]
4	V	35.1	38.1	3.0	2.1[b]	0.9[c]
5	V	34.5	37.2	2.7	2.1[b]	0.6[c]

[a] The contact of this cell was damaged during the I-V curve measurements.

[b] This is assumed to be the same as for the control device.

[c] This is calculated by assuming an equal benefit due to optical coupling with the control device.

These first positive results for encapsulated CIGS devices show that it is possible for the LDS technology to be introduced in a production-feasible design of a CIGS PV module. Additionally, higher J_{SC} gains are expected if LDS layers are applied to larger area devices. This is, firstly, because the losses from the edges of the LDS layer are greater when the ratio between the device area and the LDS perimeter area is smaller. In [27], this ratio was 0.6 for small area solar cells (0.5 cm^2) and the edge losses were too high to report any improvement due to LDS. In this work however, the corresponding ratio is 5 (with cell area of 1 cm^2), mainly due to the six times thinner LDS layer, and it has been possible to demonstrate an improvement. Positive results were also reported in [27] when a thinner varnish layer (corresponding ratio of ~3.6) and larger-area mini-modules (corresponding ratio of 6.1) were used. These losses were previously quantified in 2.3, where it was shown that they become very small once a typical cell size (> 10 cm^2) of a commercial CIGS PV module is reached. Secondly, there is emission of photons towards the direction of the underlying sample and not the top or side escape cones of the LDS layer, but at large enough angles for a fraction of the photons to reach the sample outside of the active area of the cell directly beneath the area of illumination (from either the monochromatic beam in

EQE measurements or the solar simulator's beam for *I—V* curves). This is again a mechanism which is size dependent and, for small area devices, can reduce the impact of LDS measured via EQE curves (the significance is defined by the ratio between the monochromatic beam's area and the area of the cell) as well as via *I—V* curves (the significance is defined solely by the active area of the devices, as the illuminated area is equal to that).

6.6 Additional Potential Benefits of LDS for CIGS PV Modules

The possibility to modify the spectrum that a CIGS solar cell receives when exposed to sunlight can potentially play a role in the design of the cell itself. CdS is the most commonly used buffer layer for its electronic properties [148, 150, 151] and its relatively high E_g that allows good transmission of visible light [149]. If it is made possible to successfully down-shift the higher energy photons of the solar spectrum, alternative materials with lower band gap could become a more feasible option. For example, one of the best candidates towards Cd-free buffers, which is a research direction driven primarily by environmental considerations, are indium sulphide (In_2S_3)-based layers [148, 150, 151]. However, In_2S_3 has an E_g of 2—2.2 eV [153], which is lower than that of CdS (~2.4 eV) and this is a fundamental problem. However, it can be potentially overcome by means of LDS. In this work it has been shown that most photons of $\lambda < 480$ nm can be successfully absorbed and down-shifted with very high efficiency. In principle, there is no barrier why it should not be possible to actively control the incident to a solar cell spectrum by means of LDS, other than the availability of suitable materials that will satisfy all the necessary requirements for doing it successfully (as listed in 1.6). This possibility could additionally allow a greater flexibility in growing slightly thicker TCO or buffer layers from the chosen materials, if that can lead to a more robust manufacturing process and higher throughput in production, without suffering the higher optical losses that are currently associated with such an action. For example, the ZnO window must be significantly thicker in the case of modules than for small-area high-efficiency laboratory cells [154, 155] and this is one reason for the commonly achieved lower efficiencies at module versus cell level [154]. The gap between production- and laboratory-quality devices may be possible to be reduced via LDS.

Finally, as in the case of mc-Si PV modules, the introduction of luminescent material in the encapsulation layer of a CIGS PV module has the additional aesthetic effect of colouring the devices, due to luminescence to all directions. LDS EVA layers of many colours have been manufactured and presented in this thesis and it is possible to produce many more colour variations, although not all will result in equal device efficiencies. This aspect of LDS was discussed earlier to be important when considering applications where colour is a requirement from the PV industry for further development of niche markets, such as the BIPV [92, 93]. This is particularly interesting for thin-film technologies like CIGS, given that these technologies are often associated with possible properties such as light-weight and flexibility, which target alternative applications to the flat-panel PV. A picture of the coloured CIGS devices manufactured for this work is shown as Figure 37.

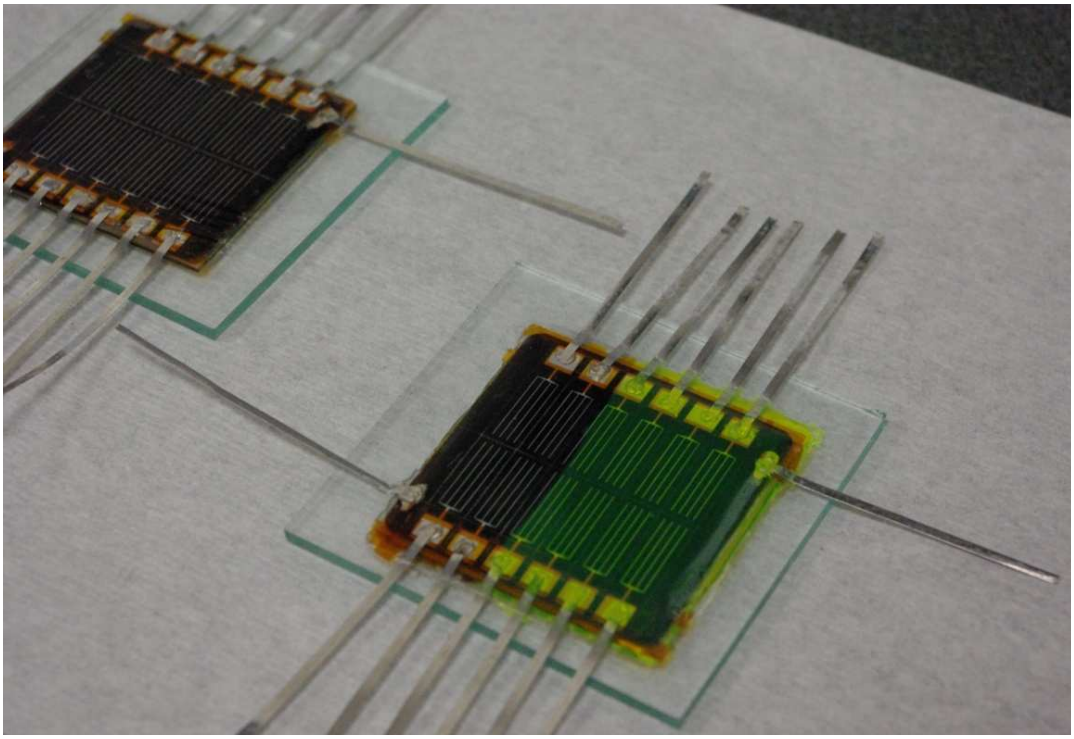

Figure 37: Coloured CIGS devices due to luminescence to all directions.

CHAPTER 7 – CONCLUSIONS AND SUGGESTIONS FOR FUTURE RESEARCH

A review of the most important findings of this thesis is given in this chapter, including:

- *the findings resulting from the critical literature review of previous works in the field of LDS;*
- *the results of characterisation for a range of luminescent materials and mixtures thereof in EVA host;*
- *the results experimentally obtained for mc-Si and CIGS devices with the use of LDS EVA layers;*
- *the potential implications of introducing the LDS technology to commercial PV modules.*

Certain suggestions on future research on the LDS technology for PV devices are also found in this final chapter.

7.1 Summary of Results and Implications for PV Devices

This thesis focused on the technology of LDS, with a primary aim to identify and investigate a production-feasible methodology to introduce the luminescent species into the design of commercial PV modules. The first step to this direction was a thorough critical literature review in order to establish a good understanding of the strengths and weaknesses of previous research works in the field. It was shown and discussed that the great disparity of the reported results was mainly due to researchers not following a uniform protocol in their experiments and reports, as well as the differences in performance between older and modern PV devices. The establishment of a standard protocol to perform experiments and report their results is necessary if different works are to be comparatively evaluated. Certain suggestions were made towards this direction, including the use of standard spectra where that is possible and the reporting of the illuminating spectrum in all cases. In addition, the inclusion in experiments of a suitable reference non-LDS device, with the only difference to the LDS samples being the absence of the luminescent species, is necessary for resolving the impact of the LDS layer to the reflection properties of the devices and to their J_{SC} due to LDS. The correct attribution of any benefit to LDS requires the

accurate resolution between these two distinct mechanisms of impact that an LDS layer will introduce to a PV device.

Following the review of all previous works on the LDS technology, an opportunity, which had not been previously explored experimentally, was identified on how to include the luminescent species in the design of a commercial PV module. This is to use as host for the luminescent species the polymeric encapsulation layer that certain in-production PV technologies rely on for protection from the environment. This approach affords the advantage of not requiring the introduction of any additional layer(s) and/or process(es) to the established manufacturing methodology of the devices.

The inclusion of several luminescent materials in EVA matrix was investigated experimentally in order to determine whether the standard encapsulant for Si wafer-based PV modules can provide a suitable host environment for them. Organic dyes and a ligand sensitised complex based on emission from the Eu^{3+} ion were investigated. The results showed that all these materials can be successfully incorporated in EVA encapsulation sheets. The luminescent materials retain the high PLQY values that they exhibit in solution and/or in alternative polymeric hosts and they do not impair the transmittance of the encapsulant. This was shown to be true when EVA is doped with either single luminescent materials or mixtures thereof. Two different methodologies were followed for the manufacture of EVA sheets and these conclusions are true for both. However, the in-house solution-based mixing and pressure moulding methodology resulted in slightly superior transmittance for $\lambda < 600$ nm, due to the actively induced faster cooling rate. The organic dyes were shown to fully tolerate the conditions during lamination of PV devices; however, this was not the case for the Eu^{3+} complex, which exhibited a reduction of its PLQY and a change of emission profile post lamination. The approach of mixing up to three organic dyes in the same sheet resulted in broader overall absorption bandwidth and greater wavelength shift for UV photons due to cascade absorption-emission events compared to what single dyes can offer.

The impact of LDS to mc-Si PV modules' EQE was shown to be positive for the region of $\lambda < 400$ nm in all cases of doped EVA sheets that were manufactured for these experiments. The enhancement of the short-λ response was greater when dye mixtures were used, due to cascade absorption-emission events and the resulting greater wavelength shift. The highest

absolute improvement for the UV region of the spectrum was up to 25 % increase in EQE and it was achieved with the use of a three-dye mixture. However, the dye mixtures that were studied also resulted in an EQE decrease of up to 20 % for the region of 400 nm < λ < 550 nm. That was because the overall optical trade-off due to the introduction of the luminescent material was negative, given that the optical losses that LDS targets are relatively lower in this region and light is already utilised very efficiently (> 65 %). The best result in terms of overall performance was achieved for mc-Si mini-modules with the use of the V at a concentration that lead to OD = 3 at peak absorption λ of the dye (375 nm). This was on overall gain in photocurrent of 0.2 mA / cm^2. However, it must be noted that a very similar improvement can be achieved by using one third of dye only. A rough cost estimate for the introduction of the LDS technology to an existing production line of mc-Si PV modules indicates that this can be realised at < 1 % added cost to solar power generation.

The impact of LDS with the use of doped EVA encapsulation was also investigated for CIGS devices. By experimenting with devices equipped with different CdS layer thicknesses, it was shown that the choice of the optimal luminescent species to perform LDS depends on the exact profile of the PV devices. As in the case of mc-Si devices, there was an EQE increase for the region of λ < 400 nm in all cases, but also a decrease for longer wavelengths within the absorption band of the luminescent species. The best overall improvement in the case of 50-nm-thick CdS layer laminated devices was achieved with the use of the V alone. That was an increase in short-λ EQE of up to 20 %, which resulted in an overall gain in J_{SC} of 0.2 mA / cm^2. In the case of 100-nm-thick CdS laminated devices, the short-λ EQE enhancement is up to 40 % and the gain in J_S up to 0.6 mA / cm^2. This was achieved with the use of the V and Y_{083} dyes in mixture.

7.2 Future Research on LDS

LDS is a technology that attempts to address an existing weakness of commercial PV modules. This means that it will continue to attract the interest of scientists and engineers working in the field of increasing the efficiency of PV devices. The suitability of the available luminescent materials is the most decisive factor for performing LDS successfully. It is very likely that a significant breakthrough may come through the development of rare-earth ion complexes for PV applications, which is a research area that

attracts the attention of several research groups in the world the recent years. Chemists and material scientists working in this area are encouraged to expand the absorption band that these complexes exhibit so that to afford broadband UV absorption. Such an improvement would make their materials very attractive candidates for LDS applications.

The photostability of EVA sheets doped with organic dyes must be investigated in order to experimentally demonstrate that this is a viable suggestion for commercialisation. The adequate stabilisation of doped EVA sheets can be relatively simply achieved with the use of additives that will provide the necessary protection, as is the standard practice for undoped EVA in the industry today. However, the real challenge is how to harness the energy content of very high energy photons and not just waste it as is the case with the use of such additives. This requires the development of LDS materials that are highly stable for long-term exposure to sunlight and this is another challenge for the researchers working in the area of material development.

The overall benefit in terms of J_{SC} and η that has been demonstrated in this thesis is rather small for the mc-Si and CIGS PV technologies. At the same time, efficiencies of commercial modules will continue to rise by further improving their optoelectronic properties and the repeatability of practices at production scale. Thus, it is an open question whether LDS will be transferred to production of mainstream high-efficiency flat-plate mc-Si and CIGS PV modules. This is more realistic to be considered in the near future by CdTe module manufacturers, given the significantly lower spectral response of their products for a broader part of the spectrum compared with mc-Si and CIGS. Having said this, there are possibilities to further increase the gains via LDS for mc-Si and CIGS devices by reconfiguring the solar cells to perform optimally under the modified spectrum. This refers primarily to the thickness and the refractive index of the AR-coatings currently in use, which can be modified to afford a better performance for visible wavelengths without the associated consequences for high energy photons, which will be down-shifted by the LDS process. In addition, certain production-related parameters, such as the emitter doping level for mc-Si and the thickness of the ZnO window for CIGS, may also be re-optimised based on the modified spectrum. These actions may yield further small improvements in the overall efficiency of commercial PV modules, or contribute towards more robust manufacturing processes, which are also highly desirable in production. A

particular possibility for the CIGS PV technology that is not as mature as the mc-Si is to investigate buffer materials with lower band gap than that of CdS, with the intention to substitute this material with a Cd-free alternative. Such an action would be based on environmental considerations rather than efficiency enhancement, due to the toxicity of Cd and the chemical bath deposition method that is used to deposit this layer.

Finally, LDS can prove to afford a breakthrough in encouraging the further uptake of PV in applications other than the flat-plate panels. The vast majority of PV products on sale today are of either dark-blue or black colour and this can be said to be an aesthetical disadvantage of PV products. If colourful, more aesthetically pleasing PV devices are an option, they can play a role in boosting emerging PV markets, such as the BIPV that has been given emphasis in this thesis, as well as niche applications that can be envisaged, including PV for textiles, PV for electrical vehicles, PV with decorative content, consumer-product integration for powering small electronic devices, education PV kits, eco-branding and many others. This aspect of LDS is in the view of the author the most outstanding outcome of this work, which can potentially have a similar impact in commercial exploitation with the development of colour TV compared with black and white. PV scientists and engineers are encouraged to investigate the potential applications that can be invented if colourful PV products are possible.

REFERENCES

[1] International Energy Association, 2011 Key world energy statistics. Available at: http://www.iea.org/textbase/nppdf/free/2011/key_world_energy_stats.pdf (Last accessed on 20-4-2012).

[2] International Energy Association, World Energy Outlook 2011 Factsheet: How will global energy markets evolve to 2035? Available at: http://www.iea.org/weo/docs/weo2011/factsheets.pdf (Last accessed on 20-4-2012).

[3] O. Morton, Solar energy: A new day dawning?: Silicon Valley sunrise, *Nature* 443 (2006): 19—22.

[4] W.A. Hermann, Quantifying global exergy resources, *Energy* 31(12) (2006) 1685—1702.

[5] W.G. Adams and R.E. Day, The action of light on selenium, *Proceedings of the Royal Society* A25 (1877) p. 113.

[6] C.E. Fritts, New Form of Selenium Cell, with some Remarkable Electrical Discoveries made by its Use, *Proceedings of the American Association for the Advancement of Science* 33 (1883) p. 97.

[7] C.E. Fritts, New Form of Selenium Cell, *American Journal of Science* 26 (1883) p. 465.

[8] R.S. Ohl, Light-sensitive electric device, US Patent No. 2402622 (1941).

[9] R.S. Ohl, Light-sensitive device including silicon, US Patent No. 2443542 (1941).

[10] D.M. Chapin, Solar Energy Converting Apparatus, US Patent No. 2780765 (1954).

[11] D.M. Chapin, C.S. Fuller and G.L. Pearson, A new silicon p-n junction photocell for converting solar radiation into electrical power, *Journal of Applied Physics* 25 (1954) 676—677.

[12] M.A. Green, K. Emery, Y. Hishikawa, W. Warta and E.D. Dunlop, Solar cell efficiency tables (version 39), *Progress in Photovoltaics: Research and Applications* 20 (2012) 12—20.

[13] W. Shockley and H.J. Queisser, Detailed balance limit of efficiency of p-n junction solar cells, *Journal of Applied Physics* 32 (3) (1961) 510—519.

[14] S.M. Bedair, M.F. Lamorte and J.R. Hauser, A two-junction cascade solar-cell structure, *Applied Physics Letters* 34 (1) (1979) 38—39.

[15] C.R. Wronski and D.E. Carlson, Amorphous silicon solar cells in: M.D. Archer, R. Hill (Eds.), *Clean Electricity from Photovoltaics, Series on Photoconversion of Solar Energy Volume 1*, Imperial College Press, London, U.K., 2001, pp. 199—236.

[16] D. Bonnet, Cadmium telluride solar cells, in: M.D. Archer, R. Hill (Eds.), *Clean Electricity from Photovoltaics, Series on Photoconversion of Solar Energy Volume 1*, Imperial College Press, London, London, U.K., 2001, pp. 245—269.

[17] U. Rau and H.W. Schock, Cu(In,Ga)Se_2 solar cells, in: M.D. Archer, R. Hill (Eds.), *Clean Electricity from Photovoltaics, Series on Photoconversion of Solar Energy Volume 1*, Imperial College Press, London, U.K., 2001, pp. 277—332.

[18] M. Grätzel, Perspectives for dye-sensitized nanocrystalline solar cells, *Progress in Photovoltaics: Research and Applications* 8 (1) (2001) 171—185.

[19] J.J.M. Halls and R.H. Friend, Organic photovoltaic devices in: M.D. Archer, R. Hill (Eds.), *Clean Electricity from Photovoltaics, Series on Photoconversion of Solar Energy Volume 1*, Imperial College Press, London, U.K., 2001, pp. 377—432.

[20] NREL, Best research-cell efficiencies 2012. Available at: http://www.nrel.gov/ncpv/ (Last accesses on 14-6-2012).

[21] European Photovoltaic Industry Association, Global market outlook for photovoltaics until 2015. Available at: http://www.epia.org/publications/epiapublications/global-market-outlook-for-photovoltaics-until-2015.html (Last accessed on 19-4-2012).

[22] S. Siebentritt, What limits the efficiency of chalcopyrite solar cells? Solar Energy Materials and Solar Cells 95 (2011) 1471–1476.

[23] W.P. Mulligan, D.H. Rose, M.J. Cudzinovic, D.M. de Ceuster, K.R. McIntosh, D.D. Smith and R.M. Swanson, Manufacture of solar cells with 21% efficiency, in: *Proceedings of the 19th EU PVSEC*, Paris, France, 2004, p. 387.

[24] K.R. McIntosh and B.S. Richards, Increased mc-Si module efficiency using fluorescent organic dyes: a ray-tracing study, in: *Conference record of the IEEE 4th World Conference on Photovoltaic Energy Conversion*, Hawaii, USA, 2006, vol. 2, pp. 2108—2111.

[25] A.W. Bett, F. Dimroth, G. Stollwerck and O.V. Sulima, III–V compounds for solar cell applications, Applied Physics A: Materials Science & Processing 69 (1999) 119—129.

[26] S.H. Demtsu, J.R. Sites, Quantification of losses in thin-film CdS/CdTe solar cells, in: *Proceedings of the IEEE 31st Photovoltaic Specialists Conference*, Florida, USA, 2005, pp. 347–350.

[27] G.C. Glaeser and U. Rau, Improvement of photon collection in Cu(In,Ga)Se_2 solar cells and modules by fluorescent frequency conversion, *Thin Solid Films* 515 (15) (2007) 5964–5967.

[28] J. Meier, J. Spitznagel, U. Kroll, C. Bucher, S. Fay, T. Moriarty and A. Shah, High-efficiency amorphous and micromorph silicon solar cells, in: *Proceedings of the 3rd World Conference on Photovoltaic Energy Conversion*, Osaka, Japan, 2003, vol. 3, pp. 2801–2805.

[29] X. Deng and E.A. Schiff, Amorphous Silicon Based Solar Cells, in: A. Luque, S. Hegedus (Eds.), *Handbook of Photovoltaic Science and Engineering*, Wiley, New York, USA, 2004, pp. 505–565.

[30] L.H. Slooff, R. Kinderman, A.R. Burgers, N.J. Bakker, J.A.M. van Roosmalen, A. Büchtemann, R. Danz and M. Schleusener, Efficiency enhancement of solar cells by application of a polymer coating containing a luminescent dye, Journal of Solar Energy Engineering 129 (3) (2007) 272–276.

[31] G. Dennler, K. Forberich, M.C. Scharber, C.J. Brabec, I. Tomiš, K. Hingerl, T. Fromherz, Angle dependence of external and internal quantum efficiencies in bulk-heterojunction organic solar cells, Journal of Applied Physics 102 (5) (2007) 054516–054517.

[32] H.J. Hovel, R.T. Hodgson and J.M. Woodall, The effect of fluorescent wavelength shifting on solar cell spectral response, *Solar Energy Materials* 2 (1979) 19–29.

[33] M. Taguchi, K. Kawamoto, S. Tsuge, T. Baba, H. Sakata, M. Morizane, K. Uchihashi, N. Nakamura, S. Kiyama and O. Oota, HIT^{TM} cells—high-efficiency crystalline Si cells with novel structure, *Progress in Photovoltaics: Research and Applications* 8 (5) (2000) 503–513.

[34] A. Luque and A. Marti, Increasing the efficiency of ideal solar cells by photon induced transitions at intermediate levels, *Physical Review Letters* 78 (1997) 5014–5017.

[35] A. Goetzberger, W. Greubel, Solar energy conversion with fluorescent collectors, *Applied Physics A: Materials Science & Processing* 14 (1977) 123–139.

[36] W.H.Weber and J. Lambe, Luminescent greenhouse collector for solar radiation, *Applied Optics* 15 (1976) 2299—2300.

[37] BASF, Lumogen F datasheets. Available at: http://www.performancechemicals.basf.com/ev-wcms-in/internet/en_GB/portal/show-content_cps/function:evproducts:/multilist/basic/4704/4732 (last accessed on 18-10-2008).

[38] ASTM Standard G-173-03. Available at: http://rredc.nrel.gov/solar/spectra/am1.5 (last accessed on 24-2-2012).

[39] T. Maruyama, A. Enomoto and K. Shirasawa, Solar cell module colored with fluorescent plate, *Solar Energy Materials & Solar Cells* 64 (3) (2000) 269–278.

[40] B. S. Richards and K. R. McIntosh, Overcoming the poor short wavelength spectral response of CdS/CdTe photovoltaic modules via luminescence down-shifting: ray-tracing simulations, *Progress in Photovoltaics: Research and Applications* 15 (1) (2007) 27–34.

[41] S. Marchionna, F. Meinardi, M. Acciari, S. Binetti, A. Papagni, S. Pizzini, V. Malatesta and R. Tubino, Photovoltaic quantum efficiency enhancement by light harvesting of organo-lanthanide complexes, *Journal of Luminescence* 118 (2006) 325–329.

[42] A. Le Donne, M. Acciarri, D. Narducci, S. Marchionna and S. Binetti, Encapsulating Eu^{3+} complex doped layers to improve Si-based solar cell efficiency, *Progress in Photovoltaics: Research and Applications* 17 (2009) 519–525.

[43] K. Kawano, N. Hashimoto and R. Nakata, Effects on solar cell efficiency of fluorescence of rare-earth ions, Materials Science Forum 239–241 (1997) 311–314.

[44] K. Kawano, K. Arai, H. Yamada, N. Hashimoto and R. Nakata, Application of rare-earth complexes for photovoltaic precursors, *Solar Energy Materials & Solar Cells* 48 (1–4) (1997) 35–41.

[45] V. Švrček, A. Slaoui and J. C. Muller, Silicon nanocrystals as light converter for solar cells, *Thin Solid Films* 451–452 (2004) 384–388.

[46] K. Yamada, Y. Wada and K. Kawano, Improvement of efficiency of solar cells by application of the rare earth ions doped fluorescent glass, *Kidorui (Rare Earths)* 36 (2000) 252–253.

[47] S. Inoue, T. Jin, K. Machida and G. Adachi, Luminescence property and application of rare earth complexes incorporated in ORMOSIL matrices, *Kidorui (Rare Earths)* 30 (1997) 190–191.

[48] T. Jin, S. Inoue, K. Machida and G. Adachi, Photovoltaic cell characteristics of hybrid silicon devices with lanthanide complex phosphor-coating film, *Journal of the Electrochemical Society* 144 (11) (1997) 4054–4058.

[49] K. Machida, H. Li, D. Ueda, S. Inoue and G. Adachi, Preparation and application of lanthanide complex incorporated ormosil composite phosphor films, *Journal of Luminescence* 87–89 (2000) 1257–1259.

[50] T. Maruyama and J. Bandai, Solar cell module coated with fluorescent coloring agent, *Journal of the Electrochemical Society* 146 (12) (1999) 4406–4409.

[51] T. Maruyama and Y. Shinyashiki, Solar cells coated with fluorescent coloring agent, *Journal of the Electrochemical Society* 145 (8) (1998) 2955–2957.

[52] T. Maruyama, Y. Shinyashiki and S. Osako, Energy conversion efficiency of solar cells coated with fluorescent coloring agent, *Solar Energy Materials & Solar Cells* 56 (1998)1–6.

[53] B.S. Richards and A. Shalav, The role of polymers in the luminescence conversion of sunlight for enhanced solar cell performance, *Synthetic Metals* 154 (1–3) (2005) 61–64.

[54] A.W. Czanderna and F.J. Pern, Encapsulation of PV modules using ethylene vinyl acetate copolymer as a pottant: a critical review, *Solar Energy Materials & Solar Cells* 43 (1996) 101–181.

[55] H.-J. Muffler, M. Bär, I. Lauermann, K. Rahne, M. Schröder, M.C. Lux-Steiner, C.-H. Fischer, T.P. Niesen and F. Karg, Colloid attachment by ILGAR-layers: creating fluorescing layers to increase quantum efficiency of solar cells, *Solar Energy Materials & Solar Cells* 90 (2006) 3143–3150.

[56] W.G.J.H.M. van Sark, A. Meijerink, R. Schropp, J.A.M. van Roosmalen and E.H. Lysen, Modeling improvement of spectral response of solar cells by deployment of spectral converters containing semiconductor nanocrystals, *Semiconductors* 38 (8) (2004) 962–969.

[57] W.G.J.H.M. van Sark, Enhancement of solar cell performance by employing planar spectral converters, *Applied Physics Letters* 87 (15) (2005) 151113–151117.

[58] W.G.J.H.M. van Sark, A. Meijerink, R.E.I. Schropp, J.A.M. van Roosmalen and E.H. Lysen, Enhancing solar cell efficiency by using spectral converters, *Solar Energy Materials & Solar Cells* 87 (2005) 395–409.

[59] F. Galluzzi and E. Scafé, Spectrum shifting of sunlight by luminescent sheets: performance evaluation of photovoltaic applications, *Solar Energy* 33 (6) (1984) 501–507.

[60] T. Maruyama and R. Kitamura, Transformations of the wavelength of the light incident upon solar cells, *Solar Energy Materials & Solar Cells* 69 (3) (2001) 207–216.

[61] T. Maruyama and R. Kitamura,Transformations of the wavelength of the light incident upon CdS/CdTe solar cells, *Solar Energy Materials & Solar Cells* 69 (1) (2001) 61–68.

[62] D. Sarti, F. Le Poull and P. Gravisse, Transformation du rayonnement solaire par fluorescence: Application a l'encapsulation des cellules, *Solar Cells* 4 (1981) 25–35.

[63] A. F. Mansour, On enhancing the efficiency of solar cells and extending their performance life, *Polymer Testing* 22 (2003) 491–495.

[64] W. Viehmann, Thin-film scintillators for extended ultraviolet (UV) response silicon detectors, *Measurements of Optical Radiations-SPIE Proceedings* 196 (1979) 90–96.

[65] K.R. McIntosh, G. Lau, J.N. Cotsell, K. Hanton, D L. Bätzner, F. Bettiol and B.S. Richards, Increase in external quantum efficiency of encapsulated silicon solar cells from a luminescent down-shifting layer, *Progress in Photovoltaics: Research and Applications* 17 (3) (2008) 191–197.

[66] R. Nakata, N. Hashimoto and K. Kawano, High-conversion-efficiency solar cell using fluorescence of rare-earth ions, *Japanese Journal of Applied Physcis* 35 (1B) (1996) L90–L93.

[67] T. Jin, S. Inoue, S. Tsutsumi, K. Machida and G. Adachi, High conversion efficiency photovoltaic cell enhanced by lanthanide complex phosphor film coating, *Chemistry Letters* 26 (1997) 171–172.

[68] A. Le Donne, M. Dilda, M. Crippa, M. Acciarri and S. Binetti, Rare earth organic complexes as down-shifters to improve Si-based solar cell efficiency, *Optical Materials* 33 (7) (2011)1012–1014.

[69] B.C. Rowan, L.R. Wilson and B.S. Richards, Advanced material concepts for luminescent solar concentrators, *IEEE Journal of Selected Topics in Quantum Electronics* 14 (5) (2008) 1312–1322.

[70] G. Seybold and G. Wagenblast, New perylene and violanthrone dyestuffs for fluorescent collectors, *Dyes and Pigments* 11 (1989) 303–317.

[71] R.E. Sah and G. Baur, Influence of the solvent matrix on the overlapping of the absorption and emission bands of solute fluorescent dyes, *Journal of Applied Physics* 23 (1980) 369–372.

[72] C. Strümpel, M. McCann, G. Beaucarne, V. Arkhipov, A. Slaoui, V. Švrček, C. del Cañizo and I. Tobias, Modifying the solar spectrum to enhance silicon solar cell efficiency—an overview of available materials, *Solar Energy Materials & Solar Cells* 91 (2007) 238–249.

[73] G.A. Crosby, R.E. Whan and R.M. Alire, Intramolecular energy transfer in rare earth chelates: Role of the triplet state, *Journal of Chemical Physics* 34 (3) (1961) 743–748.

[74] M.G. Debije, P.P.C. Verbunt, B.C. Rowan, B.S. Richards and T.L. Hoeks, Measured surface loss from luminescent solar concentrator waveguides, *Applied Optics* 47 (2008) 6763-6768.

[75] A. Parretta, A. Sarno, P. Tortora, H. Yakubu, P. Maddalena, J. Zhao and A. Wang, Angle-dependent reflectance measurements on photovoltaic materials and solar cells, *Optics Communications* 172 (1999) 139–151.

[76] Newport Corporation, Technical information. Available at: http://www.newport.com/350—1000-W-Arc-Spectral-Irradiance-Data/409190/1033/catalog.aspx (last accessed on 18-10-2008).

[77] Newport Corporation, Technical information. Available at: http://www.newport.com/Quartz-Tungsten-Halogen-Lamps/378263/1033/info.aspx (last accessed on 27-02-2012).

[78] ASTM Standard E-490-00. Available at: http://rredc.nrel.gov/solar/spectra/am0/ (last accessed on 27-02-2012).

[79] G. Hering, Cell production 2011: Survey, *Photon International*, March 2012, pp. 132-161.

[80] E. Klampaftis, B.S. Richards, L.R. Wilson, K.R. McIntosh, A. Cole and K. Heasman, Improving spectral response of mc-Si cells via luminescent down-shifting of the incident spectrum, in: *Proceedings of the 4th PVSAT Conference*, Bath, UK, 2008, pp. 59—62.

[81] C.P. Thomas, A.B. Wedding and S.O. Martin, Theoretical enhancement of solar cell efficiency by the application of an ideal 'down-shifting' thin film, *Solar Energy Materials & Solar Cells* 98 (2012) 455-464.

[82] R.A. Zakhidov and A.I. Koifman, Solar cell with a protecting coating, *Applied Solar Energy* 30 (4) (1994) 22–25.

[83] D.Z. Garbuzov, V. Bulović, P.E. Burrows and S.R. Forrest, Photoluminescence efficiency and absorption of a luminum-tris-quinolate(Alq3) thin films, *Chemical Physics Letters* 249 (1996) 433–437.

[84] D.Z. Garbuzov, S.R. Forrest, A.G. Tsekoun, P.E. Burrows, V. Bulović and M.E. Thompson, Organic films deposited on Si p–n junctions: accurate measurements of fluorescence internal efficiency, and application to luminescent antireflection coatings, *Journal of Applied Physics* 80 (8) (1996) 4644–4648.

[85] Z. Cheng, L. Pan, F. Su, M. Cao and Z. Sun, Eu^{3+} Doped Silica Film as Luminescent Down-Shifting Layer for Crystalline Si Solar Cells, *Surface Review and Letters* 16 (5) (2009) 669—673.

[86] Z. Cheng, F. Su, L. Pan, M. Cao and Z. Sun, CdS quantum dot-embedded silica film as luminescent down-shifting layer for crystalline Si solar cells, Journal of Alloys and Compounds 494 (1–2) (2010) L7–L10.

[87] X. Pi, Q. Li, D. Li and D. Yang**,** Spin-coating silicon-quantum-dot ink to improve solar cell efficiency, *Solar Energy Materials & Solar Cells* 95 (10) (2011) 2941-2945.

[88] T. Fukuda, S. Kato, E. Kin, K. Okaniwa, H. Morikawa, Z. Honda, N. Kamata, Wavelength conversion film with glass coated Eu chelate for enhanced silicon-photovoltaic cell performance, *Optical Materials* 32 (1) (2009) 22-25.

[89] J. Liu, K. Wang, W. Zheng, W. Huang, C.H. Li and X.Z. You, Improving spectral response of monocrystalline silicon photovoltaic modules using high efficient luminescent down-shifting Eu^{3+} complexes, *Progress in Photovoltaics: Research and Applications* DOI: 10.1002/pip.1251.

[90] ASTM Standard E-927-05. Available at: http://www.astm.org/Standards/E927.htm (last accessed on 04-03-2012).

[91] S. Riekeberg, P.P. Altermatt and R. Brendel, Decoupling thermalisation from solar cells, in: *Proceedings of the 21st EUPVSEC*, Dresden, Germany, 2006, pp.294–297.

[92] J. Cace and E. ter Horst, The Netherlands, Amersfoort, Nieuwland 1MW Project, in: B. Gaiddou, H. Kaan, and D. Munro (Eds), *Photovoltaics in the Urban Environment. Lessons Learnt From Large-Scale Projects*, Earthscan, London, U.K., 2009, p. 64.

[93] T.H. Reijenga, PV in architecture, in: A. Luque, S. Hegedus (Eds.), Handbook of Photovoltaic Science and Engineering, second ed., John Wiley & Sons, Chichester, UK, 2011, pp. 1043–1077.

[94] D. Walsh, Y. Shing, ZnSe solar spectrum converter for GaAs solar cells, in: *Conference Record of the IEEE 14th Photovoltaic Specialists Conference*, New Jersey, USA, 1980, pp. 476–477.

[95] M. Stan, D. Aiken, B. Cho, A. Cornfeld, J. Diaz, V. Ley, A. Korostyshevsky, P. Patel, P. Sharps and T. Varghese, Very high efficiency triple junction solar cells grown by MOVPE, *Journal of Crystal Growth* 310 (23) 5204–5208.

[96] S. Bailey and R. Raffaelle, Space Solar Cells and Arrays, in: A. Luque, S. Hegedus (Eds.), *Handbook of Photovoltaic Science and Engineering*, John Wiley & Sons, Chichester, U.K., 2003, pp. 413—448.

[97] M. Laczka and L. Stoch, Rare earth elements as components of special glasses, *Journal of the Less-Common Metals* 166 (1) (1990) 163–171.

[98] R. R. Reisfeld, H. Minti, A. Patra, D. Ganguli and M. Gaft, Spectroscopic properties of cerium in glasses and their comparison with crystals, *Spectrochimica Acta Part A* 54 (1998) 2143–2150.

[99] R. L. Crabb, Evaluation of cerium stabilized microsheet cover slips for higher solar cell outputs, in: *Conference Record of the IEEE 9th Photovoltaic Specialist Conference*, Silver Springs, USA, 1972, p. 329.

[100] H.R. Moutinho, F.S. Hasoon and L.L. Kazmerski, Studies of the micro-and nanostructure of polycrystalline CdTe and $CuInSe_2$ using atomic force and scanning tunneling microscopy, *Progress in Photovoltaics: Research and Applications* 3 (1) (1995) 39–46.

[101] B.C. Hong and K. Kawano, PL and PLE studies of $KMgF_3$:Sm crystal and the effect of its wavelength conversion on CdS/CdTe solarcell, *Solar Energy Materials & Solar Cells* 80 (4) (2003) 417–432.

[102] B.C. Hong and K. Kawano, Organic dye-doped thin films for wavelength conversion and their effects on the photovoltaic characteristics of CdS/CdTe solar cells, *Japanese Journal of Applied Physics* 43 (4a) (2004) 1421–1426.

[103] L. Danos, T. Parel, T. Markvart, V. Barrioz, W.S.M. Brooks and S.J.C. Irvine, Increased efficiencies on CdTe solar cells via luminescence down-shifting with excitation energy transfer between dyes, *Solar Energy Materials & Solar Cells* 98 (2012) 486-490.

[104] D. Ross, E. Klampaftis, J. Fritsche, M. Bauer and B.S. Richards, Increased short-circuit current density of production line CdTe mini-module through luminescent down-shifting, *Solar Energy Materials and Solar Cells* 103 (2012) 11-16

[105] M. Gloeckler and J. R. Sites, Apparent quantum efficiency effects in CdTe solar cells, *Journal of Applied Physics* 95 (8) (2004) 4438–4445.

[106] M. Kontges, R. Reineke-Koch, P. Nollet, J. Beier, R. Schaffler and J. Parisi, Light induced changes in the electrical behavior of CdTe and $Cu(In,Ga)Se_2$ solar cells, *Thin Solid Films* 403–404 (2002) 280–286.

[107] A.O. Pudov, J.R. Sites, M.A. Contreras, T. Nakada and H.W. Schock, CIGS J-V distortion in the absence of blue photons, *Thin Solid Films* 480–481 (2005) 273–278.

[108] M. Sendova-Vassileva, Model calculation of the effectiveness of Tb^{3+} containing glass as a wavelength converter in thin film solar cells, *Journal of Material Science* 46 (22) (2011) 7184-7190.

[109] J. Liu, Q. Yao and Y. Li, Effects of downconversion luminescent film in dye-sensitized solar cells, *Applied Physics Letters* 88 (17) (2006) 173113–173119.

[110] BASF Corproration, Colorants for plastics colorations. Available at: http://www.basf.es/ecp1/Poland/pl/function/conversions:/publish/upload/02_Products_Industries/04_Business_Segments/Pigmenty/Pigmenty_do_tworzyw.pdf (last accessed on 7-4-2011).

[111] L.R. Wilson, PhD Thesis: "Luminescent solar concentrators: A study of optical properties, re-absorption and device optimisation", Heriot-Watt University, May 2010. Available at: http://www.imajeenyus.com/about_me_files/phd_thesis_061127579_lindsay_wilson.pdf (last accessed on 7-4-2012).

[112] L.R.Wilson and B.S. Richards, Measurement method for photoluminescent quantum yields of fluorescent organic dyes in polymethyl methacrylate for luminescent solar concentrators, *Applied Optics* 48 (2) (2009) 212–220.

[113] BASF Corproration, Lumogen F Violet 570. Available at: http://www2.basf.us/additives/pdfs/lumvio570.pdf. (last accessed on 7-2-2011).

[114] BASF Corproration, Plastic additives. Available at: http://worldaccount.basf.com/wa/NAFTA~en_US/Catalog/PlasticAdditives/pi/BASF/range/prod_br_col_pl_lumog (last accessed on 7-2-2012).

[115] O. Moudam, B.C. Rowan, M. Alamiry, P. Richardson, B.S. Richards, A.C. Jones, and N. Robertson, Europium complexes with high total photoluminescence quantum yields in solution and in PMMA, *Chemical Communications* 43 (2009) 6649–6651.

[116] S.I. Weismann, Intramolecular energy transfer: The fluorescence of complexes of europium, *Journal of Chemical Physics* 10 (4) (1942) 214–217.

[117] N. Sabbatini, M. Guardigli and J.M. Lehn, Luminescent lanthanide complexes as photochemical supramolecular devices, *Coordination Chemical Review* 123 (1–2) (1993) 201–228.

[118] L. Porres, A. Holland, L.O. Palsson, A.P. Monkman, C. Kemp and A. Beeby, Absolute measurements of photoluminescence quantum yields of solutions using an integrating sphere, *Journal of Fluorescence* 16 (2006) 267–272.

[119] A.M. Gabor, J.R. Tuttle, D.S. Albin, M.A. Contreras and R. Noufi, High efficiency $CuIn_xGa_{1-x}Se_2$ solar cells made from $(In_x,Ga_{1-x})_2Se_3$ precursor films, *Applied Physics Letters* 65 (2) (1994) 198—200.

[120] Schott, Borofloat 33 brochure. Available at: http://www.schott.com/hometech/english/download/brochure_borofloat_e.pdf. (last accessed on 7-2-2012).

[121] K.R. McIntosh, J.N. Cotsell, J.S. Cumpston, A.W. Norris, N.E. Powell and B.M. Ketola, Optical modeling results comparing silicone and EVA photovoltaic encapsulants, in: *Proceedings of the 34th IEEE Photovoltaic Specialist Conference*, Philadelphia, USA, 2009, pp. 544–549.

[122] DuPont Corporation, DuPont FEP Fluorocarbon Film. Available at: http://www2.dupont.com/Teflon_Industrial/en_US/assets/downloads/h55008_FEP_Film_Properties_Bulletin.pdf (last accessed 29-3-2012).

[123] G.P. Smestad, F.C. Krebs, C.M. Lampert, C.G. Granqvist, K.L. Chopra, X. Mathew and H. Takakura, Reporting solar cell efficiencies in solar energy materials and solar cells, *Solar Energy Materials & Solar Cells* 92 (4) (2008) 371–373.

[124] A. Böhm, A. Grimm and B.S. Richards, Photovoltaic modules with improved quantum efficiency, Patent International Publication Number: WO/2008/110567 (2007).

[125] M.A. Green, Self-consistent optical parameters of intrinsic silicon at 300 K including temperature coefficients, *Solar Energy Materials & Solar Cells* 92 (2008) 1305–1310.

[126] P.P.C. Verbunt, A. Kaiser, K. Hermans, C.W.M. Bastiaansen, D.J. Broer and M.G. Debije, Controlling light emission in luminescent solar concentrators through use of dye molecules aligned in a planar manner by liquid crystals, *Advanced Functional Materials* 19 (2009) 2714-2719.

[127] C.L. Mulder, P.D. Reusswig, A.M. Velázquez, H. Kim, C. Rotschild and M.A. Baldo, Dye alignment in luminescent solar concentrators: I. Vertical alignment for improved waveguide coupling, *Optics Express* 18 (2010) A79-A90.

[128] A. Böhm, ColorFlex GmbH & Co KG, Kirchwaldstrasse 75, Mannheim, Germany, PLZ: 68305, Personal communication (2008).

[129] MarketBuzz, Annual World Photovoltaic Market Review, SolarBuzz LLC (2009) p. 301.

[130] International Renewable Energy Agency, Renewable energy technologies: cost analysis series, Solar Photovoltaics (June 2012). Available at: http://www.irena.org/DocumentDownloads/Publications/RE_Technologies_Cost_Analysis-SOLAR_PV.pdf (last accessed 29-6-2012).

[131] A. Böhm, ColorFlex GmbH & Co KG, Kirchwaldstrasse 75, Mannheim, Germany, PLZ: 68305, Personal communication (2012).

[132] N.B. Mason, T.M. Bruton and R. Russell, Properties and performance of coloured solar cells for building facades, in: *Proceedings of the 13th EU PVSEC*, Nice, France, 1995, pp. 2218–2219.

[133] S. Devenport, S. Roberts, T.M. Bruton, K. Heasman, L. Brown, A. Cole, I. Baistow, K. Webster and B. Garrard, Summary of the Havemor project - Process development of shaped and coloured solar cells for BIPV Applications, in: *Proceedings of the 24th EU PVSEC*, Hamburg, Germany, 2009, pp. 4276-4279.

[134] W.G.J.H.M. van Sark, K.W. Barnham, L.H. Slooff, A.J. Chatten, A. Büchtemann, A. Meyer, S.J. Mc.Cormack, R. Koole, D.J. Farrell, R. Bose, E.E. Bende, A.R. Burgers, T. Budel, J. Quilitz, M. Kennedy, T. Meyer, S.H. Wadman, G.P. van Klink, G. van Koten, A. Meijerink and D. Vanmaekelbergh, Luminescent solar concentrators – a review of recent results, *Optics Express* 16 (2008) 21773-21792.

[135] R. Kinderman, L.H. Slooff, A.R. Burgers, N.J. Bakker, A. Büchtemann, R. Danz, J.A.M. van Roosmalen, I–V performance and stability study of dyes for luminescent plate concentrators, *Journal of Solar Energy Engineering* 129 (2007) 277–282.

[136] A.A. Earp, T. Rawling, J.B. Franklin and G.B. Smith, Perylene dye photodegradation due to ketones and singlet oxygen, *Dyes and Pigments* 84 (2010) 59–61.

[137] D. Ross, E. Klampaftis, J. Fritsche, M. Bauer and B.S. Richards, Measured increased J_{sc} in production quality CdTe cells and mini-Modules through luminescent down-shifting, in: *Proceedings of the 26th EUPVSEC*, Hamburg, Germany, 2011, pp. 2463 – 2466.

[138] J. Perrenoud, B. Schaffner, S. Buecheler and A.N. Tiwari, Fabrication of flexible CdTe solar modules with monolithic cell interconnection, *Solar Energy Materials & Solar Cells* 95 (S1) (2011) S8–S12.

[139] C. Hindle, Napier Edinburgh University. Personal Communication (2009).

[140] M. Vogt, Etimex GmbH. Personal Communication (2009).

[141] M.J. Weber, T.E. Varitimos and B.H. Matsinger, Optical intensities of rare-earth ions in yttrium orthoaluminate, *Physical Review B* 8(1) (1973) 47–53.

[142] M.H.V. Werts, R.T.F. Jukes and J.W. Verhoeven, The emission spectrum and the radiative lifetime of Eu^{3+} in luminescent lanthanide complexes, *Physical Chemistry Chemical Physics* 4 (9) (2002) 1542–1548.

[143] C. Gorller-Walrand and K. Binnemans, Rationalization of crystal-field parametrization, in: K.A. Gschneidner, L. Eyring (Eds.), *Handbook on the Physics and Chemistry of Rare Earths*, vol. 23, Elsevier, Amsterdam, Netherlands, 1996, pp. 121–283.

[144] A.M. Klonkowski, S. Lis, M. Pietraszkiewicz, Z. Hnatejko, K. Czarnobaj and M. Elbanowski, Luminescence properties of materials with Eu(III) complexes: Role of ligand, coligand, anion, and matrix, *Chemistry of Materials* 15 (3) (2003) 656–663.

[145] P. Jackson, D. Hariskos, E. Lotter, S. Paetel, R. Wurz, R. Menner, W. Wischmann and M. Powalla, New world record efficiency for Cu(In,Ga)Se_2 thin-film solar cells beyond 20%, *Progress in Photovoltaics: Research and Applications* 19 (7) (2011) 894–897.

[146] W.N. Shafarman, S. Siebentritt, L. Stolt, Cu(In,Ga)Se_2 solar cells, in: A. Luque, S. Hegedus (Eds.), *Handbook of Photovoltaic Science and Engineering, second ed.*, John Wiley & Sons, Chichester, UK, 2011, pp. 546–599.

[147] R. Klenk and M.C. Lux-Steiner, Chalcopyrite based solar cells, in: J. Poortsmans, V. Arkhipov (Eds.), *Thin Film Solar Cells vol. 275*, John Wiley & Sons, Chichester, 2006, p. 237.

[148] N. Naghavi, D. Abou-Ras, N. Allsop, N. Barreau, S. Bucheler, A. Ennaoui, C.-H. Fischer, C. Guillen, D. Hariskos, J. Herrero, R. Klenk, K. Kushiya, D. Lincot, R. Menner, T. Nakada, C. Platzer-Bjorkman, S. Spiering, A.N. Tiwari and T. Torndahl, Buffer layers and transparent conducting oxides for chalcopyrite Cu(In,Ga)$(S,Se)_2$ based thin film photovoltaics: present status and current developments, *Progress in Photovoltaics: Research and Applications* 18 (2010) 411–433.

[149] K. Orgassa, U. Rau, Q. Nguyen, H.W. Schock and J.H. Werner, Role of the CdS buffer layer as an active optical element in Cu(In,Ga)Se_2 thin-film solar cells, *Progress in Photovoltaics: Research and Applications* 10 (2002) 457–463.

[150] D. Hariskos, S. Spiering and M. Powalla, Buffer layers in Cu(In,Ga)Se_2 solar cells and modules, *Thin Solid Films* 480–481 (2005) 99–109.

[151] S. Siebentritt, Alternative buffers for chalcopyrite solar cells, *Solar Energy* 77 (2004) 767–775.

[152] Solar Frontier, Product Datasheet. Availabale at: http://www.solar-frontier.com/UserFiles/file/20110722_Datasheet_SF140-155_A4%281%29.pdf (last accessedon 16-4-2012).

[153] P. Pistor, R. Caballero, D. Hariskos, V. Izquierdo-Roca, R. Wachter, S. Schorr and R. Klenk, Quality and stability of compound indium sulphide as source material for buffer layers in Cu(In,Ga)Se_2 solar cells, *Solar Energy Materials and Solar Cells* 93 (2009) 148–152.

[154] J. Kessler, J. Wennerberg, M. Bodegard and L. Stolt, Highly efficient Cu(In,Ga)Se_2 mini-modules, *Solar Energy Materials and Solar Cells* 75 (2003) 35–46.

[155] D. Hariskos, B. Fuchs, R. Menner, N. Naghavi, C. Hubbert, D. Lincot and M. Powalla, The Zn(S,O,OH)/ZnMgO buffer in thin film Cu(In,Ga)$(Se,S)_2$-based solar cells, Part II: magnetron sputtering of the ZnMgO buffer layer for in-line co-evaporated Cu(In,Ga)Se_2 solar cells, *Progress in Photovoltaics: Research and Applications* 17 (2009) 479–488.